UCL Université catholique de Louvain

École polytechnique de Louvain (EPL)

epl

Comparison between different muscular models

Dissertation presented by
Alexandra HAMBURGER

for obtaining the Master's degree in
Biomedical Engineering

Supervisor(s)
Renaud RONSSE, François HEREMANS

Reader(s)
François HENROTTE

Academic year 2016-2017

Abstract

Muscles are crucial to any living creature since the muscular system is responsible for the movement of the body. Muscles allow us to speak, breath, walk or run for example. They are capable to turn energy into motion and are tremendously sophisticated. They thus aroused the interest of scientists to understand how muscles work and how they can be modelled. Muscle models have been developed for different reasons such as trying to better understand how muscles work by isolating the important components or to explain and predict a force response. Understanding how a healthy muscle works can be crucial to comprehend muscle pathologies in order to heal them. Understanding a muscle and being able to predict its force response can also be used to create prostheses that replace a body segment. Another application for muscular models can be humanoid robots where the muscle activity of humans is more or less duplicated. Most muscular models focus on skeletal muscles since these are the ones that allow us to interact with the environment. The purpose of this master thesis is to review some muscular models of the skeletal muscle and compare them according to different criteria in order to see whether there is a model better than the others and whether it takes the whole complexity of the muscle into account. First, an isolated muscle and its force response with the different muscular models will be compared and then, since a skeletal muscle is usually connected to bones, a bi-muscular articulation will be implemented and compared for the different muscular models.

Four types of models, found in the literature, were implemented in this master thesis by using the MATLAB® software. These models were chosen for the reason that they all focused on a different aspect of the muscle modelization. All the models work according to a common framework: each model takes as input the muscle length and velocity as well as an activation level. The main output is the force response. Mathematical functions, different for each model, predict the force-response from these inputs. The force-response from each model for the same inputs were then compared to each other and to the literature. They were compared in terms of different criteria such as computation time, their biophysical meaning or their activation dynamics to name a few. Their mechanical impedance, how the muscle resists to an oscillating perturbation, was also analysed for each model. The bi-muscular articulation analysed in this master thesis is the human ankle and two antagonist muscles. The tibia was fixed and only the foot could move with respect to the tibia. The muscles were given similar activation levels for the models and the resulting change in angle and torque could be obtained and compared. The mechanical impedance, of the ankle this time, was analysed for each model as well.

Although all four models had similar force responses, one dominated in terms of biophysical meaning and accuracy. The price of this is a heavy computation time that made it unsuited for the implementation of an articulation. The other models had better computational times with a loss of accuracy and biophysical meaning. The activation dynamics of the four models were quite dissimilar: some were more complex and physiologically meaningful than others. Two models had as output only the force-response while one gave also the muscle stiffness and one, the slowest one, gave the muscle stiffness as well as the stored elastic energy in the muscle. Finally, some differences in terms of impedance of the modelled isolated muscle could be noted. The simulated ankle articulation moved in a similar way with the three remaining muscular models and their impedance did not differ much.
The models presented in this master thesis are only a handful of the diversity of models that exists in the literature. The models discussed here modelled all the skeletal muscle but there exist also models for other types of muscle.

Acknowledgements

I would like to take this opportunity to thank all the people who have contributed to this master thesis.

I would first like to thank my thesis advisor Renaud Ronsse for the subject of this thesis, taking the time to read my manuscripts and steering me in the right direction with constructive comments and suggestions.

I would like to thank François Heremans for his help and patience as well as reading my manuscripts too.

I would also like to thank François Henrotte for accepting and taking the time to read this master thesis.

Finally, I would like to thank my parents and friends for their support and encouragements during this final master year.

Contents

Introduction

About half of the human weight is made of muscles, around 650 of them [1], that allow us not only to move, speak, eat or interact with the environment but also to maintain our posture and circulate blood throughout the body as well as many other functions. Despite their great number, they can be classified into three types: skeletal, cardiac and smooth muscles [2]. The skeletal muscles are the ones we think of first when we hear the word "muscle". They are the muscles linked to our bones and allow us to run, maintain our posture or open a jar of jam for example. The second type contains the muscles of the heart and is for example responsible for the heartbeat and the blood circulation in our body. The last type can be found around hollow organs such as in lungs to regulate the airflow.

Scientists have tried to understand the functioning of muscles through experiments since early on, for instance Luigi Galvani who discovered in the mid-1780s that a dead frog legs twitched when stimulated with an electrical impulse [3]. Discoveries have been made and theories formulated over time. A possible way to better understand the muscle is by trying to model it. In order to build a muscle model, the important features responsible for muscle responses have to be discerned and the less important discarded. Several muscle models have been created the last decades. But is there a model better than the other ones? To what extent do they have a biophysical meaning? Is the phenomenological model, based on empirical research, to be discarded? Are the highlighted features of each model truly the most important ones?

The goal of this master thesis is to provide an answer to these questions. The focus will be on skeletal muscles as most muscle models found in the literature focus on them. They interest scientist most since these muscles allow us to move and interact with the environment. Modelling them is can thus be interesting to better understand how a muscle works, how pathologies can affect them or for humanoid robotics to name a few examples. Several different muscle models have been chosen and will be compared in order to provide an answer to these questions.

This master thesis has been divided into four parts. In the first part, the muscle physiology will be reviewed. It is the basis for the rest of the work since, before modelling a muscle, it is first needed to understand how it works.
The second part will introduce and detail different muscular models. Each model has its features and works differently to represent the muscle response to a stimulation. There are other muscle models present in the literature than these; however these were chosen because of their specific features and different approaches to model the muscle.
The third part will focus on the comparison between the models presented in the second part. In this part, the muscle to be modelled will be considered to be isolated. The computation time, the muscle features that are taken into account or left aside, what they have in common, their activation dynamics and the mechanical impedance will be discussed.
In the final part, a multi-muscle single-joint is implemented with the different muscular models. An ankle joint simulation has been chosen due to its abundance in the literature making it easier to compare the obtained results with the models to the literature.

Part I

Muscle physiology

Chapter 1

Review of the muscle physiology

This chapter about muscles physiology is mainly based on "Vander's Human Physiology: The Mechanisms of Body Function" by E. P. Widmaier, H. Raff, and K. T. Strang [2]. The elements of the muscle physiology explained in this chapter coming from a different source will be explicitly specified. The purpose of this part is to review the muscle physiology on which the models discussed in this master thesis are based upon.
First, the muscle and the motor unit will be defined. Secondly, the muscular fiber organisation in skeletal muscles will be discussed. Thirdly, the sliding-filament mechanism responsible for muscle contraction will be explained. Then, the mechanics of single-fiber as well as the whole muscle contraction will be discussed. The different types of muscle contraction will then be explained. A few words will be given about the muscle pennation and contraction. Finally, the specific features of smooth and cardiac muscles - which are not central to the present thesis - will be briefly described.

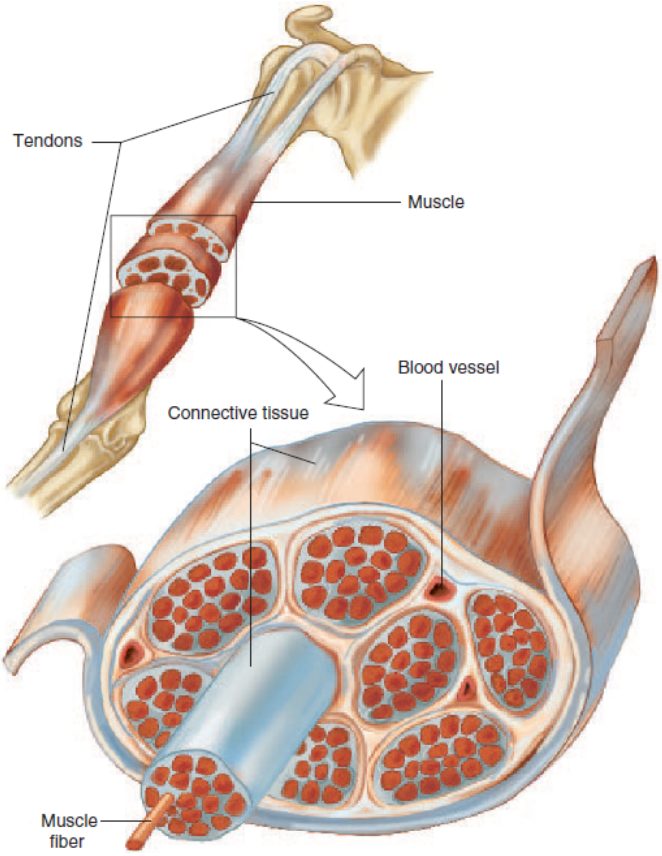

Figure 1.1: Skeletal muscle, and its organisation, attached to the bones by the tendons

1.1 Muscle and motor unit

Muscles are organs transforming a chemical energy into a mechanical movement by producing a force. It allows to bring bone segments closer to each other, about a joint. Since a muscle cannot elongate on its own, antagonist muscles are needed to achieve bidirectional movements.
There are three types of muscles: skeletal, cardiac, which are both striated muscles, and smooth muscles. The skeletal muscle is the one that allows the human body to move freely and can contract voluntarily. It is schematically represented in Figure 1.1. The cardiac muscle propels, by contraction, the blood through the circulatory system. Unlike skeletal muscles, it is regulated by the autonomic nervous system and cannot contract voluntarily. Smooth muscles can mostly be found around hollow organs. They are also controlled by the autonomic nervous system.
Since most muscle models focus on the skeletal muscle, this type of muscle will mostly be reviewed in this chapter. Another reason for focusing on skeletal muscles is that these are interesting to be emulated for bio-inspired robotics.

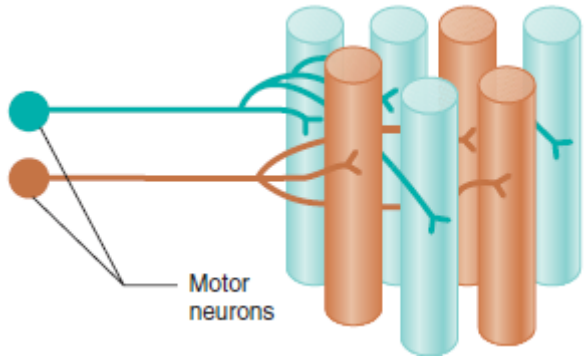

Figure 1.2: Two motor units innervating muscle fibers [2]

A motor unit is the smallest contractile element that the nervous system can modulate. A single motor neuron innervates several muscle fibers whereas a single muscle fiber is innervated by only one motor neuron. A motor unit therefore consists in a motor neuron and the muscle fibers that it innervates. This is schematically represented in Figure 1.2. An action potential in a motor neuron will only stimulate innervated muscle fibers.

1.2 Muscular fiber organization of the skeletal muscle

Muscles are linked to the bone by the tendons which consist of bundles of collagen fibers. A muscle is composed of many subentities such as muscles fibers that are bound together by connective tissue. These muscle fibers, for adults, can have diameters varying from 10 to 100 μm and a length up to 20 cm.

Each muscle fiber is a bundle of myofibrils and each myofibril is made of even smaller, repeating entities: sarcomeres. The configuration of the sarcomeres is so that each thick filament is surrounded by six thin filaments, and each thin filament is surrounded by three thick filaments.

Each sarcomere consists of two contractile proteins: actin for thin filaments and myosin for thick filaments. Thin filament also comprises troponin and tropomyosin whereas thick filament consists almost only of myosin. These two filaments are positioned so that they overlap. This organization can be visualized in Figure 1.3.

Those thick and thin filaments are the contractile elements of the muscle. The thick filament can, through myosin heads, create bridges, called "cross-bridges", between them and the thin filaments. During the contraction, those bridges connect to thin filament and push it toward the center of the sarcomere by exerting a force. This can reduces the length of the sarcomeres and thus of the whole muscle during contraction.

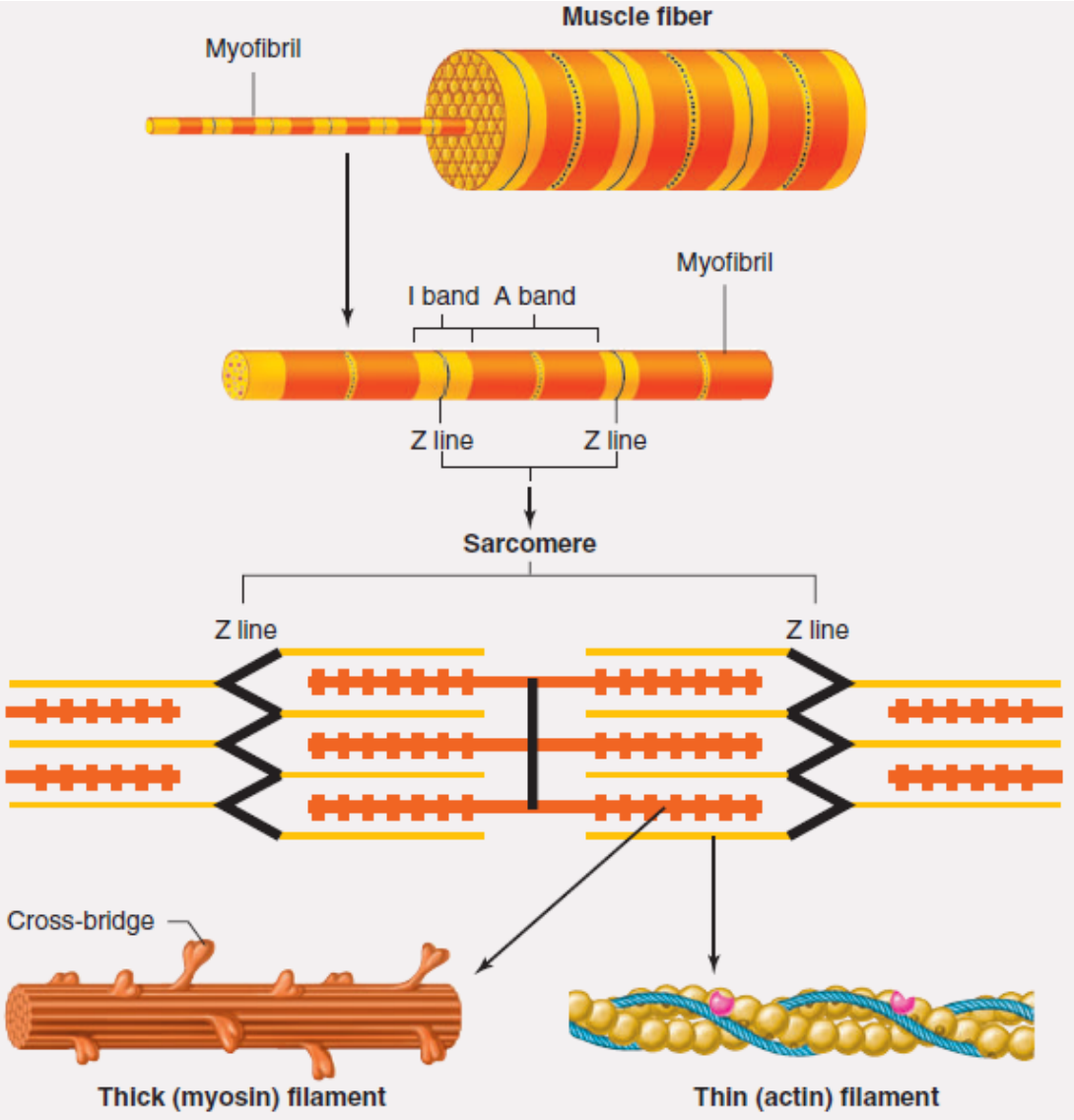

Figure 1.3: Organization of a muscle fiber[2]

1.3 Sliding-Filament mechanism

The thick and thin filaments never change in length, it is the movement of the thin filament with respect to the thick filament that contracts the muscle. The myosin cross-bridges attach to the actin filament and produce strokes that move it toward the center of the sarcomere. This induces the shortening of the sarcomeres and therefore of the muscle.
Each actin molecule contains a binding site for myosin heads. The myosin molecule has a more complicated configuration. It is constituted of two heavy chains and four light chains. This configuration gives to the myosin molecule two globular heads and a long tail. These myosin tails are directed toward the center of the sarcomere to form the myosin filament while the myosin heads stick out of this filament to form the cross-bridges. Each myosin head has a binding site for the actin molecules and one for adenosine triphosphate (ATP). ATP is a small molecule that transports chemical energy to the place where energy is needed. Once it is there, it breaks into adenosine diphosphate (ADP) and phosphate (P_i) by a breakdown of the last covalent link of the phosphate which liberates energy.

At rest, there is ADP on the myosin head and the actin filament is in a configuration such that

the myosin heads cannot attach to the actin molecules. An increase in cytoplasmic calcium concentration induces the change of the actin filament configuration so that the myosin head can interact with it. There are altogether four steps to move the actin filament toward the center of the sarcomere. These four steps form a cycle that is called the "cross-bridge" cycle and are:

1. The cross-bridge attaches to the thin filament.
2. The ADP on the myosin head is released which induces the movement of the cross-bridge and thus the muscle contraction.
3. ATP links with the myosin head which causes the detachment of the cross-bridge from the actin molecule.
4. The myosin head hydrolyzes the ATP into ADP and phosphate so that it can restart the cycle.

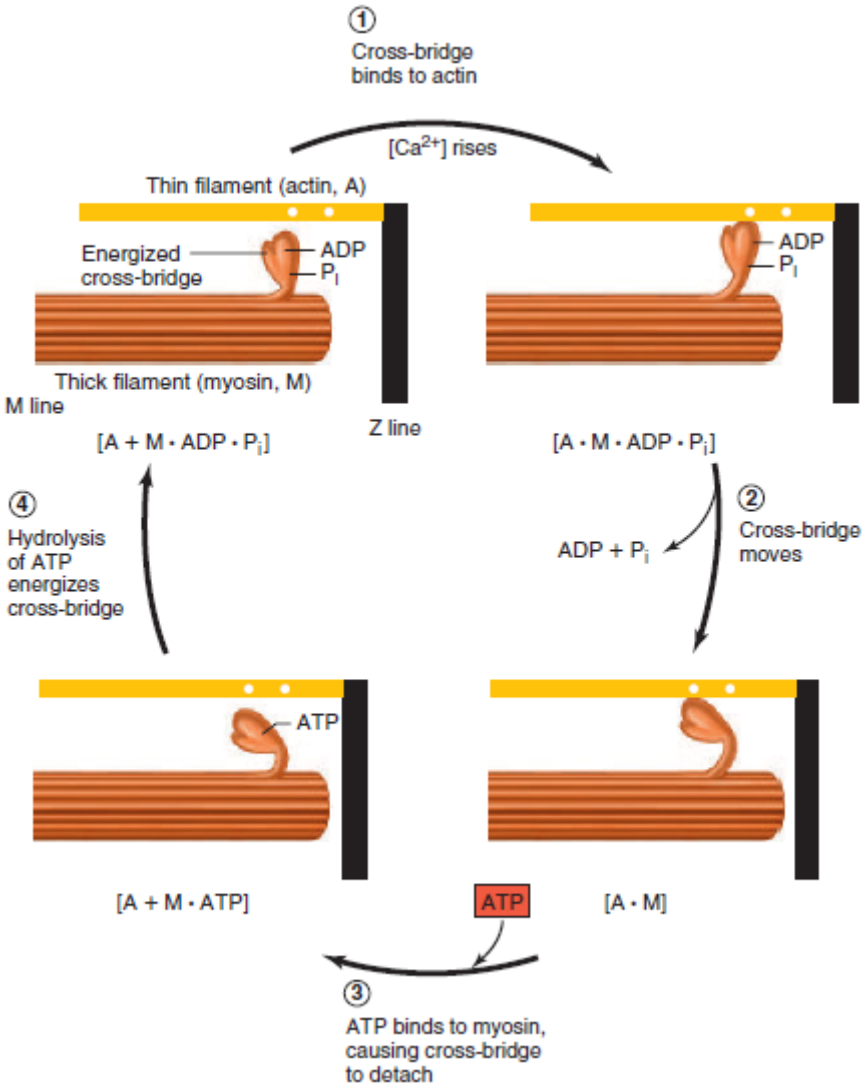

Figure 1.4: The four steps of the cross-bridge cycle [2]

These four steps can be visualized in Figure 1.4. The thin filament movement does not mean that all the myosin heads are attached simultaneously to the thin filament. Each myosin head follows the cross-bridge cycle independently from the other heads which means that only a portion of the heads are attached simultaneously while the other heads are detached. As long as

there is enough calcium being delivered, this cycle will continue.

Calcium is therefore the contraction regulatory element. At low calcium concentration, the tropomyosin molecule, shaped as a rod, covers the myosin-binding sites preventing any binding between the actin and the myosin cross-bridges. It is the troponin molecule, bound to the actin and tropomyosin, that maintain the tropomyosin rod into this position. When calcium binds to the troponin molecules, they change their shape so that the tropomyosin rod is moved away from the binding sites. A decrease in calcium will result in the opposite effect, making the cross-bridge attachment again impossible. Thus, it is the calcium concentration, itself modulated by electric signals from the nervous system, that modulates the muscle contraction.

The electric activation signal is called an "action potential". It propagates through the excitable muscle plasma membrane. It lasts only one or two milliseconds to increase the cytosolic calcium concentration in the sarcoplasmic reticulum and stops before the muscle contraction starts. The change of calcium concentration last longer than the action potential and causes the muscle to contract by the mechanism seen above. The muscle contraction can last more than hundred milliseconds. After the action potential, the calcium release is quick but pumping it back, which also requires ATP, into the sarcoplasmic reticulum takes much longer. This explains the shape of the muscle fiber tension with respect to time depicted in Figure 1.5. Thus, the force generated by the muscle is directly proportional to the calcium concentration and therefore to the firing frequency of the motor neurons, i.e. the muscle nerve cells.

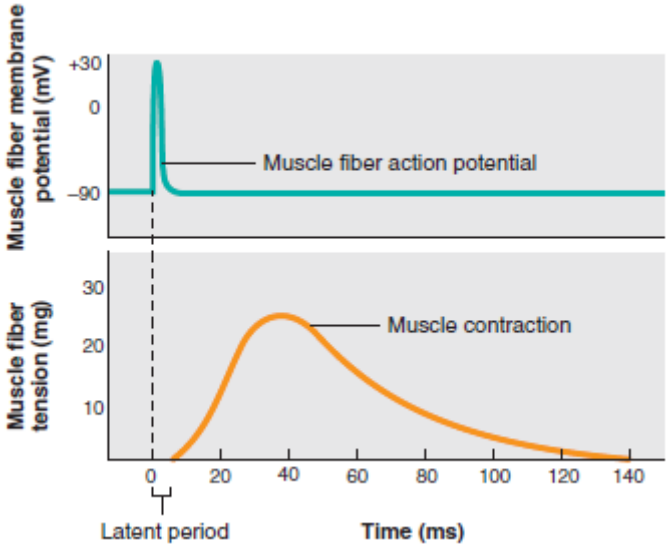

Figure 1.5: Muscle fiber tension induced by an action potential with respect to time [2]

1.4 Mechanics of single-fiber contraction

When a single muscle fiber is excited by a single action potential, the resulting mechanical response is called a "twitch". The contraction time of a muscle fiber depends on its type, whether is is a fast or a slow fiber.

Isometric and isotonic twitch

In an isometric contraction, the muscle does not change its length but the generated force in the muscle does. This force generation is progressive and takes some time before reaching the maximal force. The relaxation is not immediate either.

In an isotonic contraction, the muscle length can change while the contraction force stays the same. The change in length changes with the applied load and this can be used to measure the muscle velocity with respect to the load.

Length-tension relationship

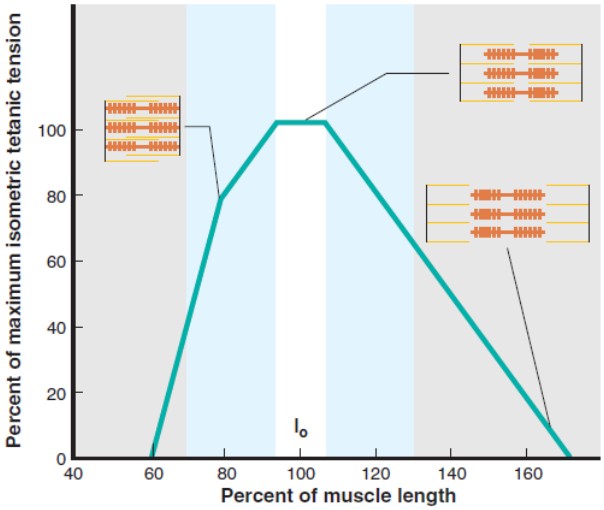

Figure 1.6: Muscle active tension with respect to fiber length [2]

The sarcomeres are capable of producing not only an active tension, with the cross-bridges, but also a passive stiffness due to the titin protein present in the sarcomeres that has a spring-like behavior.
The amplitude of the active tension developed by a muscle fiber also depends on the length of the muscle fiber.
To produce the force-length diagram in Figure 1.6, the muscles fibers were tetanically stimulated at various lengths. The maximal isometric force is attained when the muscle fiber is at its optimal length. The length at which the active maximal isometric force is reached is called the "optimal muscle length". At this optimal length, the actin and myosin filaments perfectly overlap so that all cross-bridges could potentially be used. Below this optimal length, the filaments overlap too much and above this length they do not overlap enough so that the cross-bridges do not work optimally.

Force-velocity relation

The shortening velocity of a muscle decreases as the load increases. It is indeed slower to move a heavy object than a lighter one. The shortening velocity is greatest when there is no load applied to the muscle and it is null when the loads becomes equal to the maximal isometric tension. Once the load is even greater, the muscle is not capable of contracting anymore. The cross-bridges are activated but cannot move the actin filament toward the center of the sarcomere anymore and the muscle lengthens. This lengthening velocity (i.e. negative shortening velocity) increases with an increasing load.
This relationship can be visualized in Figure 1.7.

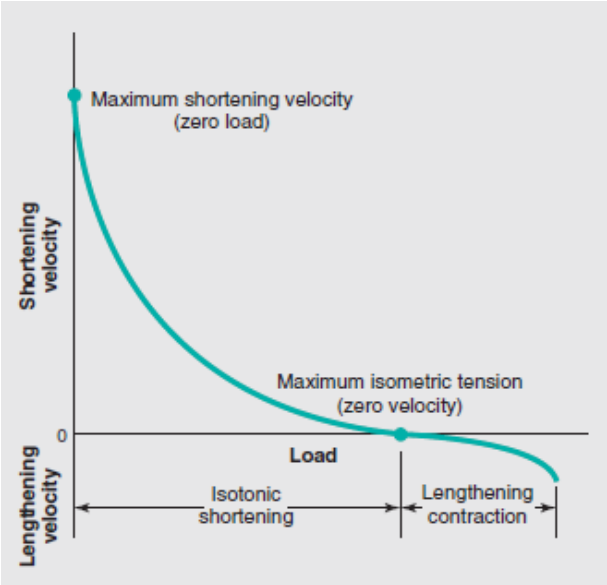

Figure 1.7: Muscle fiber velocity with respect to load [2]

Frequency-tension relationship

If the interval between successive stimuli is large enough, which means longer than the time needed by the muscle to twitch, the twitches will have the same amplitude and contraction time. If the time interval is smaller so that another stimulus is applied when the previously induced muscle contraction is not completely over, the twitches will overlap and sum up. This results in a higher twitch amplitude and an oscillating tension. This phenomena is called "unfused tetanus". If this time interval is even smaller, around 10 milliseconds, the mechanical response is the smooth summation of the twitches induced by those almost simultaneous stimuli.
However, this cannot go indefinitely because the produced tension will eventually saturate when the firing frequency becomes too high. This will induce a contraction that is maintained by the repetitive stimuli and is called a "fused tetanus". This tetanic tension is about three to five times bigger than for a simple isometric twitch. This is due to the fact that the actions potentials are so close to each other in time that the released calcium does not have time to be pumped back into the reticulum. This maintains all the available actin binding site unblocked.
These types of twitch, unfused and fused tetanus are depicted in Figure 1.8.

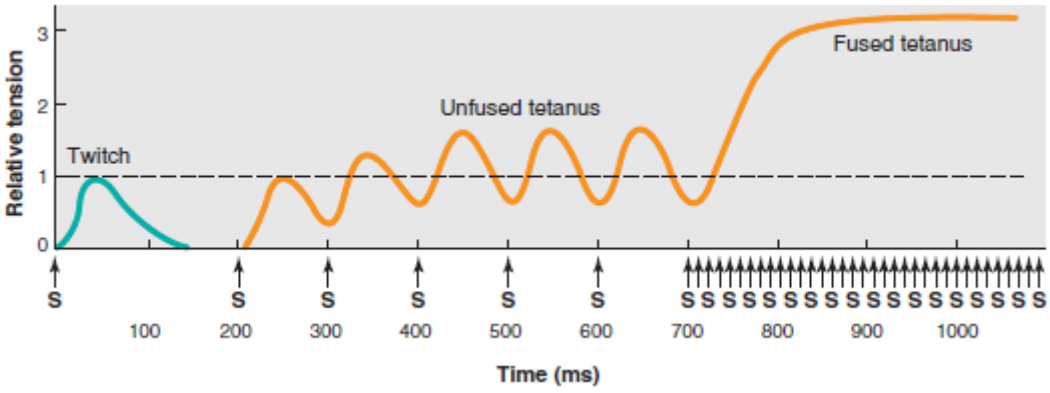

Figure 1.8: Twitch, unfused and fused tetanus. S represents a single stimulation of the muscle; the closer in time these stimulation are, the more the relative tensions will sum up. From [2]

1.5 Whole muscle contraction

The total muscle tension depends on the amount of tension that is developed by each single muscle fiber and by the number of contracting muscle fibers. If the exerted force is large enough, the bones are moved by the shortening muscle. Since a muscle can only shorten, there is a need for antagonist muscles that will pull it in opposite directions with respect to each other.

1.6 Contraction types

Unlike one may think, the word "contraction" does not necessarily imply a shortening of the muscle. It rather refers to the activation of the muscle. An activated muscle without change of length is called an "isometric contraction".

Altogether, there are three different muscle contractions: the isometric contraction, the concentric contraction and the eccentric contraction. An isometric contractions means that the muscle is activated but the muscle lengths does not change. An example for this type of contraction could be to carry an object without moving it; the muscle does not change its length but there is force needed to maintain the object at its position. A concentric contraction is a contraction where the muscle shortens in order to bring the connected bone segments together. The eccentric contraction of a muscle can only happen by an external force since a muscle has only the capacity to contract. This external force can be exerted by an antagonist muscle as well as a force external to the body. Those three types of contractions can be visualized in Figure 1.9.

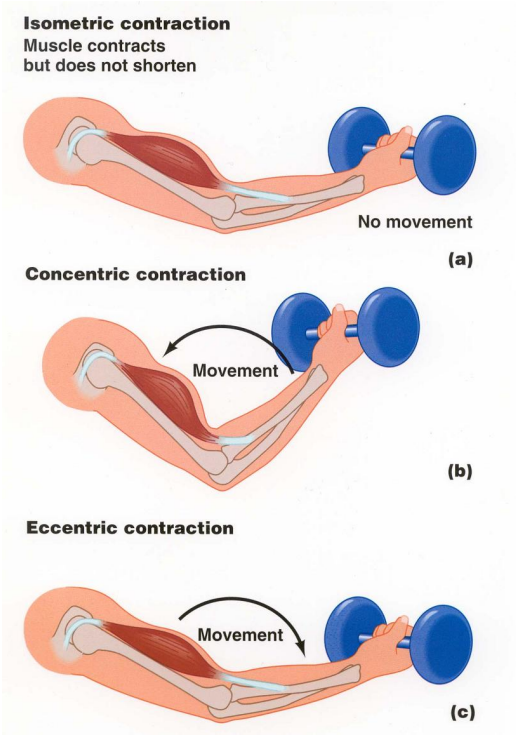

Figure 1.9: Types of muscular contraction [4]

1.7 Muscle fiber pennation

This section is mostly based on [5].
Muscles can have different architectural arrangements where the fibers have a specific orientation with respect to the tendon they are attached to. They can either be parallel or pinnated. This arrangement is called the muscle pennation and is depicted in Figure 1.10.

In parallel-fibered muscles, the fibers go from one tendon to another and their length corresponds to the length of the muscle. In this arrangement, the power loss is minimum during contraction and these fibers will remain more in the isometric condition because the deformation is only a small fraction of the total fiber length. Due to this, the force per fiber will be maximum.

In pinnate-fibered muscles, the fibers are oriented at a certain angle with the direction of the tendon motion and therefore the direction of the induced force. Since these fibers are not parallel to the force direction, only the contractile fiber component parallel to the tendon axis will contribute to the total force. The perpendicular force component is hence lost. The produced force will therefore be lower than for a parallel-fibered muscle where the fiber contributes

maximally. However, they have an advantage compared to the parallel-fibered muscles: since a single pinnate muscle fiber does not go completely from one tendon to the other, much more fibers can be placed in the same volume, thus producing more power.

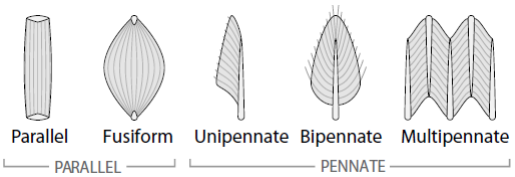

Figure 1.10: Types of muscle pennation[6]

1.8 Smooth muscle

This section on smooth muscles and the next section on cardiac muscles are given as additional information but do not present any interest for the rest of this master thesis as the muscular models focus on skeletal muscles. Even if they are not used by the muscular models presented in this work, a few words about them are given here as it is interesting to understand what differentiates them from skeletal muscles and why they are as important for the living body.

Smooth muscle are different from the skeletal muscle due to their lack of cross-striated banding pattern; they have neither troponin nor T tubules. A second difference is that smooth muscles are innervated by nerves derived from the autonomic nervous system. Smooth muscle therefore contract involuntarily, as opposited to skeletal muscles.

However skeletal and smooth muscle both use cross-bridge movements between the actin and the myosin filaments to produce a force. Calcium controls the contraction activity for both muscle types. However, the calcium activation works differently for the smooth muscle. Since there are no calcium-binding troponin proteins in smooth muscles, the calcium binds to another protein called calmodulin. Then, this complexes binds to a myosin light-chain kinase which uses ATP to phosphorylate the myosin cross-bridges. The phosphorylated cross-bridges can then bind to the actin filaments and induce the cross-bridge cycle. So, in skeletal muscle, calcium changes the configuration of the thin filament whereas in smooth muscle, calcium changes the thick filament configuration. This has a considerable effect on the contraction speed making the smooth muscle much slower than skeletal muscles.

There are neither myofibrils nor sarcomeres in the smooth muscle; therefore the organization of the thin an thick filaments are not aligned as regularly as in the skeletal muscle. The thin filaments are oriented diagonally to the longer axis of the cell and directly attached to the plasma membrane or to cytoplasmic structures. Even though there are actin and myosin filaments as in the skeletal muscle, their proportions are not the same: there is much more actin and less myosin.

The force produced by smooth muscles is similar to skeletal muscles and also varies with the fiber length. Smooth muscles, however, can stretch more than skeletal muscles and still produce a certain force.

1.9 Cardiac muscle

Cardiac muscles have properties from both skeletal and smooth muscles. They have, like skeletal muscles, troponin and T tubules. They also have myosin and actin filaments arranged similarly

to skeletal muscles. However, they have much shorter fibers than skeletal muscle fibers.

In skeletal muscles, the action potential is very short and stops before the muscle contraction even began. It is different for cardiac muscle; an action potential from a cardiac muscle cell has a long refractory period lasting almost as long as the cardiac muscle contraction. This is to avoid tetanus which would interrupt the cardiac cycle. A cardiac muscle cell contracts and relaxes periodically to create the heartbeat.

1.10 Tendons

This section is based upon [8].
Tendons bind the muscles to the bones, and are therefore passive elements. They are made of soft connective tissue that is composed of collagen fibers. Due to this, they are white and undergo small deformations. They are oriented in the same direction as the tensile force.
They have several functions: firstly, since they transmit the force from the muscle to the bone, they need to be able to sustain high stresses. However, tendons have low shear resistance. Secondly, they need to remain flexible enough to bind at joints. Thirdly, they also have a damping function to absorb shocks and limit potential damage to the muscle. Fourthly, they can store energy when the muscle is lengthened and release it later as an elastic recoil to reduce the muscles work.

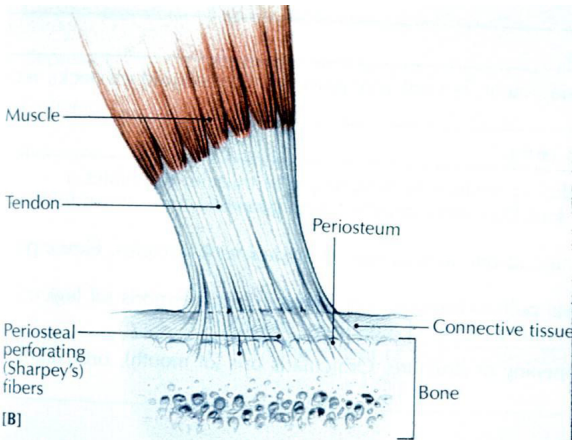

Figure 1.11: Tendon linked to a muscle on one side and to the bone through the Sharpey's fibers on the other side. From [7]

The part where the tendon joins the bone is called the "osteotendinous junction". The collagen fibers from the tendon enter the bone as so called Sharpey's fibers [8]. A tendon linked to a muscle and a bone, through the Sharpey's fibers, is represented in Figure 1.11.

1.11 Summary

This chapter mainly reviewed the mechanisms responsible for the contraction in skeletal muscles. Most of the concepts and mechanisms presented in this chapter are based on "Vander's Human Physiology: The Mechanisms of Body Function" by E. P. Widmaier, H. Raff, and K. T. Strang [2]. The concepts from other sources were specifically mentioned.
A motorneuron is connected to muscle fibers and a nervous signal propagates through it until it reaches the muscle fibers. This causes an increase in calcium concentration in the muscle which in turn causes a change of configuration of the actin filaments. This change of configuration makes the binding site accessible for the cross-bridges. The cross-bridges from the myosin filaments can bind to the actin filaments and move them which induces the shortening of the sarcomeres and eventually the whole muscle contraction. Without another electrical stimulation, the calcium is pumped back resulting in a decrease in calcium concentration inside the muscle and the actin filaments go back to their resting configuration which does not allow any interaction between thin an thick filaments.
A few words about smooth and cardiac muscles and on how they differ from skeletal muscles were given. Their most important dissimilarity with skeletal muscles is that they cannot contract voluntarily because they are regulated by the autonomic nervous system.

Part II

Muscular models

Introduction of Part II

In this part, different muscular models will be introduced. The comparison of the models in the last two parts will be based upon this part.

The first chapter will describe and discuss the first type of skeletal muscle model. This model is so-called Hill model [9]. It is the most famous and used model for understanding how a muscle works or for i.e. bio-inspired robots. First, the original model, published in 1938 by A.V. Hill, will be described. Then a Hill-type model, a muscular model based on the model developed by A.V. Hill, will be described and explained. There are many Hill-type models, each having its own particularities, but only one will be developed in this work for illustration. The introduced Hill-type model was developed by D.F.B. Haeufle et al. in 2014 [10] and has the particularity that it focuses not only on the concentric contractions but also on the eccentric contractions. At the end of this chapter, a comparison of different Hill-type models, including the one developed by D.F.B. Haeufle, will be given. The comparison will focus on the force-length and force-velocity relationships that are defined differently in each model.

The second type of introduced models will be discussed in the second chapter. It was developed by A.F. Huxley in 1957 [11]. Unlike the Hill model which is phenomenological, based on empirical observations, the Huxley model is based on the cross-bridge dynamics introduced in the first part. This model, due to its biological precision, is complex and computational greedy. G.I Zahalak published a model in 1981 [12], the distribution-moment model, that approximates the Huxley model. This was done in order to simplify the model while keeping it as biologically correct as possible.

The third chapter will focus on a third type of model which is a model developed by T.L. Williams [13]. One particularity about this model is the activation which is different from the Hill model. The activation is governed by the concentration of calcium inside the muscle and follows a differential equation. Another particularity of this model is the so-called "work-dependent deactivation" which takes into account that a muscle that has been shortening under a load generates less force after the shortening stops. One last particularity is that the stiffness of the muscle depends on the activation and is thus not constant.

The last chapter and type of model introduced in this part is the so-called multiscale model by H.E. Makssoud et al. which was developed in 2011 [14]. It is based on the distribution-moment model for the microscopic elements and on the Hill model for the macroscopic elements. This model has the particularity that is covers different scales: the sarcomere scale, the muscle fiber scale and the whole muscle scale.

Each of these models have their pros and cons which will be surveyed at the end of each model description. Despite the variety between the models, their inputs and outputs are similar. The input for each model is the muscle activation. However, each model treats the activation dynamics differently. The muscle length and velocity are also inputs for all the models. Each model can be separated into two parts: the activation dynamics and the mechanical model.

The output of the different models is the force resulting from their corresponding activation mechanism. Two models give additional outputs such as the stiffness and one even gives the elastic energy stored inside the muscle.

Chapter 2

Hill and Hill-type models

2.1 Hill model

This model has been developed by A.V. Hill [9] and this chapter is also based on the article [16]. This model is a phenomenological model, build from empirical relationships, that were developed by A.V. Hill with his associates and published in 1938. This chapter will first describe the original model that was published in 1938 [9]. Then the activation dynamics as well as the mechanical model will be described.
Then, a Hill-type model, developed by Daniel Haeufle in 2014 [10], will be introduced. The equations needed to compute a force response from inputs such as activation and muscle velocity will be given and discussed.
Finally, a comparison between several Hill-type models will be provided.

2.1.1 Description

In order to build this phenomenological model, A.V. Hill and his associates experimentally measured the behavior of an isolated animal muscle which was maximally stimulated [17] [18]. From the observed mechanical behavior, they concluded that it resembled the behavior of a viscoelastic system.
However, after a few years, other experiments led by A.V. Hill showed that the shortening of the muscles and their work production were not governed by the release of elastic energy but by chemical reactions. This observation led to the rejection of the viscoelastic theory. These experiments measured the heat production of the muscle during contraction and were later published by A.V. Hill [9].

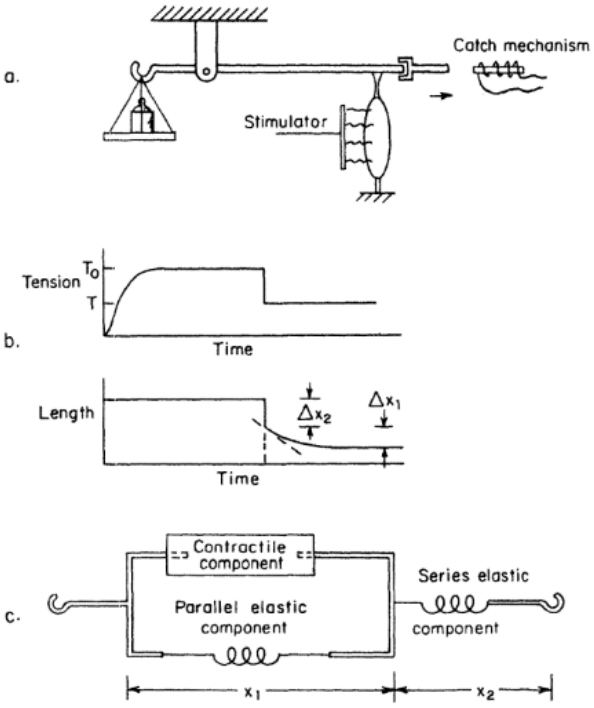

Figure 2.1: Quick-release experiment (a) and results (b). (a) shows the experimental setup for the quick release experiment: the muscle is fixed and cannot change its length. The muscle is stimulated until it reaches its maximal isometric force (T_0). The muscle is then quickly released and the muscle length can change. The change in muscle tension and length is represented in (b). (c) represents the components of the muscle: a contractile element, a series elastic element and a parallel elastic element. From [15]

The main experiment of this paper is the "isotonic quick-release" [9]. The set-up for this experiment can be visualized in Figure 2.1a. First, the muscle is fixed so that its lengths cannot change. Then it is stimulated to produce an isometric peak force (T_0) and one end of the muscle is quickly released so that the muscle can freely change its length but the tension is constant (T) when the muscle is released because the muscle is attached to a weight equal to T/g. This new constant value of tension is determined by the weight in the pan. After the release, the muscle shortens almost instantly by a distance Δx_2 as can be observed in Figure 2.1b. The value of this Δx_2 depends on the difference in force before and after the release ($T_0 - T$). It then shortens more slowly by an amount Δx_1 where it reaches a resting length.

A.V. Hill measured the muscle heat production during the second phase of shortening (Δx_1). From this he made two important observations [16]:

1. The additional heat that is released during the shortening is proportional to the shortening distance: $\Delta E_1 = -a\Delta x_1$ (with ΔE_1 the increment of extra energy released). The released energy also depends on the tension so that $\Delta E = -(a + T)\Delta x_1$

2. The rate of extra energy release during the shortening phase is proportional, even linear, to the force applied to the muscle: $\Delta \dot{E} = b(T_0 - T)$.

a and b are both constants that are characteristic of the muscle. a is a heat shortening constant and depends on the cross-section of the muscle. b is a constant for the absolute rate of energy liberation. From these two observations, Equation 2.1 can be obtained, with V the shortening velocity of the muscle ($V = -\Delta \dot{x}$).

$$(a + T)V = b(T_0 - T) \tag{2.1}$$

From Equation 2.1, Equation 2.2 can be found by adding ab on every side of the equation and by rearranging the terms. This equation relates the speed and the tensile force of the muscle in an isotonic shortening. It represents the force-velocity relationship described by a hyperbola with two asymptotes.

$$(T + a).(V + b) = (T_0 + a).b = \text{const.} \tag{2.2}$$

Years later however, A.V. Hill found through more refined experiments [19], that the heat shortening a is not constant as was first assumed. Nevertheless, Equation 2.1 is still considered to be a good empirical fit to the force-velocity data.

The force-velocity relationship firstly defined by Hill took only the shortening of the muscle into account. This relation had thus to be generalized to the lengthening case too. It is one of the aspects on which the Hill-type model presented later on in this chapter will focus on.

From this, A.V. Hill developed a simple model for the muscle in an isotonic quick-release test [16]. This model separates the elasticity and the contractility of the muscle into two component connected in series. These elements have been represented schematically in Figure 2.1c.
Firstly, a "series elastic" element (SE) which is assumed to be a spring that has a characteristic length and stiffness. It represents the tendon of the muscle tendon unit and is function of the tendon length.

The second element is the "contractile" element (CE) that is characterized by a force-velocity relationship. Since the muscle force is held constant in the isotonic quick-release, this model implies that the muscle velocity V is equal to the CE velocity. Equation 2.2 is thus the force-velocity relationship of the CE element. The capacity of the muscle to contract voluntarily

is modelled trough that element. The force generated by the contractile element is usually represented by Equation 2.3 [20].

$$F_{CE}(A, l_{CE}, v_{CE}) = AF_{max} f_l(l_{CE}) f_v(v_{CE}) \tag{2.3}$$

The term A represents an activation state and is a function in time that varies between 0 (relaxed muscle) to 1 (fully activated muscle). F_{max} corresponds to the maximal force that the muscle can generate in isometric condition. The force-length relationship is modelled by a function $f_l(l_{CE})$ which is depends on the contractile elements length. It is a function that has a similar form as Figure 1.6 in Chapter 1 where the physiological force-length relationship is presented. Finally, the force-velocity relationship is modelled by the function $f_v(v_{CE})$ which depends on the contraction velocity of the contractile element. It is a function that has a similar form as the physiological force-velocity relationship presented in Figure 1.7 in Chapter 1. Several mathematical representations of these two relationships will be computed and compared in Section 2.3.

And finally, there is an elastic element in parallel to the contractile element that represents the passive characteristics of the muscle when it is for example stretched. It is usually represented by a spring with a characteristic stiffness and is function of the contractile element length l_{CE}.

Other investigators tried to generalize this model to be more representative of *in-vivo* muscles. Some examples are represented in Figure 2.2 where different configurations were introduced. This led to Hill-type muscle models [16]. An enhancement has been to add another elastic element but in parallel and not in series this time. This has been named the "parallel elastic" element (PE) and is shown in 2.2(b). This element has been added to model that the muscle can passively resist to a stretch.

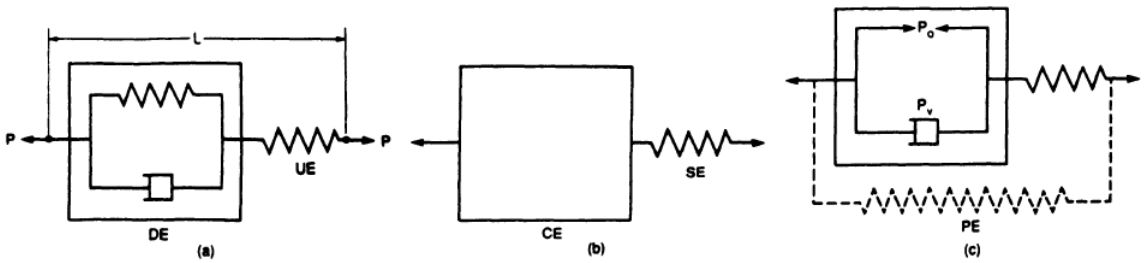

Figure 2.2: Three different Hill-type muscle models from [16]. (a) undamped elastic element (UE) in series with a damped elastic element (DE) from Levin-Wyman. (b) a series elastic element (SEE) with a contractile element (CE). (c) same model as (b) where the inside of the contractile element is shown in parallel with a passive elastic element

The Hill model considers that the muscles activation, the force-length, and force-velocity relationships are independent of each other.

2.1.2 Pros of Hill-type models

The main advantages of this model are its simplicity and its direct connection with the macroscopic muscle experiments. The force-length and force-velocity relationships presented in Chapter 1 are used to model the force generated by the contractile element.
It has been developed more than hundred years ago and is now widely used. This model is almost universally accepted as an appropriate phenomenological and mathematical representation of the muscle dynamics.

2.1.3 Cons of Hill-type models

The Hill model is based on viscoelastic analogies. However, the underlying physiological mechanism of the muscle has little connection with these analogies.
The phenomenological model has been build with different elements such as the contractile or elastic elements. These elements have little to no physical meaning and are purely conceptual constructs.
Another deficiency of this model is that it gives no information about the biochemical energetics responsible for the activation of the muscle.

2.2 Hill-type model with serial damping and eccentric force-velocity relation

This model was developed by D.F.B. Haeufle, M. Günther, A. Bayer and S. Schmitt [10]. Most of this section is based upon the article describing their model [10]. It focuses mainly on eccentric contractions unlike many Hill-type models which focus more on the concentric contractions. In order to do this, a damping element (SDE) was added in series to the contractile and parallel elastic elements (CE and PEE) and in parallel with the series elastic element (SEE). The structure of this model is schematically represented in Figure 2.3. This damper in the series elastic structure was added to predict muscle forces with more realism.

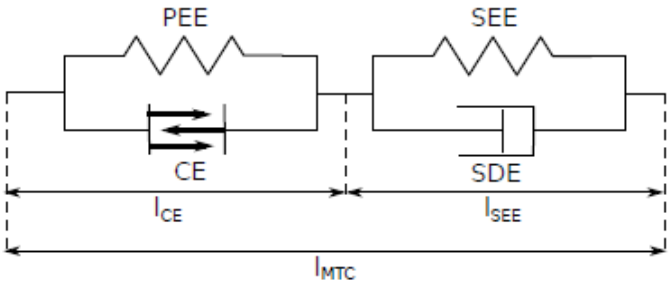

Figure 2.3: Structure of the proposed Hill-type model. From [10]

2.2.1 Simulation protocol

A Simulink® model created by the authors of this model is freely available[1].
The model was however reimplemented in MATLAB® since the other models were implemented in MATLAB® as well.
This model possesses a large number of open parameters. Added to this, the concentric and eccentric cases are considered separately, resulting in even more parameters. All the needed constants are given in the provided MATLAB® function `muscle_param_mus01.m` that stores all constants in a structure array. Only a few of them are muscle dependent such as the optimal muscle length which need to be changed for the particular muscle being modelled.

First, the initial conditions such as the muscle muscle-tendon and contractile element lengths as well as their respective velocities are set. An activation function also needs to be set. It is a function between 0 (no activation) and 1 (muscle fully activated).
Secondly, the force-length and force-velocity functions are computed with the contractile element length and velocity. These are then used to compute the force of the contractile element (F_{CE}) which is a function of the contractile element length, velocity and activation level.
The next force to be computed is the parallel elastic element F_{PEE} which is a function of the

[1] https://nl.mathworks.com/matlabcentral/fileexchange/56950-daniel-haeufle-macroscopic-muscle-model. Last accessed 17-05-2017

contractile element length since this element is in parallel with the contractile element and have thus the same length.
The following force to be computed is the serial damping element force F_{SDE}. This elements depends on the muscle-tendon and contractile element velocities, the contractile element and parallel elastic element forces.
The last element to be computed is the series elastic element F_{SEE} . It is a function of the series element length.
The whole muscle force is then computed by summing the force of the series elastic element and the serial damping element. This is the output of the muscle model.

New values of the lengths and velocities of the muscle tendon unit and contractile element need to be recomputed for the next time step. The velocity of the muscle tendon unit is an input of the model and depends on the load impedance, i.e null for the isometric case. The muscle tendon length is its integrated value and stays constant in the isometric case. The velocity of the contractile element can be found by solving the equation $F_{SEE}(l_{CE}, l_{MTC}) + F_{SDE}(l_{CE}, \dot{l}_{CE}, \dot{l}_{MTC}, A) = F_{CE}(l_{CE}, \dot{l}_{CE}, A) + F_{PEE}(l_{CE})$ which gives a quadratic equation of the form $C_2\dot{l}_{CE}^2 + C_1\dot{l}_{CE} + C_0$. It is then integrated to obtain the contractile element length.

2.2.2 Mechanical model

The equations presented in this section were defined in the article presenting this model [10].
The total force of the muscle-tendon complex (MTC) is given by Equation 2.4. Since the CE-PEE and SDE-SEE elements are in series, the forces across both units should be the same.

$$\begin{aligned} F_{MTC} &= F_{SEE}(l_{CE}, l_{MTC}) + F_{SDE}(l_{CE}, \dot{l}_{CE}, \dot{l}_{MTC}, A) \\ &= F_{CE}(l_{CE}, \dot{l}_{CE}, A) + F_{PEE}(l_{CE}) \end{aligned} \tag{2.4}$$

l_{CE} and l_{MTC} are the lengths of the contractile element CE and the muscle-tendon complex which vary with time. $\dot{l}_{CE}$ and $\dot{l}_{MTC}$ are their respective velocities. A is the activation factor and is between 0 (non activated muscle) and 1 (maximally activated muscle).

Contractile element CE: The contractile element is defined, as in other Hill-type models, by a force-length and a force velocity relationship. The force-length relationship is given by Equation 2.5.

$$F_{isom}(l_{CE}) = \exp\left(-\left|\frac{l_{CE}/l_{CE,opt} - 1}{\Delta W_{limb}}\right|^{\nu_{CE,limb}}\right) \tag{2.5}$$

$L_{CE,opt}$ is the optimum muscle length. $\nu_{CE,limb}$ and ΔW_{limb} are constants which are different for the concentric case ($l_{CE} < l_{CE,opt}$) or the eccentric case ($l_{CE} \geq l_{CE,opt}$). This is a specific feature of this model, in contrast to many other models that use the same parameters for both cases.

The force-velocity relation is given by Equation 2.6.

$$F_{CE}(\dot{l}_{CE}) = F_{max}\left(\frac{A.F_{isom} + A_{rel}}{1 - \frac{\dot{l}_{CE}}{B_{rel}.l_{CE,opt}}} - A_{rel}\right) \tag{2.6}$$

A_{rel} and B_{rel} are functions that depend on l_{CE} and A. These functions are given in [10]. As for the force-length relationship, they are different for the case of concentric shortening or eccentric lengthening. The force-length and force-velocity relationships can be visualized in Figure 2.4.

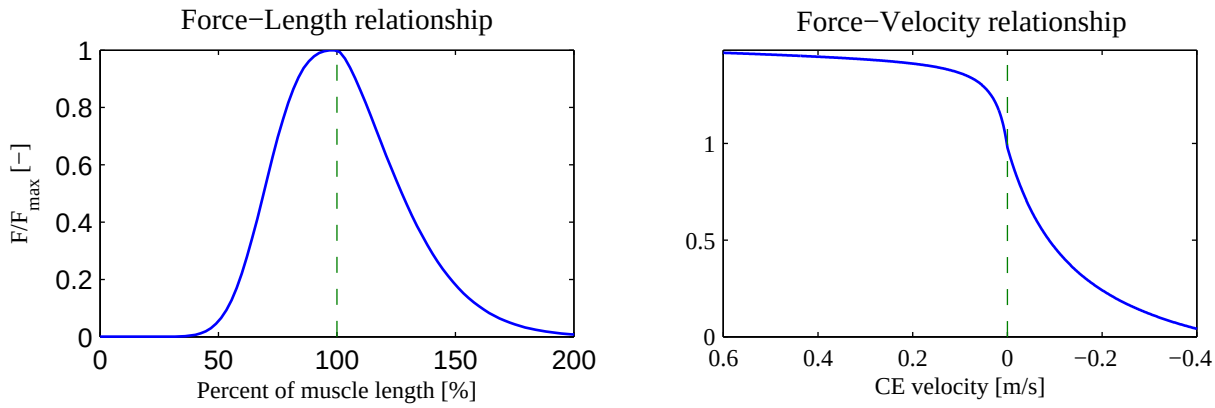

Figure 2.4: Force-length (left) and force-velocity (right) relationships of the Haeufle model

A comparison of force-length and force-velocity relationships from different Hill-type models, including those from the Haeufle model, can be found in Section 2.3.

Parallel elastic element PEE: The force generated by this element is given by Equation 2.7.

$$F_{PEE}(l_{CE}) = \begin{cases} 0 & \text{for} \quad l_{CE} < l_{PEE,0} \\ K_{PEE}(l_{CE} - l_{PEE,0})^{\nu_{PEE}} & \text{for} \quad l_{CE} \geq l_{PEE,0} \end{cases} \tag{2.7}$$

The constant $l_{PEE,0}$ is the rest length of the parallel elastic element. K_{PEE} is a defined constant and ν_{PEE} a factor of non-linearity that is given in [10].

Serial damping element SDE: The force generated by the serial damping element is given by Equation 2.8.

$$F_{SDE}(l_{CE}, \dot{l}_{CE}, \dot{l}_{MTC}, A) = D_{SDE,max}\left((1 - R_{SDE}).\frac{F_{CE} + F_{PEE}}{F_{max}} + R_{SDE}\right).\left(\dot{l}_{MTC} - \dot{l}_{CE}\right) \tag{2.8}$$

R_{SDE} is a constant that represents the damping at $F_{MTC} = 0$ whereas $D_{SDE,max}$ is a constant that represents the maximum damping coefficient at $F_{MTC} = F_{max}$. It is a damper-like force with a damping coefficient that is proportional to the muscle-tendon complex force $F_{MTC} = F_{CE} + F_{PEE}$.

Serial elastic element SEE: The force generated by the serial elastic element is given by Equation 2.9. It is modeled by a non-linear toe zone with a linear continuation.

$$F_{SEE}(l_{SE}) = \begin{cases} 0 & \text{for} \quad l_{SE} < l_{SEE,0} \\ K_{SEE,nl}(l_{SE} - l_{SEE,0})^{\nu_{SEE}} & \text{for} \quad l_{SE} < l_{SEE,nll} \\ \Delta F_{SEE,0} + K_{SEE,l}(l_{SE} - l_{SEE,nll}) & \text{for} \quad l_{SE} \geq l_{SEE,nll} \end{cases} \tag{2.9}$$

$l_{SEE,0}$ is the rest length of the SEE. $l_{SEE,nll}$ is the length of the SEE at the non-linear/linear transition. ν_{SEE} is a defined constant. $\Delta F_{SEE,0}$ is the force at the transition and the force increase in the linear part. $K_{SEE,nl}$ and $K_{SEE,l}$ are two constants given in [10] for the non-linear and linear parts.

Contractile element velocity $\dot{l}_{CE}$: The contractile element velocity depends on its length l_{CE}, the length of the muscle-tendon complex l_{MTC} and its velocity $\dot{l}_{MTC}$ as well as on the activation factor A. Calculating and then integrating $\dot{l}_{CE}$ allows to obtain le length of the contractile element l_{CE}.
It can be found by solving Equation 2.4 for $\dot{l}_{CE}$ which gives a relationship of the form $C_2\dot{l}_{CE}^2 + C_1\dot{l}_{CE} + C_0$. Since this is a quadratic equation it can easily be solved and is given by Equation 2.10.

$$\dot{l}_{CE} = \begin{cases} \dfrac{-C_1 - \sqrt{C_1^2 - 4C_2C_0}}{2C_2} & \text{for} \quad \dot{l}_{CE} \leq 0 \\ \dfrac{-C_{1,e} + \sqrt{C_{1,e}^2 - 4C_{2,e}C_{0,e}}}{2C_{2,e}} & \text{for} \quad \dot{l}_{CE} > 0 \end{cases} \tag{2.10}$$

The coefficients C_i (with $i = 0, 1, 2$) are given by Equation 2.11.

$$\begin{aligned} C_0 &= D_0\dot{l}_{MTC} + l_{CE,opt}B_{rel}(F_{SEE} - F_{PEE} - F_{max}AF_{isom}) \\ C_1 &= -\left(C_2\dot{l}_{MTC} + D_0 + F_{SEE} - F_{PEE} + F_{max}A_{rel}\right) \\ C_2 &= d_{SE,max}\left(R_{SE} - \left(A_{rel} - \frac{F_{PEE}}{F_{max}}\right)(1 - R_{SE})\right) \end{aligned} \tag{2.11}$$

Where

$$D_0 = l_{CE,opt}B_{rel}d_{SE,max}\left(R_{SE} + (1 - R_{SE})\left(AF_{isom} + \frac{F_{PEE}}{F_{max}}\right)\right) \tag{2.12}$$

$d_{SE,max}$ is the maximum damping coefficient at $F_{MTC} = F_{max}$. R_{SE} is a given constant. The coefficient $C_{i,e}$ are similar except for the fact that $A_{rel,e}$ and $B_{rel,e}$ are used instead of A_{rel} and B_{rel} respectively.

2.2.3 Numerical implementation

The force-response F_{MTC} for different activation factors A of different amplitudes (1, 0.4 and 1) and durations (0.05s, 0.05s and 0.3s) can be observed in Figure 2.5.

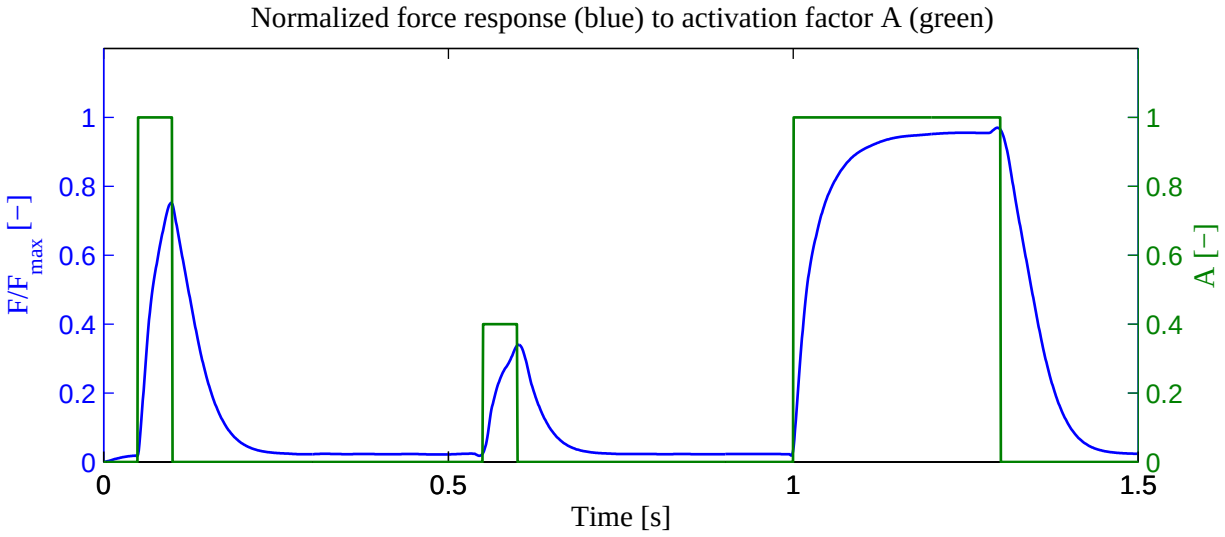

Figure 2.5: Normalized force-response F_{MTC} for different activation factors A of different amplitudes (1.0, 0.4 and 1) and durations (0.05s, 0.05s and 0.3s). This figure was obtained according to the simulation protocol presented in subsection 2.2.1

2.2.4 Pros of the Haeufle model

By adding the serial damping element and the eccentric force-velocity relationship, the model is more detailed and realistic also for eccentric movements. Even with the added complexity, the model is still suitable for multi-body simulations with many muscles [10].

2.2.5 Cons of the Haeufle model

It does not consider some known effects that are relevant for muscle force generation. It does not correctly represent the force-generation at submaximal contraction activation and will overestimate it. [10]
Also, the model does not reproduce contraction history effects as well as the recruitment of fast or slow muscle fibers.

2.3 Comparison of the force-length and force-velocity relationships of Hill-type models

The Hill-type models all use two relationships to define the produced force: the force-length relationship and the force-velocity relationship. In this section, these relationships were computed with MATLAB® and compared for different Hill-type models.

2.3.1 Force-length relationship

Three Hill-type models are compared here: the Geyer [21], Haeufle [10] and Yun [22] models. The force-length-relationships of these models are given in Table 2.1 and plotted in Figure 2.6. It can be observed that the force-length relationship was approximated by a Gaussian function for the Geyer and Yun models. The Haeufle model divided this relationship into an ascending branch, when the length of the contractile element is smaller than the optimal length of the muscle ($l_{CE} < l_{opt}$), and a descending branch, when $l_{CE} > l_{opt}$. The force-length relationship of Figure 1.6 in Chapter 1 was plotted additionally for a better comparison.

Model	**Force-length relationship**
Geyer [21]	$f_l(l_{CE}) = \exp\left[c\left\lvert\frac{l_{CE}-l_{opt}}{l_{opt}w}\right\rvert^3\right]$
Haeufle [10]	$f_l(l_{CE}) = \begin{cases} \exp\left(-\left\lvert\frac{l_{CE}/l_{opt}-1}{\Delta W_{limb,asc}}\right\rvert^{\nu_{CE,limb,asc}}\right) & \text{if} \quad l_{CE} < l_{opt} \\ \exp\left(-\left\lvert\frac{l_{CE}/l_{opt}-1}{\Delta W_{limb,des}}\right\rvert^{\nu_{CE,limb,des}}\right) & \text{if} \quad l_{CE} > l_{opt} \end{cases}$
Yun [22]	$f_l(l_{CE}) = \exp\left(-0.5\left(\frac{l_{CE}/l_{opt}-1.05}{0.19}\right)^2\right)$

Table 2.1: Force-length relationships equations for different Hill-type models

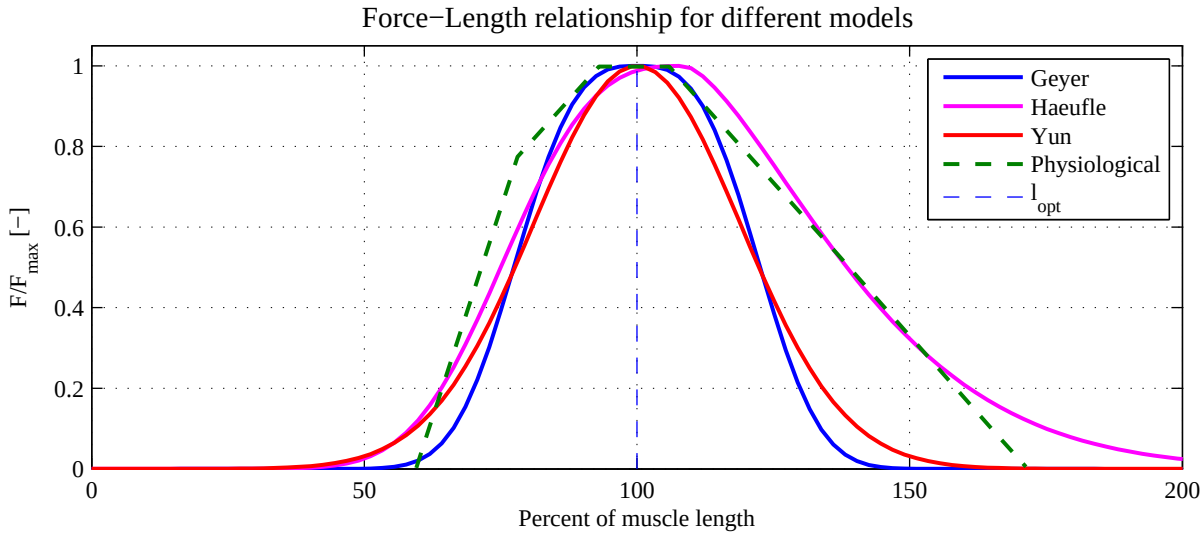

Figure 2.6: Force-length relationships for different Hill-type models. The physiological curve comes from Figure 1.6 in Chapter 1.

It can be observed that all three models fit the physiological around the optimal length rather good. In the more remote regions of the optimal length, the three relationships differ.
In the concentric contraction region ($l_{CE} < l_{opt}$), the relationships are quite similar. The force increase of the Geyer model and the physiological relationship start around the same length value. The two other models start at a smaller lengths.
In the eccentric case ($l_{CE} > l_{opt}$), the Haeufle model shows a significant difference to the other two models. The force at lengths bigger than the optimal length comes closer to the physiological relationship. The force of the Geyer and Yun models decrease faster with the length of the contractile element than the physiological case. The Haeufle model focuses on eccentric movement unlike the two other. It seems hence natural that the force-length relationships of the Haeufle model fits better the physiological relationship in the eccentric case.

2.3.2 Force-velocity relationship

The same references than for the force-length relationships have been used to compare different implementations of the force-velocity relationships. The equations for these relationships for this models are presented in Table 2.2 and depicted in Figure 2.7.
Two of the models, the Geyer and Haeufle model, divided the relationship into two subequations: one for a shortening velocity and one for a lengthening velocity. The Yun model tried to approximate it by a single sigmoid function.
All three models cross each other at the point where the muscle's velocity is null, thus the isometric condition, and where the force is equal to the maximal force in isometric condition.
As in the force-length case, the physiological case has been plotted too for comparison [23].

Model	**Force-length relationship**
Geyer [21]	$f_v(v_{CE}) = \begin{cases} \dfrac{v_{max} - v_{CE}}{v_{max} + K.v_{CE}} & \text{if} \quad v_{CE} < 0 \\ N + (N-1)\dfrac{v_{max} + v_{CE}}{7.56 K v_{CE} - v_{max}} & \text{if} \quad v_{CE} \geq 0 \end{cases}$
Haeufle [10]	$f_v(v_{CE}) = \begin{cases} F_{max}\left(\dfrac{a.f_l(l_{CE}) + A_{rel}}{1 - \frac{v_{CE}}{B_{rel} l_{opt}}} - A_{rel}\right) & \text{if} \quad v_{CE} < 0 \\ F_{max}\left(\dfrac{a.f_l(l_{CE}) + A_{rel,e}}{1 - \frac{v_{CE}}{B_{rel,e} l_{opt}}} - A_{rel,e}\right) & \text{if} \quad v_{CE} \geq 0 \end{cases}$
Yun [22]	$f_v(v_{CE}) = \dfrac{0.1433}{0.1074 + \exp\left(-1.409.\sinh(3.2 v_{CE}/v_{max} + 1.6)\right)}$

Table 2.2: Force-velocity relationships equations for different Hill-type models.

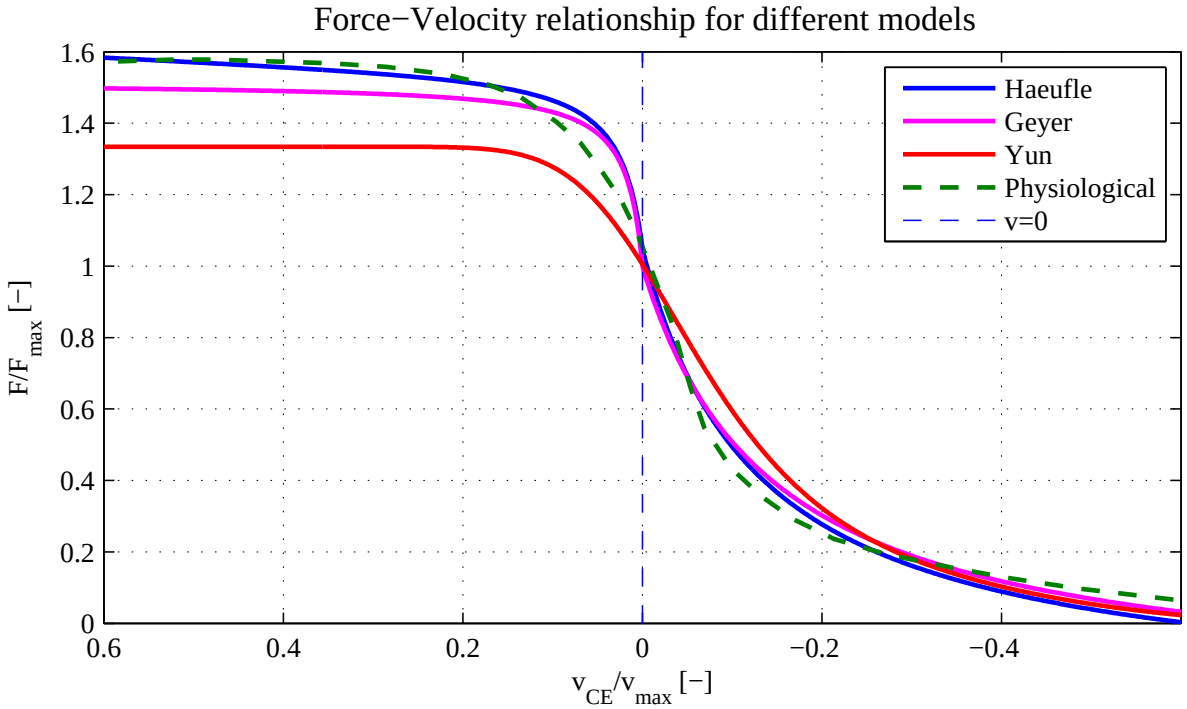

Figure 2.7: Force-velocity relationships for different Hill-type models. The physiological curve [23] has been plotted for comparison.

For contraction velocities ($v_{CE} < 0$) It can be observed that all curves are very similar, the Haeufle and Geyer model are almost identical. The dissimilarities between the models can be observed for lengthening velocities ($v_{CE} > 0$). The Yun model, due to the fact that the force-velocity relationship is approximated by a single sigmoid function, does not fit the physiological curve as well as the two other models. The two others come closer to the physiological curve due to the fact that they separated the contraction and lengthening cases. The Geyer model comes much closer to the physiological curve than the Yun model. The Haeufle model is the one that comes closest to the physiological curve. This can be explained by the fact that the Haeufle model focuses on eccentric movements.

Chapter 3

Huxley model and the distribution-moment approximation

3.1 Original Huxley model

This model was first developed by A.F. Huxley in 1957 [11] and is also partly described in [16]. It was the simplest model Huxley created to describe muscle contraction and got more complex and precise later on.

3.1.1 Description of the initial model

A.F. Huxley assumed in this model that a myosin cross-bridge can either be attached to the actin filament or detached. These cross-bridges were assumed to be attached to the myosin filament through an elastic linkage and to have an equilibrium position [11].
In this simpler version of the model, it is assumed that each cross-bridge works independently from each other. A cross-bridge binds to a nearby actin site on the actin filament inducing the stretching or compression of the elastic linkage. This, in turn, induced an interaction force between the actin and myosin filaments. The total force produced by the muscle is the sum of all the forces produced by the cross-bridges [11].

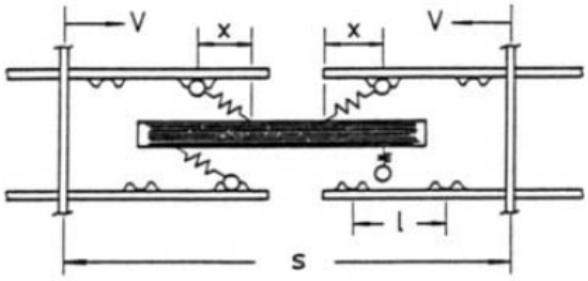

Figure 3.1: Schematical representation of the interactions of the cross bridges with the thin (actin) filaments [16]. X represents the distance between the cross-bridge and its equilibrium position where it is unattached. V represents the half-sarcomere contraction velocity. l is the distance between the actin-binding sites.

Several assumptions are made in this model [16]. Firstly, as already been said, the cross-bridges are assumed to act independently from each other. Secondly, the myofilaments are considered to be rigid. Thirdly, it is considered that there is a fixed number of active cross-bridges. Lastly, the chemical kinetics that determine the activation level are assumed to be of the first order. The mathematical description of this model will be discussed in the next section.

3.1.2 Mathematical formulation

As has been approached earlier, the elastic myosin linkage can either be attached or detached. Thus two rates are introduced into the model: f, the rate for formation of links between actin and myosin while g is the rate for breaking links [11]. These rates are functions of the displacement from its equilibrium position where the cross-bridge is not attached, x. This displacement x is

represented schematically in Figure 3.1.
The Huxley model defined a bond-distribution function, $n(t, x)$. It corresponds to the proportion of sites that are connected to the actin filament at a time t with a bond distance of x and satisfies Equation 3.1 [11].

$$\frac{\partial n}{\partial t} = (1-n)f - ng \qquad \text{or} \qquad -v.\frac{\partial n}{\partial x} = f - (f+g)n \tag{3.1}$$

All contraction sites have a same distance x to the equilibrium position. The variable v is the velocity of the actin filament with respect to the myosin filament (shortening of the muscle). The attachment and detachment of the cross-bridges varies in time. During a contraction, the cross bridges will attach to the actin site and detach according to the mechanism presented in Section 1.3 of Chapter 1. Thus at a time t, a certain percentage of cross-bridges will be attached while the others will be detached. The number of attached cross-bridges does not depend only on time. It depends also on their distance to the actin sites. If they are too far from the sites, the bond-distribution of cross-bridges is smaller than if they are close to the sites and can easily connect. The rate functions f and g model this principle.

Huxley defined in his 1957 paper [11] the rates f and g in Equation 3.2 and Equation 3.3 where f_1, g_1 and g_2 are defined constants.

$$f(x) = \begin{cases} 0 & \text{if} \quad x < 0 \text{ or } x > h \\ f_1 \dfrac{x}{h} & \text{if} \quad 0 < x < h \end{cases} \tag{3.2}$$

$$g(x) = \begin{cases} g_2 & \text{if} \quad x < 0 \\ g_1 \dfrac{x}{h} & \text{if} \quad 0 < x \end{cases} \tag{3.3}$$

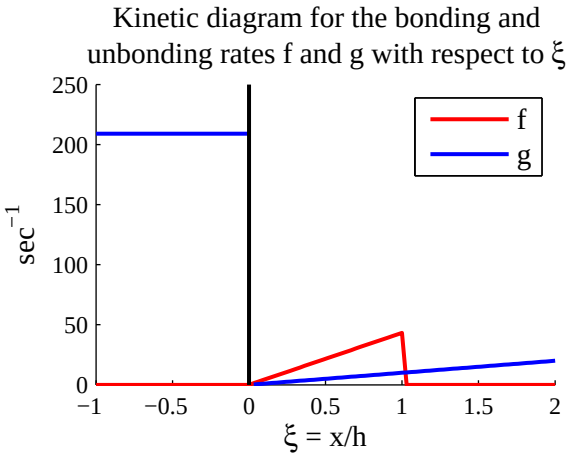

Figure 3.2: Graphical representation of the kinetic rates defined by A.F. Huxley in Equation 3.2 and 3.3

The constant h is the largest displacement at which a side-piece can become attached to an actin filament. Dividing x by h gives the normalized displacement ξ

Figure 3.2 shows how the rates for formation and breaking of links between the cross-bridges and actin sites, f and g respectively, depend on the normalized displacement ξ.
For negative values of the normalized displacement $\xi = x/h$ or values superior to ξ, the connection between the cross-bridge and the actin site cannot be made anymore; thus the rate for formation of links f is null for $\xi < 0$ or $\xi > 1$. There can only be a connection between the cross-bridge and the actin site in the range $0 < \xi < 1$. As the muscle shortens, the actin filaments move relatively to the myosin filaments and the distance ξ decreases. Once this distance becomes negative, the actin sites moved passed the equilibrium position of the cross-bridges, the tension in the elastic element of the cross-bridge becomes unfavourable and the cross-bridges can only detach from the actin sites. The detachment rate g is thus quite high in that case ($\xi < 0$) [11].
No matter the value of ξ, there is always a possibility of detachment between the cross-bridge and the actin site. The probability of detachment changes with the distance ξ: in the range

$0 < \xi < 1$, the detachement rate is quite low since it is the optimal range for the formation of links ($f > g$ in that range). The farther the actin site is away from the equilibrium position of the cross-bridge, the more it becomes probable that there will be a detachment of the link and g increases with increasing ξ.
It is assumed that the distance between the sites on each filament are far enough spaced so that they do not affect the surrounding sites [11].
The constants f_1, g_1 and g_2 cannot be directly deduced from macroscopic muscle experiments [16]. A.F. Huxley found values for these constants by trial and error to fit the relationships found experimentally by A.V. Hill [11].

After a development that can be found in [11] where Equation 3.2 and Equation 3.3 are inserted into Equation 3.1, the following set of equations for the bond distribution n can be found:

$$\begin{aligned} x > h \qquad & n = 0 \\ 0 < x < h \quad & n = \frac{f_1}{f_1 + g_1}\left(1 - \exp\left(\left(\frac{x^2}{h^2} - 1\right)\frac{\phi}{V}\right)\right) \\ x < 0 \qquad & n = \frac{f_1}{f_1 + g_1}\left(1 - \exp\left(-\frac{\phi}{V}\right)\right)\exp\left(\frac{2xg_2}{sV}\right) \end{aligned} \tag{3.4}$$

With $\phi = (f_1 + g_1)\dfrac{h}{s}$ and $V = \frac{2v}{s}$.
s is the length of a sarcomere. They are all constants and can be found in [11]. The variation of the proportion of contraction sites that are connected to the actin filament n with respect to x/h is depicted for different values of velocity V in Figure 3.3a. It can be observed that the higher the velocity, the lower n becomes. Thus, less sites are connected to the actin filament as the velocity increases.

The number of cross-bridges which are attached to the actin filament with a displacement between a and b is the integral of $n(x,t)$ between a and b.

The total muscle tension is given as the sum of the tensions that are generated by the contraction sites in a half-sarcomere. The tension per square centimeter is given by Equation 3.5 [11].

$$P = \frac{msk}{2.l}\int_{-\infty}^{\infty} nxdx \tag{3.5}$$

There are $\frac{ms}{2}$ sites in a cross-section area of 1cm^2. m is the number of myosin sites per cubic centimeter of muscle.

From Equation 3.5 with Equation 3.4, the tension-velocity relationship can be found:

$$P = P_0\left(1 - \frac{V}{\phi}\left(1 - \exp\left(-\frac{\phi}{V}\right)\right)\left(1 + \frac{1}{2}\left(\frac{f_1 + g_1}{g_2}\right)^2\frac{V}{\phi}\right)\right) \tag{3.6}$$

A positive value of V corresponds to a shortening velocity. This relationship is depicted in Figure 3.3b.

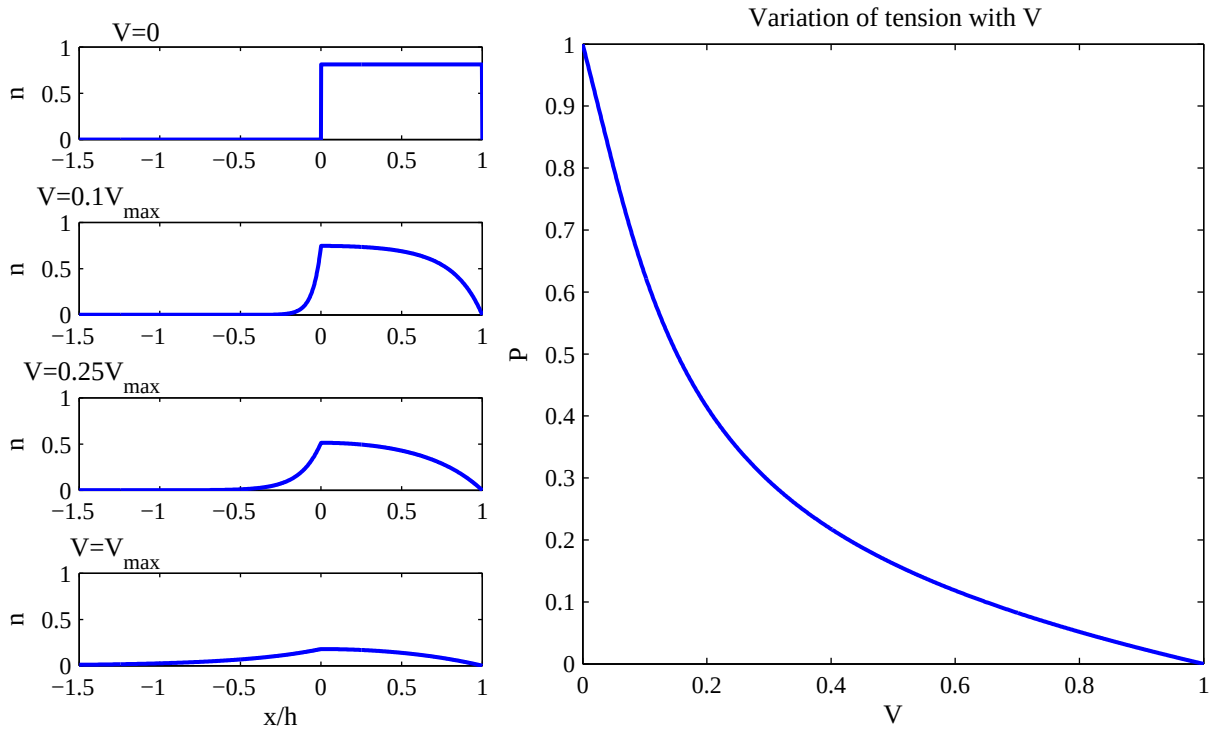

(a) Variation of n with $\frac{x}{h}$, adapted from [11]

(b) Variation of tension with V, adapted from [11]

Figure 3.3: Variation of n with x/h and of P with V

3.1.3 Pros of Huxley model

An advantage of this model, even in the simplest two-state case, is that is gives a concise mathematical description of the way a muscle works. Unlike the Hill model, this model is not phenomenological but is based on a physical meaning. This model links the mechanics, chemistry responsible for the binding between actin and myosin and the structure of the muscle. As an example, the tension per square centimeter given in Equation 3.5 is based on the distribution of bound cross-bridges inside the sarcomere unlike the Hill model which considers the contractile element as a black box.
The initial two states model may be too simple and does not take into account all the features intervening in the muscle contraction but it does deal with the most important one: the binding between actin and myosin.

3.1.4 Cons of Huxley model

In 1971, Huxley and Simmons [24] discovered that one state for the attachment and a second one for the detachment are not enough. With only two states as presented here, the model cannot predict a maximum in the steady-state rate of shortening. They then postulated later on that a second state of attachment and detachment are needed. Thus, the rates f' and g' are added to the f and g rates.
With time, more and more states were added to the original model making it more and more accurate and complicated. Each added state comes with an additional rate equation. It involves the numerical integration of several functional states of the cross-bridges. This gives a non-linear partial differential equation which is not trivial to solve [25].

3.2 Distribution-Moment (DM) model

3.2.1 Description

This model was created by George I. Zahalak and is mostly described in the first chapter of [16]. This model is a bridge between the macroscopic point of view, i.e. the Hill models, and the microscopic point of view, i.e. the Huxley model. Its goal is to generate a macroscopic model of a muscle that is simpler than the Huxley model while keeping its presumed biological relevance. It is based on the cross-bridge theories and the two-state Huxley model with an extension by integrating a model for electrical stimulation and calcium-activation dynamics into the cross-bridge model.

3.2.2 Simulation protocol

This model has been implemented in MATLAB® as the previous model. Its implementation is based upon the equations and constants found in different published articles by the author [12] [16] [26] [27].

First, the activation dynamics, which will be detailed in Subection 3.2.4, are implemented. The activation dynamics in the distribution-moment model models the calcium activation dynamics mentioned in Chapter 1. The activation depends on the total sarcoplasmic calcium ion concentration and the free calcium ion concentration. The activation of muscle can be controlled by a pulse train function that represents a sequence of action potentials.

The mechanical model is based upon three differential equations representing the "moments" Q_λ with $\lambda = 0, 1, 2$. These represent the muscle stiffness (Q_0), force (Q_1) and elastic energy stored in the muscle (Q_2) and will be explained in details in the following Subsection. The set of equations to be solved for the mechanical model are given by Equation 3.7 with $\lambda = 0, 1, 2$. How these moments were obtained from the original Huxley equation and the different terms will be explained in details in the following Subsections.

$$\frac{dQ_\lambda}{dt} = r.\alpha.\beta_\lambda - r.\phi_{1\lambda}(Q_0, Q_1, Q_2) - \phi_{2\lambda}(Q_0, Q_1, Q_2) - \lambda u(t) Q_{\lambda-1} \tag{3.7}$$

There are thus three equations that depend on an activation factor r (the link with the calcium concentration will be explained in subsection 3.2.4), a fraction of cross-bridges available to interact with the actin sites (α) which is a value between 0 and 1, the velocity of the sliding filaments $u(t)$ and the different moments Q_λ. The function β_λ, $\phi_{1\lambda}$ and $\phi_{1\lambda}$ will also be detailled in the following subsections and the explicit construction of these functions is given in Appendix A.

3.2.3 Mathematical formulation

This model concentrates on the Myosin-Actin-Troponin (MAT) complex and makes several assumptions. First, it is assumed that each cross-bridge interacts with a single actin site, the closest, and that all the cross-bridges act independently of each other. Secondly, one molecule of troponin regulates the availability of the actin binding site for each instantaneous [myosin cross-bridge]-[actin binding site] pair. Only when two calcium ions are bound to the troponin molecule, which is assumed to be fast compared to the cross-bridge reaction, the myosin can bind to the actin. Thirdly, it is assumed that only a fraction of the cross-bridges in the contractile tissue, which is assumed to be a function of the muscle length, is available to interact with actin at any given time [16].

In the distribution moment model, there are three different so-called "moments" that are defined

by Equation 3.8 [12]. These moments, particularity of this model, are based upon the original Huxley model [11] but did not define them separately as here.

$$Q_\lambda(t) = \int_{-\infty}^{\infty} \xi^\lambda n(\xi, t) d\xi \tag{3.8}$$

where $\xi = x/h$. x is the displacement of a cross-bridge from its neutral equilibrium position and h is the bond-length scaling factor. In this model, there are three moments ($\lambda = 0, 1, 2$) which correspond to the normalized stiffness of the contractile tissue, the muscle force and the stored elastic energy in the cross-bridges respectively.

So, the three moments can be defined as

$$Q_0 = \int_{-\infty}^{\infty} n(\xi, t) d\xi \qquad \text{the stiffness}$$
$$Q_1 = \int_{-\infty}^{\infty} \xi.n(\xi, t) d\xi \qquad \text{the muscle force}$$
$$Q_2 = \int_{-\infty}^{\infty} \xi^2.n(\xi, t) d\xi \qquad \text{the stored elastic energy}$$

The muscle normalized stiffness Q_0, muscle force Q_1 and stored elastic energy Q_2 are linked and functions of the cross-bridge binding distribution. It is demonstrated hereunder how these three relationships are linked to the stiffness, force and stored elastic energy.

The muscle stiffness corresponds to the stiffness of the muscle due to the cross-bridge inside the sarcomeres. It is not to be mingled with the concept of "quasi-stiffness". "Quasi-stiffness" refers to the slope of the torque-ankle relationship in an articulation during dynamic tasks [28] or the slope of the force-length relationship in an isolated muscle. The quasi-stiffness varies widely while the muscle stiffness is usually considered to be constant.

To show this, a slab of contractile tissue is taken and the following developments are based on [27]. This slab is represented schematically in Figure 3.4. The thickness of this slab is the half of a sarcomere length, $s/2$. The cross-section of this slab is denoted A. The total number of cross-bridges in this slab is thus $m.(A.s/2)$ with m the concentration of cross-bridges. Since only the bond cross-bridges produce a force, the number of cross-bridges must be multiplied by the bond-distribution function $n(x, t)$ and is thus $m.(A.s/2).n(x, t)$.
The distance between the actin binding sites is denoted l. The nearest actin-site for a cross-bridge must be between $-l/2$ and $l/2$. The number of cross-bridges with nearest actin sites lying in the interval $(x, x + dx)$ at time t is proportional to dx/l.
It is assumed that a cross-bridge is elastically attached to the myosin filament and that the elastic restoring force of each cross-bridge is linear with a spring constant k.

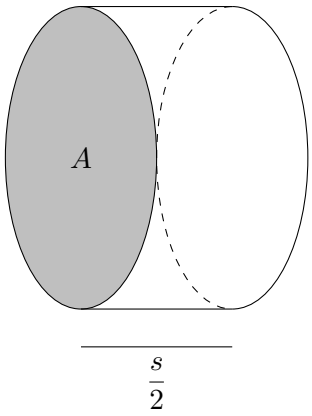

Figure 3.4: Muscle slab

Muscle force Q_1: The increment in force that is exerted by the fraction of bonded cross-bridges with bond-lengths in the range $(x, x + dx)$ is thus $m.(A.s/2).n(x, t).k.x.dx/l$.
Integrating this over all possible bond lengths gives

$$F(t) = \frac{m.A.s.k}{2.l} \int_{-\infty}^{\infty} x.n(x, t) dx$$

Scaling x with the scaling factor h such that $\xi = x/h$, it gives

$$F(t) = \frac{m.A.s.k.h^2}{2.l} \int_{-\infty}^{\infty} \xi.n(\xi, t)d\xi$$

So if the constant $\Gamma = \frac{m.A.s.k.h^2}{2.l}$ is defined, $F = \Gamma.Q_1(t)$.

Stiffness Q_0: If the slab is stretched or shorten by an amount ΔX, then all the cross-bridges in the slab will have a bond length change of $\frac{s}{2}\frac{\Delta X}{X}$ where X is the length of the slab.
The change in force in the range $(x, x + dx)$ is

$$d(\Delta F) = \left(\frac{m.A.s.k}{2}\right).\left(\frac{s}{2}\frac{\Delta X}{X}\right).n(x, t).\frac{dx}{l}$$

The stiffness is $K_c = \frac{\Delta F}{\Delta X}$ thus by integrating $d(\Delta F)$ over all bond lengths

$$K_c = \left(\frac{m.A.s^2.k}{2.l}\right).\left(\frac{1}{2X}\right)\int_{-\infty}^{\infty} n(x, t).dx$$

And by changing x to ξ

$$K_c = \left(\frac{m.A.s^2.k.h}{2.l}\right).\left(\frac{1}{2X}\right)\int_{-\infty}^{\infty} n(\xi, t).d\xi$$

Thus $K_c \propto \int_{-\infty}^{\infty} n(\xi, t).d\xi$

Stored elastic energy Q_2: The increment in energy that is associated with all the cross-bridges with bond lengths in the range $(x, x + dx)$ is $d(U_c) = (kx^2/2)(m.A.X).n(x, t)dx/l$. Integrating this over all bond lengths gives

$$U_c = \frac{k.m.A.X}{2.l} \int_{-\infty}^{\infty} x^2.n(x, t).dx$$

So, by adding the scaling factor h,

$$U_c = \frac{k.m.A.X.h^3}{2.l} \int_{-\infty}^{\infty} \xi^2.n(\xi, t).d\xi$$

Thus $U_c \propto \int_{-\infty}^{\infty} \xi^2.n(\xi, t).d\xi$

As a summary,

$$\begin{aligned} K_c(t) &= \frac{m.A.s^2.k.h}{4.l.X} Q_0(t) \\ F(t) &= \frac{m.A.s.k.h^2}{2.l} Q_1(t) \\ U_c(t) &= \frac{k.m.A.X.h^3}{2.l} Q_2(t) \end{aligned}$$

The main approximation of the Huxley model is the definition of n that depends on the moments and as a Gaussian. n is given by Equation 3.9 where $p := Q_1/Q_2$ and $q := \sqrt{(Q_2/Q_0) - (Q_1/Q_0)^2}$. p is the mean and q is the standard deviation of the approximate bond distribution.

$$n(\xi, t) := \frac{Q_0}{\sqrt{2.\pi q}} \exp\left(\frac{-(\xi - p)^2}{2.q^2}\right) \tag{3.9}$$

As a reminder, $n(\xi, t)$ corresponds to Equation 3.4 in the Huxley model. Figure 3.5 represents graphically this function $n(\xi, t)$ at different times in the lower graph. $n(\xi, t)$ was computed with the moments which were first computed with Equation 3.7. The upper graph shows the force response curve and the coloured stars represent the moments at which the corresponding $n(\xi, t_i)$ where taken. The green star is at the maximum of the force response curve and the green n curve is also the one with the greatest amplitude. Indeed, more cross-bridges are needed to create a bigger force than for the gray star for example where there is a much smaller force response.

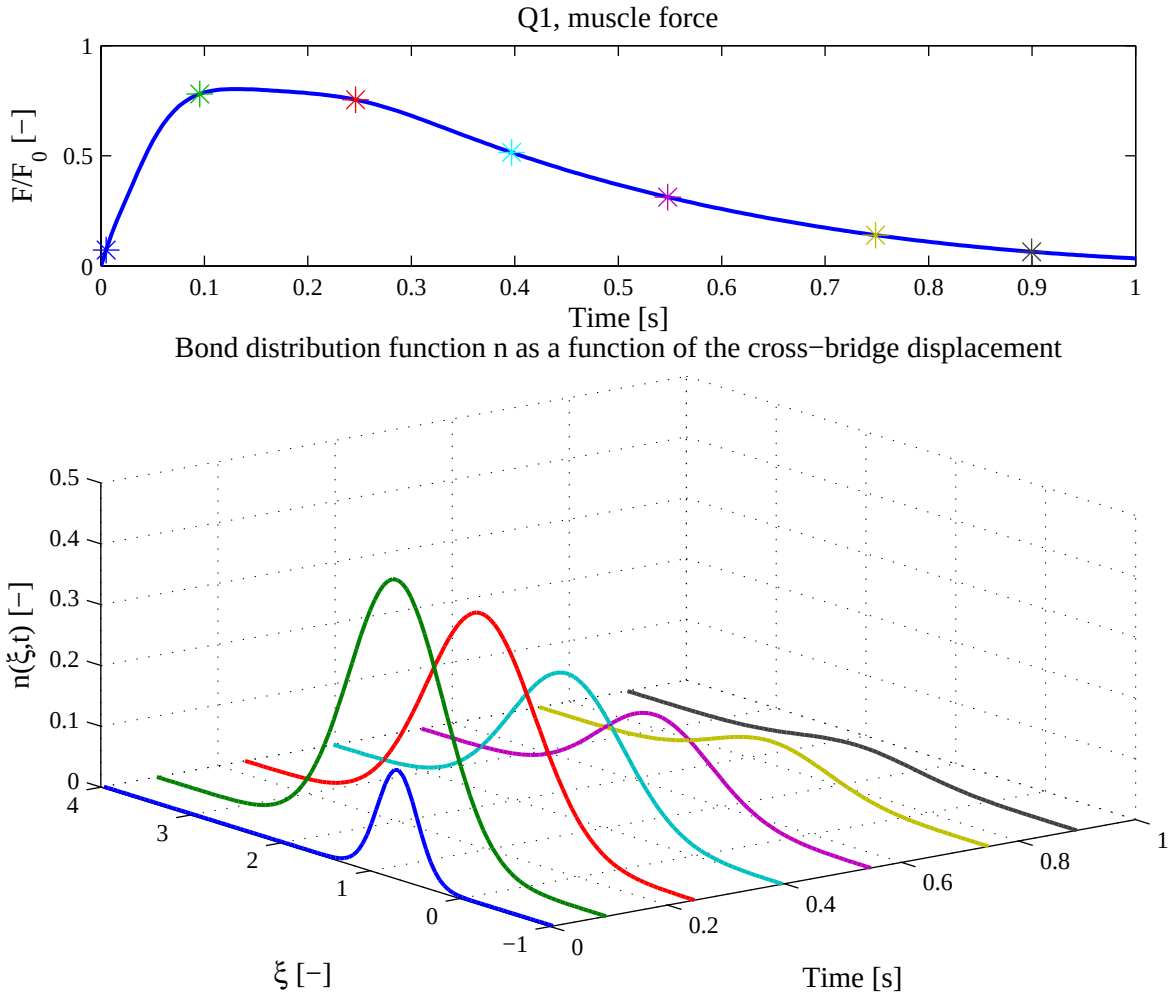

Figure 3.5: The upper graph represents the normalized force-response of a muscle. The lower graph represents the bond distribution functions $n(\xi, t_i)$ at different times indicated by the colored stars in the upper graph.

3.2.4 Activation dynamics

There is an activation factor r (see Equation 3.7) in this model that is a function of the free calcium concentration in the sarcoplasm. It is this function that is responsible for the coupling between the cross-bridge contraction dynamics and the action potential mediated calcium-activation dynamics.

In this model, there are two different activation schemes and they are represented schematically in Figure 3.6. The ball and the spring represent the cross-bridge, the hatched rectangle represents the troponin molecule and the filled hexagon represent a calcium ion. The first activation scheme is called the "loose coupling" scheme and it is represented by the solid circles. It assumes that the binding/unbinding of the calcium ions from the troponin molecules happen independently

from the state of binding between the actin and the myosin. The second scheme however, called the "tight coupling" scheme, considers that the calcium ions can only unbind from the troponin molecule only if the myosin is detached from the actin. It is represented by the solid and dashed large circles.

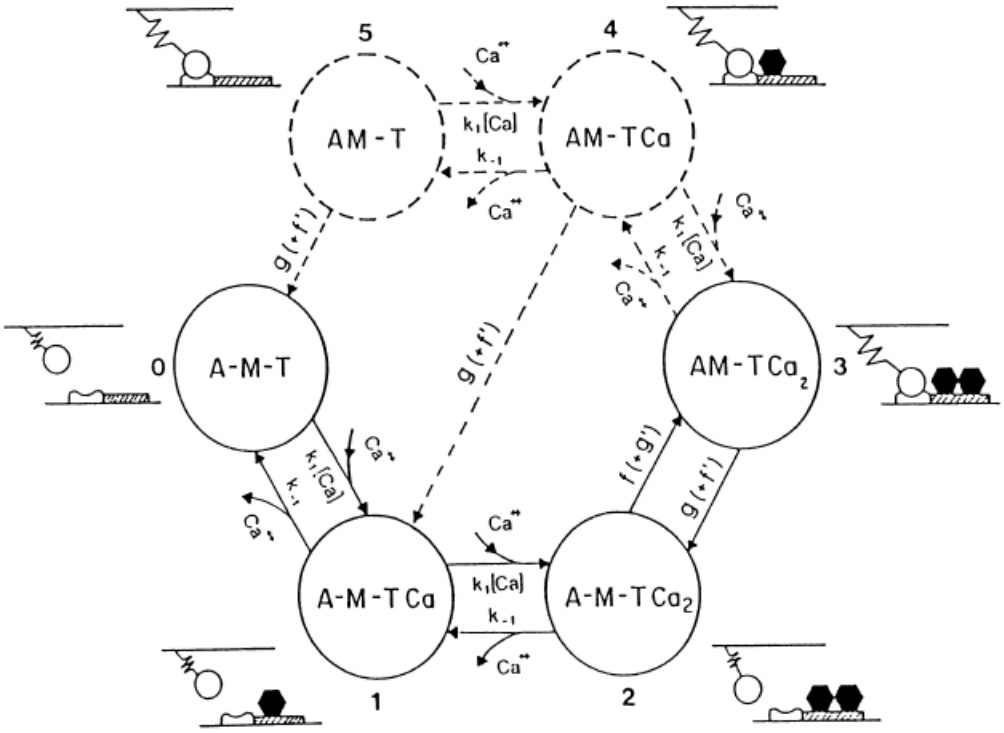

Figure 3.6: Kinetic diagram for two calcium-activation schemes. From [16]

G. I. Zahalak modified the Huxley rate equation using these activation dynamics to obtain Equation 3.10 [16].

$$\frac{\partial n}{\partial t} - v(t)\frac{\partial n}{\partial x} = (f+g')(r\alpha - n) - (f'+g)n \qquad \text{for loose coupling} \tag{3.10}$$
$$\frac{\partial n}{\partial t} - v(t)\frac{\partial n}{\partial x} = r(f+g')(\alpha - n) - (f'+g)n \qquad \text{for tight coupling}$$

G. I. Zahalak adapted the Huxley equations to both loose and tight coupling schemes and the equations for both will be given. However, experimental evidence as well as model simulations conducted by Zahalak and Ma [29] later on have suggested that the tight coupling corresponds better to reality. The different equations for loose and tight coupling will be given as there are only a few differences between these two couplings but the model implementation will be done by using the tight coupling scheme. A comparison of the force responses in both cases is given in Appendix A and shows that the force responses with both couplings are almost identical.

Equation 3.10 is similar to Equation 3.1 with some modifications. The Huxley equation was limited to two rates, f and g, whereas there are two more here, f' and g'. Also Equation 3.10 takes into account two possible couplings. There are also two terms that were not present in the Huxley equation. Firstly, α which represents the fraction of cross-bridges that are available to interact with the actin ($0 < \alpha < 1$). Secondly, r which is the activation factor and is a pure function of free calcium.

To be able to determine the activation factor, the concentration of free calcium must first be determined. The activation dynamics depend on the calcium-rate and is given by Equation 3.11

[16].

$$\frac{d[Ca]_t}{dt} = R_0 \left(1 - \frac{[Ca]}{[Ca]^*}\right) \chi(t) - V_m \frac{[Ca]}{[Ca] + K_m} \tag{3.11}$$

The terms K_m and V_m are parameters from the Michaelis-Menten kinetics. $[Ca]$ is the free calcium concentration while $[Ca]_t$ is the total sarcoplasmic calcium concentration (free and bond to troponin). R_0 is the concentration change of calcium injected into the sarcoplasm. $\chi(t)$ is the pulse train of action potentials and the input to control the activation dynamics.

The different terms of this equation can be rendered dimensionless by multiplying them by N/m where N is the Avogadro number and m is the number of cross-bridges per unit volume.

$$[Ca]\frac{N}{m} = c \quad [Ca]^*\frac{N}{m} = c^* \quad [Ca]_t\frac{N}{m} = C \quad R_0\frac{N}{m} = \rho \quad V_m\frac{N}{m} = \tau_0^{-1} \quad K_m\frac{N}{m} = k_m$$

Equation 3.11 thus becomes Equation 3.12.

$$\frac{dC}{dt} = \rho \left(1 - \frac{c}{c^*}\right) \chi(t) - \tau_0^{-1} \frac{c}{c + k_m} \tag{3.12}$$

Where $\chi(t)$ represents a sum of normalized impulse functions and a possible impulse function is defined by Equation 3.13 with $\tau_1 = 0.005$s and $\tau_2 = 0.001$s [27]. The activation dynamics can be controlled with this function.

$$\begin{aligned} \chi(t) &= \sum_i \hat{\chi}(t - t_i) \\ \hat{\chi}(t) &= \left(\exp(-t/\tau_1) - \exp(-t/\tau_2)\right)(\tau_1 - \tau_2) \end{aligned} \tag{3.13}$$

A relation between C and c was given by G. I. Zahalak in his paper [26] for the loose and tight coupling:

$$C = \begin{cases} c + r(2 + \mu/c) & \text{loose coupling} \\ c + 2bQ_0 + r(2 + \mu/c)(1 - bQ_0) & \text{tight coupling} \end{cases} \tag{3.14}$$

μ is a normalized mean calcium binding constant. The relation in the tight coupling takes into account the muscle stiffness Q_0 unlike the loose coupling case. This corresponds better to the reality as was discovered by the author [29]. By solving Equation 3.12, C can be determined and Equation 3.14 can be solved numerically to obtain c. However, solving this equation numerically at each time step makes the model run slower.

Finally, the activation factor r is given by Equation 3.15 [16].

$$r(c) = \frac{c^2}{c^2 + \mu c + \mu^2} \tag{3.15}$$

By changing the concentration of total calcium, the activation factor r is modified. This can be controlled with the nomalized impulse function $\chi(t)$. Figure 3.7 shows the muscle force response for two different impulse functions. First, in Figure 3.7a the impulse was short which resulted in a force response that does not attain its peak value. The force response is a twitch. In the second case, in Figure 3.7b, the impulse function is wider which results in a tetanic response of the muscle. The force response reaches its peak value and presents a plateau until the activation factor r starts decreasing again.

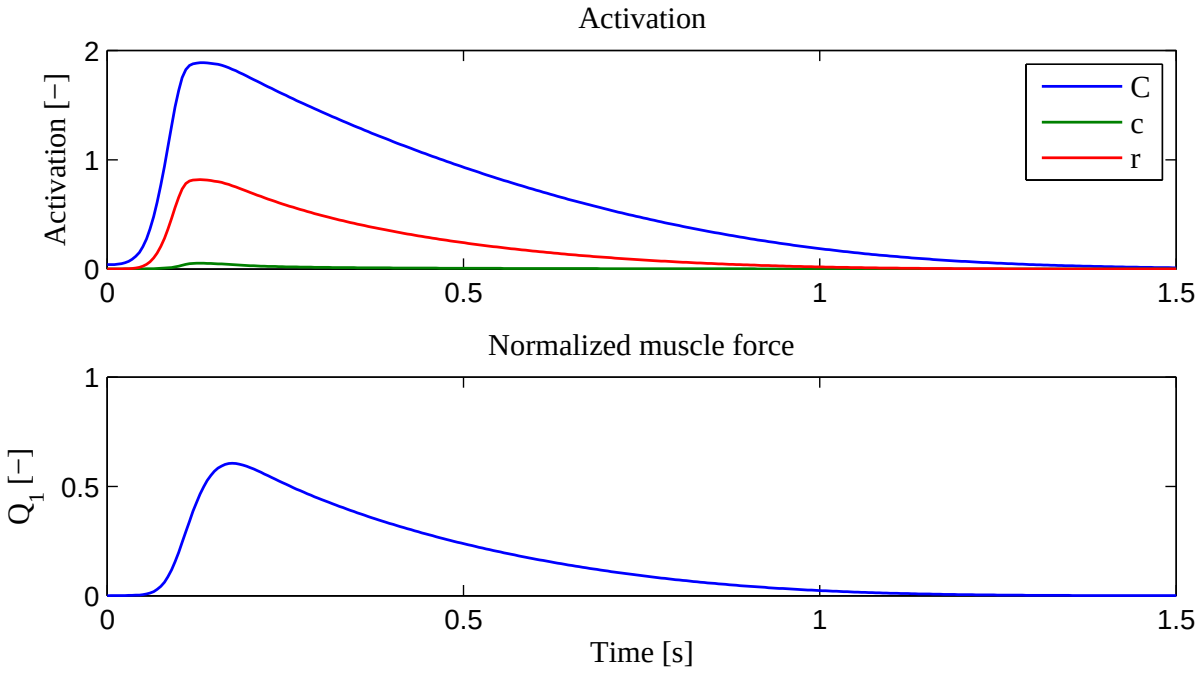

(a) Force response for short activation and a constant scaled myofilament sliding velocity u of 20 sec^{-1}

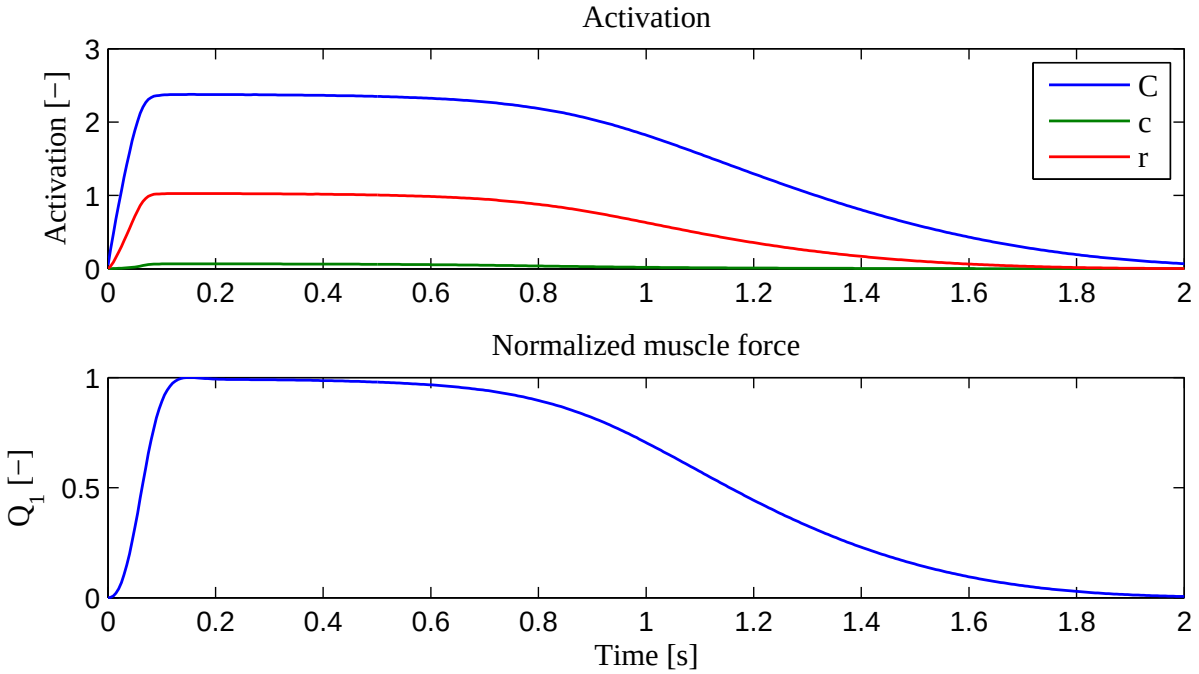

(b) Force response for longer activation and a constant scaled myofilament sliding velocity u of 20 sec^{-1}

Figure 3.7: Activation dynamics and resulting force responses for two different activation times

3.2.5 Numerical implementation for the loose coupling

The original Huxley equation is given as a reminder in Equation 3.16.

$$\frac{\partial n}{\partial t} - v(t)\frac{\partial n}{\partial x} = f(x) - (f(x) + g(x))\,.n(x,t) \tag{3.16}$$

As a reminder, $f(x)$ and $g(x)$ are the rate of binding and unbinding respectively. They are defined by Huxley in Equation 3.2 and Equation 3.3. G. I. Zahalak modified these rates

(Equation 3.17 and Equation 3.18) by introduction one additional rate parameter g_3 [12]. This modification was made to make the stretching response more realistic. Once the attachment of cross-bridges is not possible anymore, the probability of detachment will be even higher. Huxley and Zahalak rate functions can graphically be seen in Figure 3.8.

$$f(x) = \begin{cases} 0 & \text{if} \quad x < 0 \\ f_1 \dfrac{x}{h} & \text{if} \quad 0 < x < h \\ 0 & \text{if} \quad x > h \end{cases} \tag{3.17}$$

$$g(x) = \begin{cases} g_2 & \text{if} \quad x < 0 \\ g_1 \dfrac{x}{h} & \text{if} \quad 0 < x < h \\ g_1 \dfrac{x}{h} + g_3 \left(\dfrac{x}{h} - 1 \right) & \text{if} \quad x > h \end{cases} \tag{3.18}$$

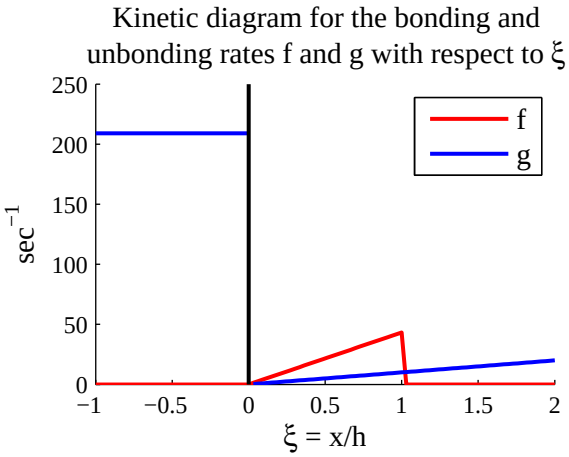

(a) Kinetic rates f and g defined by A.F. Huxley

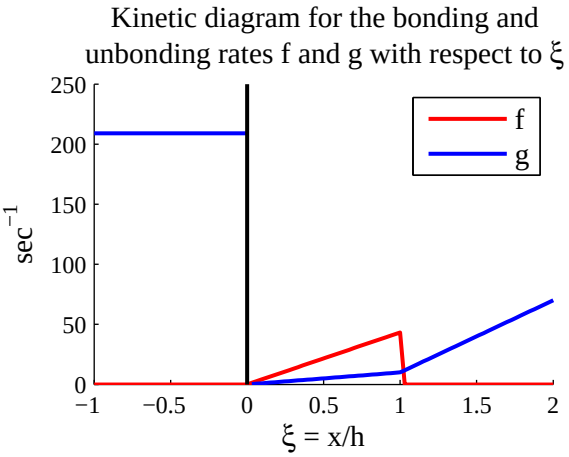

(b) Zahalak's modified version of the Huxley kinetic rates

Figure 3.8: Comparison between the kinetic rate functions of A.F. Huxley and G.I. Zahalak

Equation 3.16 is multiplied by x^λ (with $\lambda = 0, 1, 2$) and integrated over the domain of x. A more detailed explanation can be found in [12]. By defining the following:

$$Q_\lambda(t) = \int_{-\infty}^{\infty} \xi^\lambda n(\xi, t) d\xi \tag{3.19}$$

$$\beta_\lambda = \int_{-\infty}^{\infty} \xi^\lambda f(\xi) d\xi \tag{3.20}$$

$$\phi_\lambda = \int_{-\infty}^{\infty} \xi^\lambda \left[f(\xi) + g(\xi) \right] n(\xi, t) d\xi \tag{3.21}$$

$Q_\lambda(t)$ is the λth moment of the bond-distribution function and β_λ is the λth moment of the bonding rate function.

Equation 3.16 becomes

$$\frac{dQ_\lambda}{dt} = r.\alpha.\beta_\lambda - \phi_\lambda(Q_0, Q_1, Q_2) - \lambda u(t) Q_{\lambda-1} \tag{3.22}$$

With $Q_{-1} = 0$. Equation 3.22 can be constructed explicitly as is shown in details in Appendix A which is from [12].

$$\beta_\lambda = f_1 \left(\lambda + 2\right)^{-1} \tag{3.23}$$

This model can be implemented by using Equation 3.12 and Equation 3.14 for the muscles activation and Equation 3.22 for the moments.

3.2.6 Numerical implementation for the tight coupling

The tight coupling is quite similar to the loose coupling. The activation dynamics are slightly different since Equation 3.14 that gives the relation between C and c is different for the tight coupling.

Equation 3.16 becomes

$$\frac{dQ_\lambda}{dt} = r.\alpha.\beta_\lambda - r.\phi_{1\lambda}(Q_0, Q_1, Q_2) - \phi_{2\lambda}(Q_0, Q_1, Q_2) - \lambda u(t) Q_{\lambda-1} \tag{3.24}$$

The ϕ_λ function from the loose coupling is divided into $\phi_{1\lambda}$ and $\phi_{2\lambda}$ where

$$\phi_\lambda = \phi_{1\lambda} + \phi_{2\lambda}$$

$$\phi_{1\lambda} = \int_{-\infty}^{\infty} \xi^\lambda f(\xi).n(\xi, t) d\xi \tag{3.25}$$

$$\phi_{2\lambda} = \int_{-\infty}^{\infty} \xi^\lambda g(\xi).n(\xi, t) d\xi \tag{3.26}$$

A comparison between the force response between the loose and tight coupling (identical constants for both cases) for a constant and oscillating scaled sliding velocity $u(t)$ can be seen in Figure A.1 in Appendix A. As can be observed, both couplings are almost identical whether the $u(t)$ is constant or not.

3.2.7 Pros of the distribution-moment model

The main advantage of this model is that is more precise and has a physical meaning than the Hill model while being more simple than the complicated Huxley model due to its approximations. The predictions of this model are somewhat less precise because of this approximations than the Huxley model but still quite reasonable.
Unlike the Huxley model, the distribution-moment model focuses directly on the quantities of interest such as the force, the stiffness and elastic energy.
In the Hill model, the activation has no measurable physical meaning. In the distribution-moment model the activation is defined by Equation 3.11 which has a physical meaning since it is linked with the calcium ion concentration.
This model has both the macroscopic and microscopic significance which is why it a bridge between the macroscopic and microscopic.

3.2.8 Cons of the distribution-moment model

Even if it is a simpler model than the Huxley model, it is still significantly more complex than the Hill-model.
Since it has a macroscopic and a microscopic meaning, this model requires all the microscopic and macroscopic data such as the structural, chemical, mechanical, and thermodynamical data for a single muscle.
Since it is an approximation of the more accurate Huxley model, assumptions were made in order to simplify the model. However, these assumptions are not necessarily true. The sarcomeres are not necessarily uniform or the fibers are not necessarily parallel to the muscle axis, etc.

Chapter 4

Work-dependent deactivation model

4.1 Description

This model presented in [13] was developed by Thelma L. Williams in 2010 and predicts the force generated by skeletal muscle according to a lengthening, shortening or no length change of the muscle. It presents two main particularities. First, it incorporates what the authors call the "work-dependent deactivation" mechanism which considers that a shortening muscle under load generates less force after the shortening ceases [13]. Secondly, this model considers the stiffness of the muscle as a function of the activation instead of a constant.

This model is divided into two parts: the activation mechanism, based on calcium ions release from the sarcoplasmic reticulum, and the mechanical model, based on a phenomenological model.
First, the simulation protocol used to implement this model will be given. Then the activation dynamics and the mechanical model will be described. Finally, a few words about the pros and cons of this model will be given.

4.2 Simulation protocol

This model has been implemented in MATLAB®. The model has been implemented as a set of differential equations from [13], integrated with the `ode45` function.

First, the initial conditions such as the muscle and contractile elements lengths and velocities need to be set. The activation is controlled by a set stimulation time.
Secondly, the activation dynamics are computed. These consist of two differential equations of the calcium concentration released from the sarcoplasmic reticulum and the calcium concentration of ions bound to the tropomyosin rods. They depend on the stimulation time given as input. It is in these equations that the "work-dependent deactivation" is taken into account.
Thirdly, the mechanical model is implemented. The whole muscle force is defined as a differential equation dependent of the contractile element force and the muscle-tendon velocity. The contractile element force is similar to the one of the Hill-type model: it consists of the activation which is the calcium concentration of bound calcium ions, a force-length and a force-velocity relationship.
The contractile element velocity is a function of the muscle-tendon velocity which is an input of the model, the muscle force as well as the activation. Once it is calculated, it needs to be integrated to obtain the contractile element length for the next time step. Another differential equation is responsible for the work-dependent deactivation mechanism and gives variable rates for the binding and release of calcium ions to the filaments which are used by the activation dynamics.

4.3 Activation dynamics

The equations presented in this section are based upon [13] and [30].
The muscle activation is linked to the calcium concentration that is released from the sarcoplasmic reticulum (C_a) and the calcium concentration bound to the tropomyosin rods (C_{af}). Equation 4.1 and 4.2 [13] are the governing equations of the released and bound calcium respectively. These equations also show the cooperativity between released and bound calcium rates. Indeed, the calcium concentration that is released from the sarcoplasmic reticulum (C_a) depends on the calcium concentration bound to the tropomyosin rods (C_{af}) and inversely. This can be seen in Figure 4.2 on the upper right graph. When one concentration increases, so does the other.

$$\frac{dC_a}{dt} = (k_4(t)C_{af} - k_3(t)C_a)(1 - C_{af}) + k_1(C - C_a - C_{af}) + k_2C_a(C - S - C_a - C_{af}) \quad (4.1)$$

$$\frac{dC_{af}}{dt} = -(k_4(t)C_{af} - k_3(t)C_a)(1 - C_{af}) \quad (4.2)$$

The constant k_1 represents the rate for release of calcium while k_2 is the rate of binding of calcium to the sarcoplasmic reticulum. Therefore, when the stimulus is on, k_2 is negligible compared to k_1 and inversely when the stimulus is off.
In an earlier version of this model [30], k_3 and k_4 were considered to be constant. In this version of the model, they were considered to vary with the shortening of the muscle. These two non constant rates are responsible for the work-dependent deactivation. C and S are two constants that represent the total calcium concentration and the sarcoplasmic-reticular binding sites respectively [30]. They have been determined from data analysis and have no physiological meaning.

The results obtained with variable k_3 and k_4 are not very different from the constant case in isometric condition. However, the variable case makes a significant difference in non-isometric condition. The more the muscle length changes, the model with constant k cannot correctly approximate the correct force generation unlike with variable k [13]. This can be observed in Figure 4.1. The muscle length varies with a frequency of 20Hz for a same stimulus time of 0.3s. Everything is kept identical in both cases except that in one case, the red curve, k_3 and k_4 are kept to a constant value whereas in the second case, the blue curve, k_3 and k_4 are variable (with initial values of the constant case). It can be seen that at the beginning, when the stimulus is still active, both curves are very much alike. Later on, when the stimulus is off, both curves evolve differently. Corr and Herzog [31] studied the recovery from work-dependent deactivation in the cat soleus muscle and gave evidence that this work-dependent deactivation mechanism is due to the inhibition of the formation of cross-bridges. The variable k_3 and k_4 induce a faster force decrease after the stimulation stops which corresponds better to the results obtained by Corr and Herzog in their paper [31].

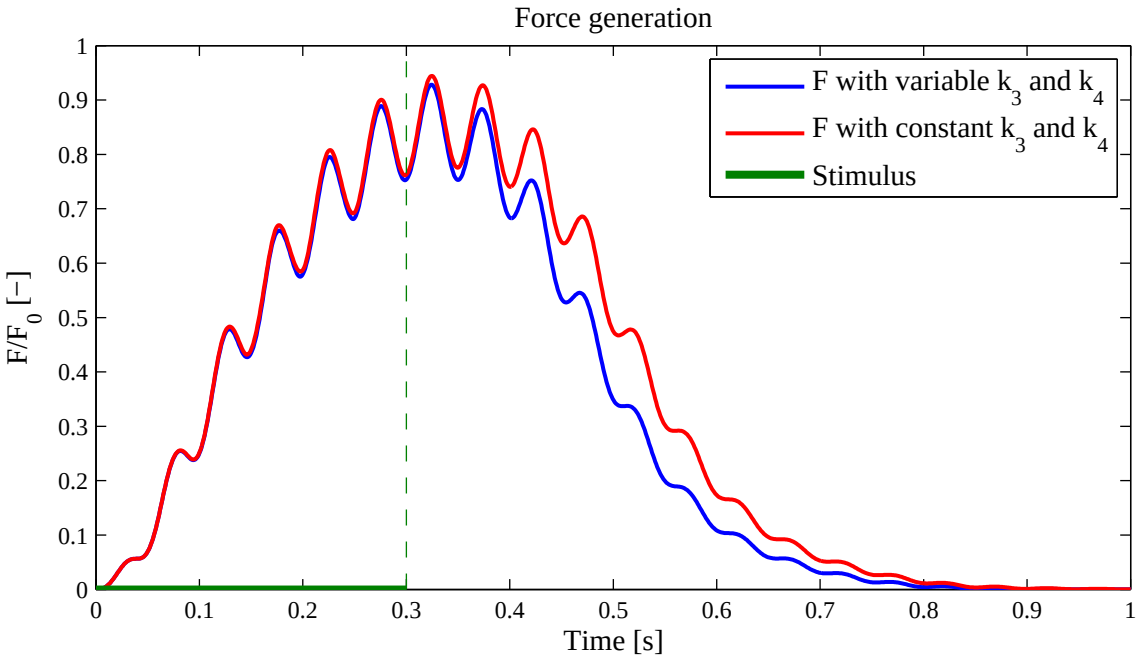

Figure 4.1: Comparison between the force-response obtained with constant and variable k_3 and k_4. The red curve represents the force response with constant k_3 and k_4 and the blue curve represents the force response with variable k_3 and k_4. The bold green line represents the stimulation time.

4.4 Mechanical model

The equations presented in this section can be found in the article presenting this model [10]. The mechanical model is based on a Hill model: a passive elastic element (SE) and a contractile element (CE) [13]. In the earlier model, the stiffness of the passive elastic element was considered constant [30]. In this model, it is not considered a constant but varies linearly with the level of activation. The force generation is quite similar for both cases, with constant and variable stiffness. However, the lengths of the contractile and elastic elements are different. In the case of variable stiffness, the elastic element stretches quicker inducing the contractile element to plateau faster, before the stimulus ends, and longer.
The active force of the contractile element has a Hill formulation as can be seen in Equation 4.3.

$$P_c = P_0 \lambda(l_c) \alpha(v_c) C_{af} \tag{4.3}$$

The active force (P_c) is the product of the maximum force produced in isometric condition (P_0), a force-length relation ($\lambda(l_c)$), a force-velocity relation ($\alpha(v_c)$) and the activation (C_{af}). This equation can be compared to the force generated by the contractile element in the Hill model (Equation 2.3). The activation A in the Hill model corresponds here to the calcium concentration bound to the tropomyosin rods C_{af} which is responsible for the muscle activation. The maximum isometric force F_{max}, usually given in Newton units, corresponds to P_0 which is mN/mm^2 units. The force-length and force-velocity relationships $f_l(l_{CE})$ and $f_v(v_{CE})$ correspond to $\lambda(l_c)$ and $\alpha(v_c)$ respectively.

The force-length relationship is approximated here by a parabolic function. In many Hill-type models however, it is approximated by a gaussian function. The force-velocity relation is approximated by two linear functions, one for shortening velocities and one for lengthening velocities. Both relations are given by Equation 4.4 and Equation 4.5 respectively [13].

$$\lambda(l_c) = 1 + 20(l_c - l_{c0})^2 \tag{4.4}$$

$$\alpha(v_c) = 1 + \begin{cases} 0.8v_c & \text{if} \quad v_c < 0 \\ 2.9v_c & \text{if} \quad v_c \geq 0 \end{cases} \tag{4.5}$$

Since the contractile element is in series with the elastic element, the forces in these two elements are nearly equal and correspond to the whole muscle force. However, the stretch of the elastic element by the contractile element cannot be instantaneous. To model this, the transfer of force is introduced in this model and presented in Equation 4.6 [13].

$$\frac{dP}{dt} = k_5(P_c - P) \tag{4.6}$$

k_5 is a constant and set to a large value so that P_c and P are almost equal.
The whole muscle force can computed with Equation 4.7 by replacing P_c by Equation 4.3, 4.4 and 4.5.

$$\frac{dP}{dt} = \frac{\lambda C_{af}\left(1 + \alpha_1 V + \alpha_1 \mu_1 P(\frac{dC_{af}}{dt})/\mu^2\right) - P}{1/k_5 + \lambda\alpha_1 C_{af}/\mu} \tag{4.7}$$

Where α_1 is equal to 0.8 if $v_c < 0$ or to 2.9 if $v_c \leq 0$. V is the whole muscle velocity which is an input of the model. μ is the stiffness which was made here dependent of the level of activation $\mu(t) = \mu_0 + \mu_1 C_{af}(t)$. μ_0 and μ_1 are the intercept and the gradient of the dependence of the series element stiffness on C_{af}.

The contractile element velocity can be found using Equation 4.7 and is given by Equation 4.8 [13].

$$v_c = V - \frac{dP}{dt}/\mu + \mu_1 P \frac{dC_{af}}{dt}/\mu^2 \tag{4.8}$$

Finally, a variable, called m, which affects the calcium binding and release rate is introduced in Equation 4.9 [13].

$$\frac{dm}{dt} = \begin{cases} -k_{m1} P_c v_c & \text{if} \quad v_c < 0 \\ -k_{m2}(m-1) & \text{if} \quad v_c \geq 0 \end{cases} \tag{4.9}$$

where k_{m1} and k_{m2} are two constants given in the article. This variable increases during muscle shortening under load and is responsible for the work dependent deactivation.
This variable m is then used to compute the variables k_3 and k_4: $k_3 = k_{30}/\sqrt{m}$ and $k_4 = k_{40}\sqrt{m}$ where k_{30} and k_{40} are the values of k_3 and k_4 when $m = 1$.

The Equations 4.3 to 4.9 have been implemented to obtain the force-response of a muscle with inputs the stimulation time and the muscle velocity. The implementation was described in Section 4.2. Figure 4.2 shows a case of isometric contraction with a stimulation of 330 ms. Four different graphs obtained with this model can be observed. In the first one, the force generation of the muscle is depicted. A stimulation of 330 ms is applied and during this time, the force rises, as does the C_a and C_{af} concentrations in the second graph. Once the stimulation stops, the force rises a bit before dropping. This can be explained with the second graph. The free calcium concentration drops almost instantly whereas the bound calcium drops more slowly. As

explained is Chapter 1, it takes time for the calcium to be pumped back. This model is therefore consistent with what happens in our muscles.
In the two other graphs, the muscle lengths and velocities are depicted. The muscle total length is constant and the velocity is null since it is in isometric condition. However, the contractile muscle length and velocity change. The contractile elements length shortens, reaches a plateau and then starts going back to its initial length some time after the stimulation has stopped.

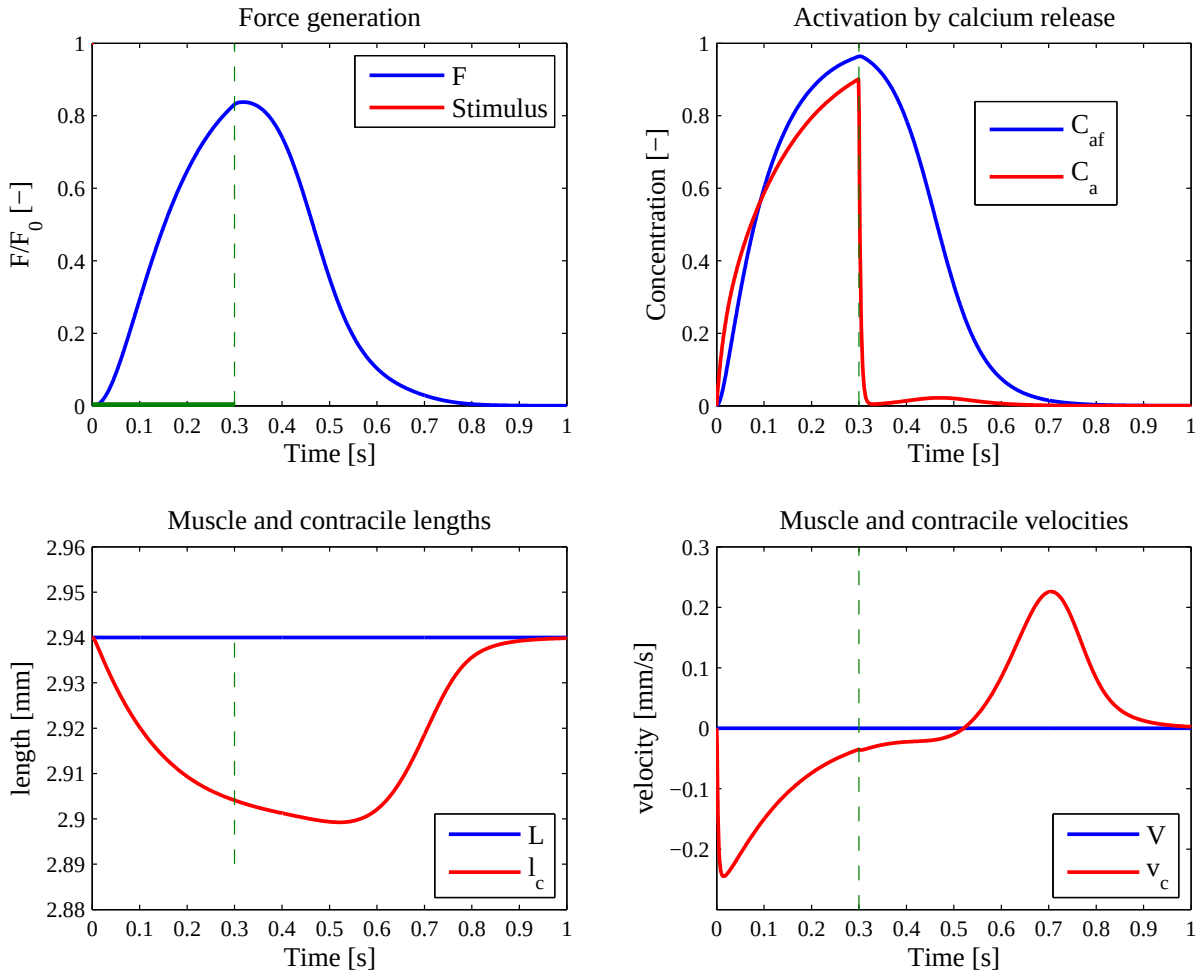

Figure 4.2: Force generation, activation, muscle lengths and velocities for a stimulus of 330 ms in isometric condition. In isometric condition, the muscle maintains its total length (L) and its velocity (V) remains null while the contractile element can vary in length (l_c) and velocity (v_c)
.

In Figure 4.3, three different graphs of force generation can be observed, with three different stimulation times: 50, 330, 700 ms. All of these cases are in isometric condition. In the first graph, with a 50 ms stimulation, the force increases quickly and, after the stimulus ends, decreases slowly. The reached force is quite low. The shape of this function is similar to the physiological case.
In the second graph, with a stimulation of 330 ms already shown in Figure 4.2, the force increases more slowly than for the shorter stimulation but decreases similarly.
In the last case with a stimulation of 700 ms, the generated force reaches a tetanic plateau and starts decreasing much later after the stimulation ends.

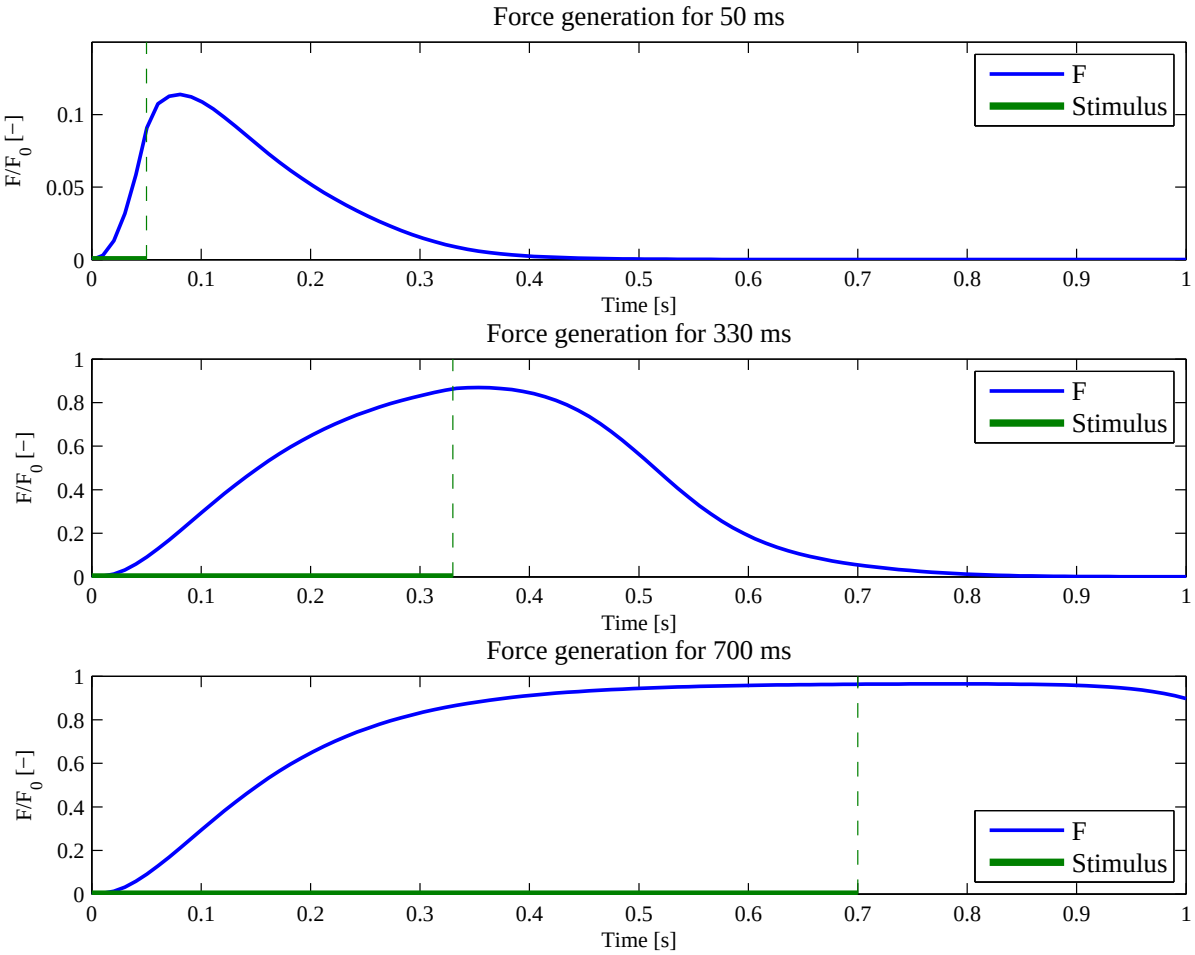

Figure 4.3: Force generation, activation, muscle lengths and velocities for a stimulus of 50 ms, 330 ms and 700 ms. The bold green line represents the stimulation time and the blue curves represent the corresponding normalized force response in isometric condition.

4.5 Pros of the work-dependent deactivation model

The activation dynamics are based on the calcium concentrations in the muscle which has a physical meaning unlike the Hill model which uses a function set between 0 and 1 with no physiological meaning.
This model also considers that the muscle stiffness is not independent of the activation level such as in the Hill model but depends on the activation. That the stiffness depends on the activation was measured in earlier papers [32].
This model tried to be more realistic by considering that there is an inhibition of the formation of cross-bridges mechanism after the end of the stimulation.

4.6 Disadvantages of the work-dependent deactivation model

Even though this model uses the calcium concentrations as activation dynamics, it is still simplified. The values of the rate constants were chosen according to a good fit and do not present a quantitative description of the reality unlike the Huxley and distribution-moment models.

Chapter 5

Multiscale model

5.1 Description

This model was developed by H.E. Makssoud et al. [14] and is based on the Huxley formulation as well as a force-length relationship. It also adds the influence of the velocity on cross-bridge breakage at the microscopic level. Macroscopic properties of skeletal muscle are introduced at the microscopic level. The outputs of this model are the muscle force and the stiffness. This model is controlled by stimulation parameters.

The model is divided into two parts: the activation dynamics and the mechanical model. A global overview of the model can be seen in Figure 5.1. The activation dynamics are controlled by an input stimulation signal that is a rectangular pulse of intensity I and width PW [14].

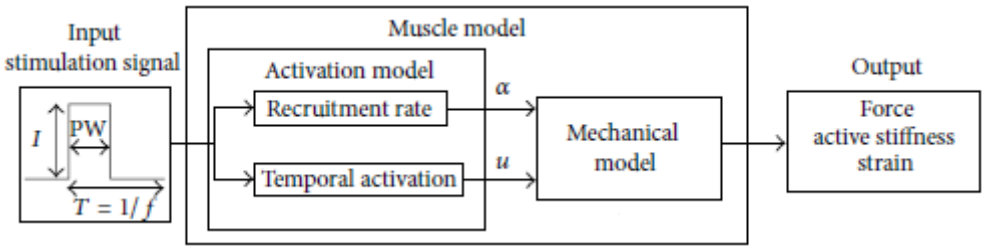

Figure 5.1: Schematical overview of the multi-scale model adapted from [33]. The input of the multiscale muscle model is a stimulation signal of intensity I, width PW and a period of T. The activation model is separated into two parts: the recruitment rate α which corresponds to the number of recruited muscle fibers and determines the activation level as well as the temporal activation $u(t)$. An example of such a function is given in Figure 5.2. The mechanical model has as input these two functions and gives an according force response.

First, the simulation protocol will be given followed by a description of the activation dynamics and the mechanical model. Finally, the pros and cons of this model will be discussed.

5.2 Simulation protocol

This model has been implemented in MATLAB® as the previous models. The set of differential equation given in [14] were integrated with the `ode45` function.

First, the initial conditions such as the muscle-tendon and contractile element lengths and velocities are set. The input for the activation is the intensity and pulse width of a pulse function. Secondly, the activation dynamics are implemented. During a contraction, the calcium concen-

tration reaches a threshold value and the activation function goes from a constant relaxation value, related to the rate of cross-bridge breakage, to a constant contraction value, linked to the rate of actin-myosin cycle.
This model considers a muscle fiber recruitment level that is a function of the pulse intensity and width [14]. An intense pulse or a long pulse will result in a stronger muscle fiber recruitment.

As for the previous models, the initial values for the muscle-tendon and contractile element lengths and velocities need to be set.
The mechanical model is defined on three scales: the sarcomere, the muscle fiber and whole muscle scales. For the three scales, differential equations are given for the stiffness and force. It is in the whole muscle scale that the recruitment level is taken into account and the differential equations are separated for the contracted and relaxed muscle fibers. All these differential equations are based on the distribution moments.
The muscle-tendon and contractile element lengths as well as a force-length relationship are based on a phenomenological Hill-type model [14].

5.3 Activation dynamics

The equations presented in this part can be found in the article presenting this model [14].
In this model, the activation dynamics are based on the number of motor units that are recruited for the whole muscle scale. When an electrical pulse of width PW and intensity I reaches a muscle fiber, the activation function $u(t)$ increases from a value U_r to U_c after a time delay τ. U_c and U_r are the chemical kinetics levels under contraction and relaxation phase. This happens when the calcium ion concentration exceeds a threshold. Since pumping back of the calcium ions takes longer than its liberation, the decrease from U_c to U_r is not instantaneous this time but lasts for a certain time. This can be schematically seen in Figure 5.2. The activation function $u(t)$ is defined by Equation 5.1 [14].

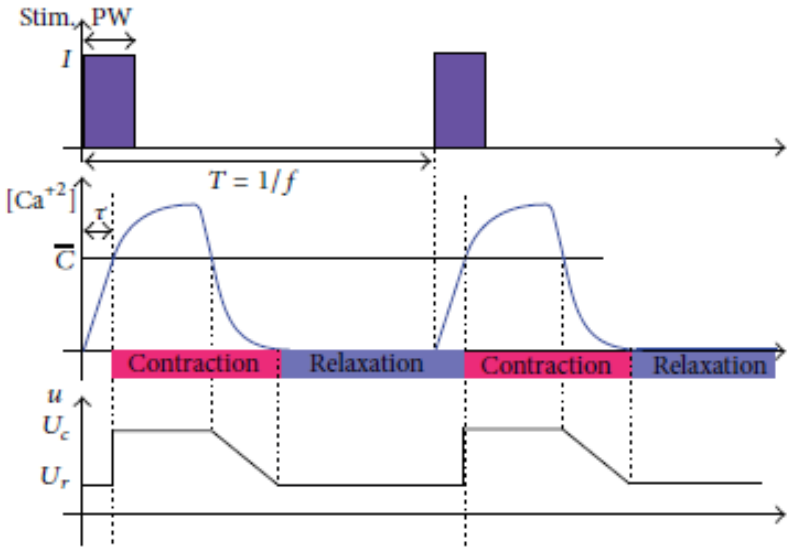

Figure 5.2: Activation dynamics. After a stimulus of intensity I and pulse width PW, the calcium concentration in the muscle increases and if it reaches a threshold value $\bar{C}$, the activation function $u(t)$ goes from a value U_r to a value U_c. It goes back to U_r when the calcium concentration goes under the threshold value. From [33]

$$u(t) = \Pi_c(t).U_c + (1 - \Pi_c(t)).U_r \tag{5.1}$$

With

$$\Pi_c(t) = \begin{cases} 1 & \text{during the contraction phase} \\ \frac{\tau_r - t_r}{\tau_r} & \text{during the relaxation phase of duration } \tau_r \\ & \text{with } t_r \text{ the relative time position} \\ 0 & \text{otherwise} \end{cases} \tag{5.2}$$

Since the activation dynamics depend on the motor unit recruitment, a recruitment model was defined for this model that depends on the current intensity of the stimulation and on the pulse width. Only a fraction α of a total number of N Motor Units is recruited. α is thus the level of recruitment and is defined between 0 and 1. The stronger the intensity of the pulse and/or the longer the pulse, the bigger α becomes. These two parameters I and PW influence the recruitment level quite differently, a recruitment model with those parameters has been defined. It is given by Equation 5.3 [14] where c and d are constants. R is defined by Equation 5.4 [14] where b, a_{PW}, a_I, PW_{max} and I_{max} are constants. q is the total injected charge $q = PW.I$. α is kept to 0 when either I or PW are 0. This recruitment rate is updated synchronously with the stimulation pulses.

$$\alpha(I, PW) = d.\left(\tanh\left(R - c\right) + \tanh\left(c\right)\right) \tag{5.3}$$

$$R = b.\left(1 + a_{PW}\frac{PW}{PW_{max}}\right)\left(1 + a_I\frac{I}{I_{max}}\right)\frac{q}{q_{max}} \tag{5.4}$$

5.4 Mechanical model

The equations presented in this part can be found in the article presenting this model [14].
The mechanical model is based on the Huxley model, and more precisely on the distribution-moment model derived from it by Zahalak [16]. As the name of the models says, the model has a multiscale approach which mean that it combines macroscopic elements from the Hill model and microscopic elements from the Huxley model. The macroscopic Hill-type part is represented in Figure 5.3. The muscle is represented by a contractile element $E_c(u, \alpha)$ with a length L_{c0} and elastic and/or damping elements. What differs from the Hill model is the expression of the force generated by the contractile element which is not a phenomenological relation anymore. It is based on the Huxley model and its distribution-moment approximation and thus based on microscopic relationships.
The passive elements of the model are on the macroscopic level. Two cases are considered (see Figure 5.3): a classical one (Figure 5.3(a)), simpler than the second one (Figure 5.3(b)), that is used in non-isometric conditions or when several muscles interact with each other. The second case (Figure 5.3(b)) is more complex than the first case (Figure 5.3(a)) and used when a single isolated muscle is simulated for more accurate results.

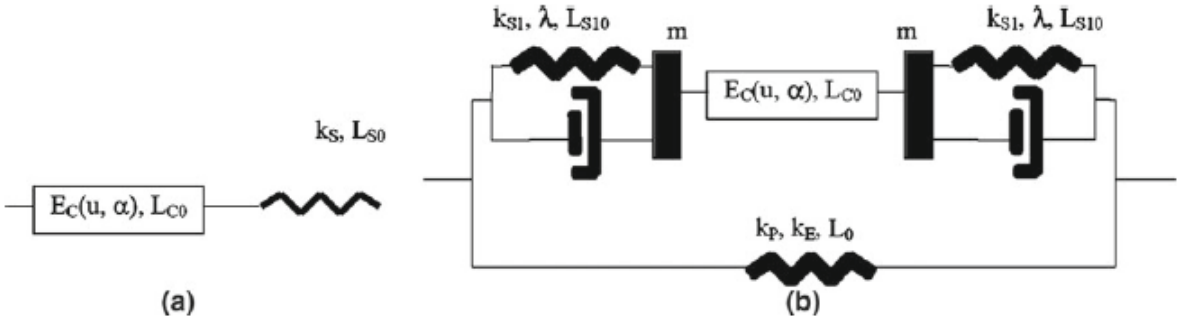

Figure 5.3: Mechanical macroscopic models a) used for non-isometric contraction or multijoint model b)used for isolated model for more accuracy. From [14].

The active element is based on a modified Huxley model to fit the macroscopic scale. This active element is thus based on the microscopic level and has physical meaning. In order to fit the microscopic Huxley model to a macroscopic one, it had to be assumed that all the sarcomeres are identical and contract/relax simultaneously [14]. This is of course not necessarily true. The evolution of the distribution of the fraction of actin-myosin pairs that are attached at time t comes directly from Equation 3.1 defined in Section 3.1 and is given by Equation 5.5 [14].

$$\frac{\partial n}{\partial t} + \frac{S_0}{h}\dot{\varepsilon}_c(t)\frac{\partial n}{\partial \xi} = f(\xi,t).fl(\varepsilon_c) - (f(\xi,t) + g(\xi,t)).n(\xi,t) \tag{5.5}$$

$v(t)$ defined in Equation 3.1 is here equal to $\frac{S_0}{h}\dot{\varepsilon}_c$. S_0 is the sarcomere length at maximum force. h is, as in the Huxley model, the maximum elongation of the myosin spring. $\dot{\varepsilon}_c$ is the time derivative of the relative variation of length of the contractile element defined as $\varepsilon_c = \frac{L_c - L_{c0}}{L_{c0}}$. L_c is the length of the contractile element and L_{c0} is the length of the contractile at maximum force. $fl(\varepsilon_c)$ is the force-length relationship that can be also found in the Hill-type models. This relationship is not present in the Huxley model since it is a microscopic level and does not take the whole muscle into account. In this model however, the macroscopic level is taken into account and the maximum number of actin-myosin pairs that can bind depends on the relative length of the contractile element ε_c. It is defined here by Equation 5.6 [14] which is a Gaussian approximation. b is the same constant as in Equation 5.4.

$$fl(\varepsilon_c) = \exp\left(-\frac{\varepsilon_c^2}{b}\right) \tag{5.6}$$

The rates f and g were modified to fit the activation dynamics of this model. They are defined by Equation 5.7 [14]. The detachment rate g is defined here so that it increases with the relative velocity between the actin and myosin filaments. This was done in order to give a more physiological meaning to it since there is a greater probability for the cross-bridges to break at higher velocities.

$$f(\xi,t) = \begin{cases} \Pi_c(t).U_c & \text{if} \quad \xi \in [0,1] \\ 0 & \text{elsewhere} \end{cases} \tag{5.7}$$
$$g(\xi,t) = u(t) + a|\dot{\varepsilon}_c(t)| - f(\xi,t)$$

Sarcomere scale Just as in the Huxley model, the myosin heads are considered to be attached to the myosin filament through an elastic linkage with a constant stiffness [14]. The moments Q_0 and Q_1 of the distribution-moment model, presented in Section 3.2, were used to generate the

stiffness and generated force of a sarcomere (Equation 5.8 where k_0 is the maximum stiffness when all the available cross-bridges are attached).

$$\begin{aligned} k_{sa}(t) &= k_0.Q_0(t) \\ F_{sa}(t) &= k_0.h.Q_1(t) \end{aligned} \tag{5.8}$$

Using the distribution-moment approximation and the f and g rates defined in Equation 5.7, Equation 5.9 [14] can be obtained. Due to the assumption that all sarcomeres are identical, the total force is the sum of all the forces generated by the sarcomeres and allows to link the microscopic scale to the macroscopic one.

$$\begin{aligned} k_{sa}(t) &= -(u + a.|\dot{\varepsilon}_c|)k_{sa} + k_0.\Pi_c.U_c.fl(\varepsilon_c) \\ F_{sa}(t) &= -(u + a.|\dot{\varepsilon}_c|)F_{sa} + k_{sa}.S_0.\dot{\varepsilon}_c + \frac{1}{2}.k_0.h.(1 + 2.y_0)\Pi_c.U_c.fl(\varepsilon_c) \end{aligned} \tag{5.9}$$

The previous equations have been implemented according to the simulation protocol and the article presenting the model. Figure 5.4 shows graphically the stiffness and force response of a sarcomere for a specific activation shown in the first subplot.

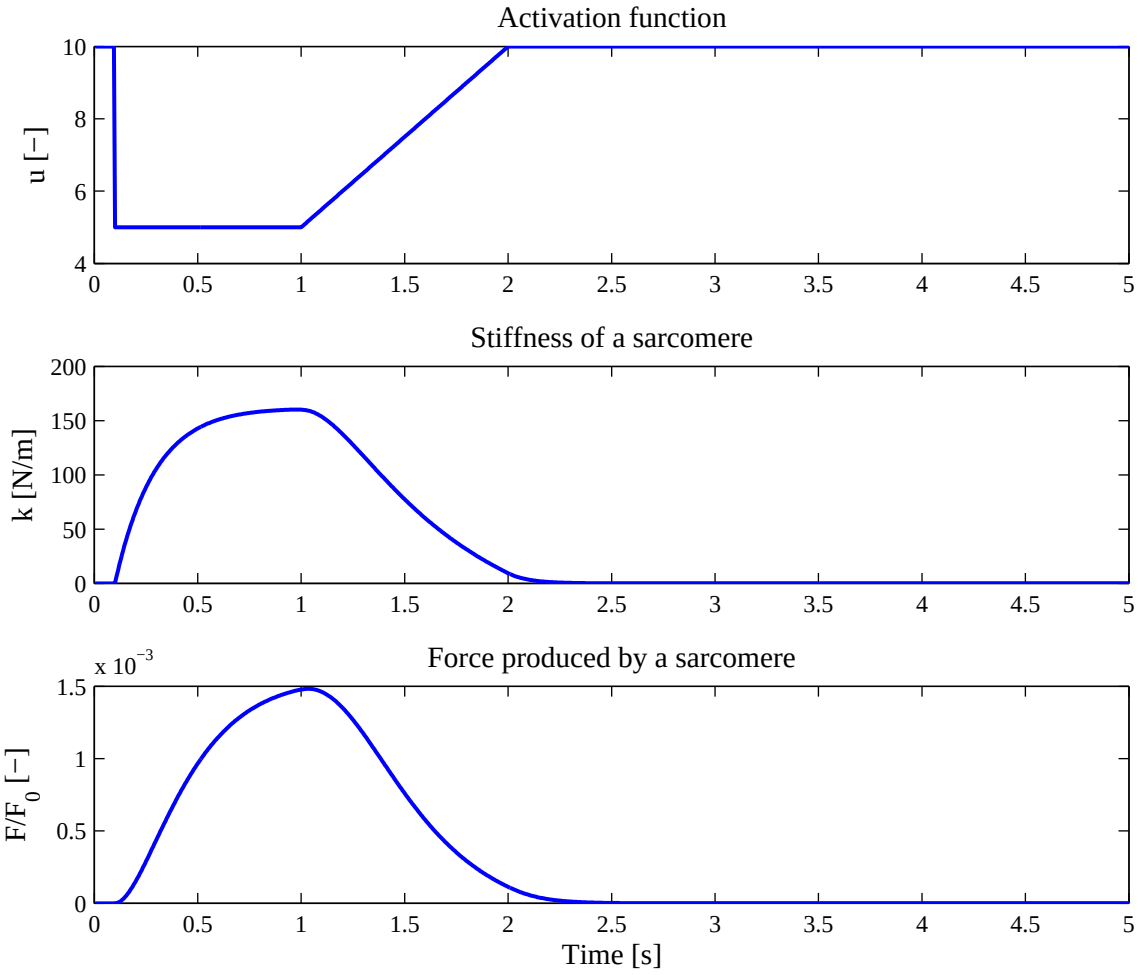

Figure 5.4: Sarcomere stiffness and generated force for a given activation function u. u varies between two threshold values that were given in [34]. The according sarcomere stiffness and normalized generated force were computed using Equation 5.9.

From the sarcomere to muscle fiber scale Since it is considered that a muscle fiber is composed of identical sarcomeres in series, the model can be extended to the muscle fiber level. So, $k_{fi} = k_{sa}\frac{S_0}{Lc0}$ and $F_{fi} = F_{sa}$ as in Equation 5.10.

$$\begin{aligned} k_{fi}(t) &= -(u + a.|\dot{\varepsilon}_c|)k_{fi} + \frac{S_0}{L_{c0}}k_0.\Pi_c.U_c.fl(\varepsilon_c) \\ F_{fi}(t) &= -(u + a.|\dot{\varepsilon}_c|)F_{fi} + k_{fi}.L_{c0}.\dot{\varepsilon}_c + \frac{1}{2}.k_0.h.(1 + 2.y_0)\Pi_c.U_c.fl(\varepsilon_c) \end{aligned} \tag{5.10}$$

From the muscle fiber to whole muscle scale It is at the whole muscle scale that the recruitment model steps in [14]. There a three possible groups of the motor units: αN contracting, βN relaxing and $(1 - \alpha - \beta)N$ completely relaxed motor units. The contribution of group of completely relaxed motor units can be discarded. The groups of contracting and relaxing motor units are treated separately.
Since the whole muscle is composed of muscle fibers working in parallel, the stiffness and force generated by the muscle are the sum of the fiber dynamics given by Equation 5.10.
So for the group of αN contracting motor units, the dynamics of the stiffness and generated force become Equation 5.11 [14].

$$\begin{aligned} k_{cu}(t) &= -(U_c + a.|\dot{\varepsilon}_c|)k_{cu} + \alpha.N.U_c.\frac{S_0}{L_{c0}}k_0.fl(\varepsilon_c) \\ F_{cu}(t) &= -(U_c + a.|\dot{\varepsilon}_c|)F_{cu} + k_{cu}.L_{c0}.\dot{\varepsilon}_c + \frac{1}{2}.\alpha.N.U_c.k_0.h.(1 + 2.y_0).fl(\varepsilon_c) \end{aligned} \tag{5.11}$$

The same is done for the group of βN relaxing motor units (Equation 5.12).

$$\begin{aligned} k_{ru}(t) &= -(U_r + a.|\dot{\varepsilon}_c|)k_{ru} \\ F_{ru}(t) &= -(U_r + a.|\dot{\varepsilon}_c|)F_{ru} + k_{ru}.L_{c0}.\dot{\varepsilon}_c \end{aligned} \tag{5.12}$$

The total stiffness is $k_c = k_{cu} + k_{ru}$ and the total generated force is $F_c = F_{cu} + F_{ru}$.

The equations for the whole muscle scale have been implemented and Figure 5.5 shows the force response and corresponding stiffness to two recruitment level: a short one and a longer one. In the first case of short lasting recruitment level, the force response is a twitch. In the second case with a longer recruitment, the force reaches a peak until the recruitment level stops.

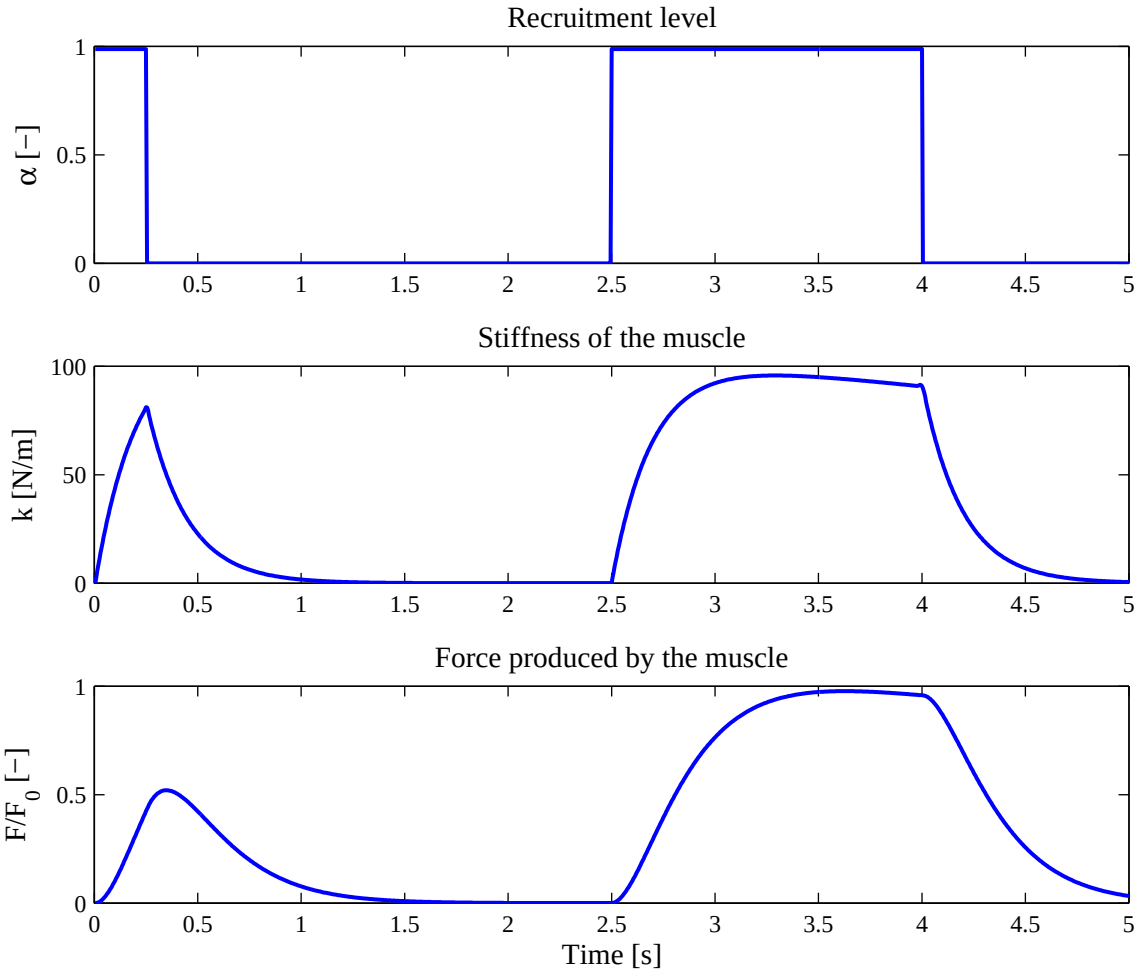

Figure 5.5: Whole muscle stiffness and generated force for a given recruitment level. The muscle stiffness and normalized generated force were computed using Equation 5.11 and 5.12.

5.5 Pros of the multiscale model

The parameters have both physiological and biomechanical meanings.
The Hill model presents limitations for the full range of movements. The multiscale model, which is itself based on the Huxley model, also considers microscopic muscle properties. This model improves the fast and slow contraction patterns that the Hill model cannot correctly approach.

5.6 Disadvantages of the multiscale model

In order to link the microscopic level to the macroscopic one, some assumptions have been made that are not necessarily correct. For instance that all the sarcomeres are identical.
The activation dynamics are too simplified compared to the distribution-moment and work-dependent deactivation models.

Part III

Comparison of the models for a single muscle

Introduction of Part III

Few muscle models comparison have been conducted and presented in the literature in the past. Tobias Siebert et al. [35] compared the nonlinearities from two common Hill-type models. F. Romero and F.J. Alonso [36] did something similar with more Hill-type models. S.H. Yeo et al. [37] compared phenomenological models during isotonic shortening. Other articles in the literature have a similar purpose. A few articles as the one by K. Jovanovic et al. [38] compared the Hill and Huxley models in terms of accurancy and efficiency. Most muscle model comparisons focus on Hill-type models and a few on the the Hill and Huxley models which are the two extreme models: a phenomenological and a biophysical model. The purpose of this master thesis, and more specifically of this part and the following one, is to compare four quite different types of muscle models: a Hill-type model since it belongs to the most used models, the work-dependent deactivation model with more physiological activation dynamics and a variable muscle stiffness, the multiscale model which tries to compute the force-response on three different muscle scales and the distribution-moment model which is based on the Huxley model.

The previous part introduced and described different muscle models individually. For each model, its strengths and weaknesses were given. However, this does not tell if one of the presented models is better than the others. In order to find whether there is a better model or a model more appropriate for a specific case, the presented models need to be compared to each other. This is the purpose of this part and the next one.

In this part, the models for isolated muscles are compared to each other.
The first chapter will compare the similarities and dissimilarities between the models in terms of the muscle structure defined in the models, the activation dynamics, their computational time as well as other criteria. A summary of this will be given in form of a comparative table.
Then, isolated muscles will be modelled with the presented models for different activation functions and the force-responses will be compared.

The second chapter will focus on the impedance of the isolated muscle modelled with the different models. First, a definition of the impedance will be given. Then, the force-response to an oscillating velocity will be shown and compared for the models. Finally, the impedance for a range of frequencies going up to 100Hz will be given for each model and compared.

The next and final part will focus on the comparison of the models implemented to model an articulation. Comparing the models in the case of an isolated muscle as in this part is interesting and gives useful information about the similarities and differences between the models. However, an isolated muscle cannot represent the main function of skeletal muscles: moving the body segments. To do that, the muscles need to be connected to bones connected by a joint. Thus the next part will focus on the comparison of the models in a more realistic configuration.

Chapter 6

Analysis of the similarities and dissimilarities between the models

6.1 Comparison of the muscle structures in the different models

All models are based on a similar structure: a contractile element and a series elastic element representing the tendon and the passive part of the muscle.

The Hill model is, as was already mentioned, a phenomenological model based on interpretations of input and output data obtained during experiments. Hence, the relationships of this model are based on experimental data and do not present a physiological meaning. The contractile element is thus represented by a black box.

In opposition, the distribution-moment model is a biophysical model and the relationships of this model have a physiological meaning. The contractile element of the distribution-moment model is made of the sarcomeres, the basic unit of muscle tissue. The force-generation is modelled by the interaction of the cross-bridges from the myosin filaments with the actin sites of the actin filaments.

A schematic representation of these two models can be seen in Figure 6.1.

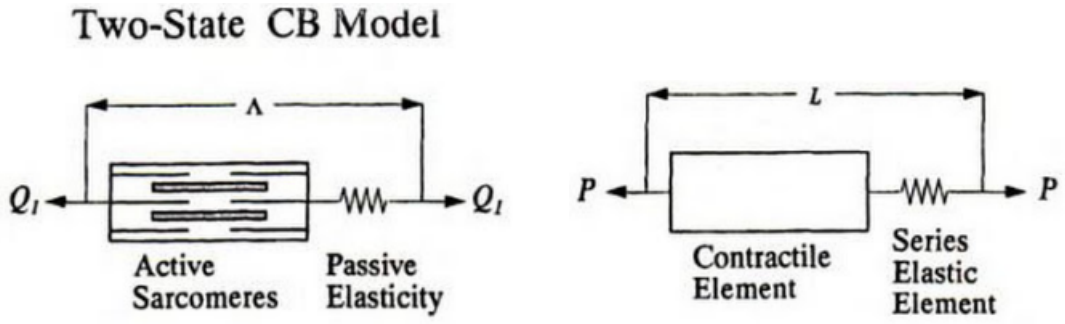

(a) Distribution-moment model (b) Hill model

Figure 6.1: Comparison between the schematic muscle structure of the distribution-moment (two-state cross-bridge model) and the Hill models. From [39]. Λ and Q_1 represent the stretch ratio and normalized force of the distribution model respectively. L and P represent the muscle length and force of the Hill model respectively.

The two other models, the work-dependent deactivation and multiscale models are somewhat in between these two structures.

The work-dependent deactivation mechanical model has a similar structure to the Hill model. The force generated by the contractile element (Equation 4.3) is very similar to the one of the Hill model given by Equation 2.3. The main difference between the work-dependent deactivation model and the Hill model are the activation dynamics.

The multiscale model is, as already mentioned, based on both distribution-moment and Hill models. This model gives the force-response for three different scales: sarcomere scale, muscle fiber scale and whole muscle scale. The generated force and muscle stiffness of all three scales are based on the distribution-moment formulations. For the whole muscle scale, elements from the Hill model such as an elastic element in series were added.

Hence, all four models present a similar structure but the modelling of the contractile element differs. The two extremes are the Hill model, which is purely phenomenological, and the distribution-moment model, which is biophysical. The work-dependent deactivation and multiscale models are in between with the first one being closer to the Hill model and the second one being closer to the distribution-moment model.

6.2 Activation dynamics in the different models

The activation of the contractile element is modelled differently in each of the presented models. As for the comparison of the structures in the previous section, the Hill model and the Huxley model are the two extreme cases.

In the Hill and Hill-type models, the activation is usually a function set between 0 (muscle fully relaxed) and 1 (muscle fully activated). Instead of using the term "activation", A.V. Hill introduced the term of "active state". The "active state" is defined as the tension generated by the contractile element without change of length after the beginning of the excitation [40]. The activation is considered to be virtually instantaneous with, often, an activation plateau. This active state was considered to be independent of the muscle length.
A widely used expression to obtain the muscle activation from a muscular excitation signal (rectangular pulse function) into an activation signal is given by Equation 6.1 [36]. These dynamics are represented in Figure 6.2.

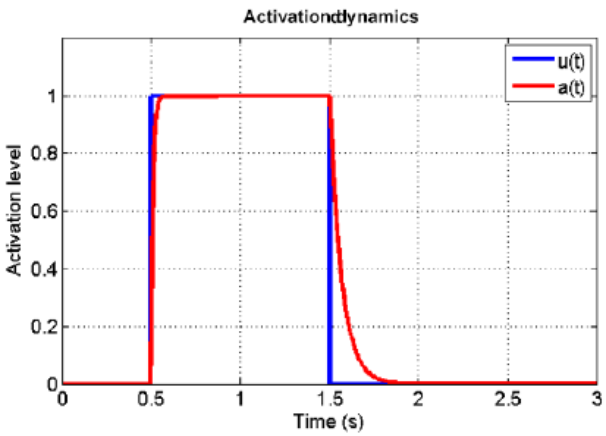

Figure 6.2: Widely used activation dynamics for the Hill-type models. From [36]

$$\dot{a} = (u(t) - a(t))(t_1 u(t) + t_2) \tag{6.1}$$

With u the neural excitation, a the muscle activation and t_1 and t_2 time constants. Another possibility for the activation dynamics of the Hill-type model is to convert an EMG signal into a muscle activation [41].

The Huxley and distribution-moment models consider the active state as the relative amount of calcium bound to troponin [40]. In the distribution-moment model, it is considered that the calcium-troponin interactions are coupled with the actin-myosin interactions. The activation

dynamics of the distribution-moment model is therefore function of the calcium concentrations inside the muscle. The distribution-moment model takes into account the sarcomere length since the rate functions f and g depend on it. Experiments [42][43][44] suggest that the activation dynamics depend indeed on the calcium-troponin interactions and the muscle dynamics [40].
The distribution-moment model, unlike the Huxley model, distinguishes between two activation cases: the "loose" and the "tight" coupling. Both couplings assume that myosin cannot bind to actin until to calcium ions are bound to troponin [40]. The difference between the two is that in the loose coupling, the calcium-troponin interactions are completely independent of the actin-myosin interactions whereas they are considered dependent in the tight coupling [16]. The experiments mentioned earlier showed indirect evidence that the tight coupling is more realistic.
In addition to the activation, the model also considers the fraction of cross-bridges in the contractile tissue that are available to interact with actin. This fraction is set between 0 and 1 and is assumed to be a function of the muscle length.

The work-dependent deactivation model considers, as the Huxley and distribution-moment models, the activation dynamics to be linked to the concentration of calcium inside the muscle. The activation dynamics of this model are however a simplified version of the Huxley and distribution-moment models and are two inter-dependent differential equations of the concentration of free and bound calcium. In addition, four rates are introduced [13]:

1. A constant calcium release rate from the sarcoplasmic reticulum.
2. A constant rate for binding of calcium ions to the sarcoplasmic reticulum.
3. A rate for binding of calcium ions to the filaments.
4. A rate for the release of calcium ions to the filaments.

In a previous version of the model, the last two rates were considered constant whereas they are considered variable in the version of the model presented in this master thesis. The constant rates and the initial values of the variable rates were found by fitting the model to isometric data and have thus less biophysical meaning than the activation dynamics of the Huxley and distribution-moment models [13].

The activation dynamics of the multiscale model are also based on the calcium concentration in the muscle. It is also a simplified version of the Huxley and distribution-moment models. Unlike the work-dependent deactivation model, the activation dynamics are not governed by differential equations. This model considers that when the concentration of released calcium in the muscle reaches a threshold value, the muscle fiber begins to contract and stops once the concentration is below the threshold value again [14]. This model considers that the calcium release in the muscle is instantaneous but that the calcium uptake is slower. This has a physiological meaning and has been explained in Section 1.3 of Chapter 1. However, it is a considerable simplification compared to the Huxley model.
This model incorporates the concept of level of muscle fiber recruitment. This level of recruitment is set to be 0 (no fiber recruitment) and 1 (maximal fiber recruitment). It is similar to the fraction of cross-bridges in the contractile tissue that are available to interact with actin of the distribution-moment model. In the distribution-moment model, it is at the cross-bridge scale (microscopic) whereas in this model it is at the whole muscle scale (macroscopic).

6.3 Computation time

The computation time of the four different models presented in the previous part have been measured. All models were set to determine the isometric muscle response for a total simulation time of 1 and 5 seconds with 1000 and 5000 time steps respectively. The models were run a

hundred times and the computation time presented in Table 6.1 corresponds to the mean time value of the 100 measured computation times. This was done on a computer with the following processor: Intel(R) Pentium(R) CPU N3540 @ 2.16GHz.

Of the four muscular models, three have similar computation times of less than a second for the simulation representing 5 seconds. The distribution-moment model takes more time due to the fact that it has to numerically solve Equation 3.14 for the muscle activation. This slows down the computation. It is also the most complex of the four models and presents a computational burden.

Model	**Computation time for 1 s**	**Computation time for 5 s**
Hill-type (Haeufle)	0.13 s	0.47 s
Distribution-moment	3.94 s	18.44 s
Work-dependent deactivation	0.14 s	0.72 s
Multiscale	0.10 s	0.38 s

Table 6.1: Mean computation time of the different models for a simulation time of 1 and 5 seconds

6.4 Muscle pennation

None of the analysed models take into account the pennation of the muscle and consider thus the muscles as parallel-fibered muscles. There are however other models that do take muscle pennation into account. Hill-type models such as suggested by F.E. Zajac [46] or D.G. Thelen [45] for example. A scheme of the muscle-tendon unit with pennation angle for a Hill-type model is shown in Figure 6.3.

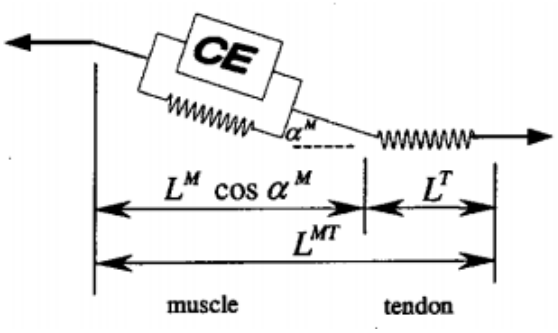

Figure 6.3: Schema of muscle-tendon unit with a muscle pennation angle α^M. l^M corresponds to the length of the muscle while $l^M \cos(\alpha^M)$ corresponds to the muscle length component in the axis parallel to force generated by the muscle-tendon unit. L^T is the tendon length and L^{MT} to the muscle-tendon unit length. From [45]

Only the force component of the muscle parallel to the tendon axis contributes to the force generated by the muscle-tendon unit. The corresponding length of the muscle parallel to the tendon axis is thus $L^M \cos(\alpha^M)$ where L^M is the muscles length and α^M is the pennation angle. Since only the force component parallel to the tendon axis contributes to the muscle-tendon unit, $F^T = F^M \cos(\alpha^M)$ with F^M the generated muscle force and F^T the force generated by the muscle-tendon unit.

Even if the four analysed models do not take muscle pennation into account, it can be incorporated without problem into the Haeufle model. It can also be incorporated into the work-dependent deactivation and multiscale (on the whole muscle scale) models since the mechanical models are, partially or completely, based upon the Hill model.

6.5 Macroscopic comparison of the models

The previous section and what has been said about the different models in the second part, gave some insight about the similarities and dissimilarities between the models. The most important features of models are given in Table 6.2. It gives a comparison of the four different models according to the following criteria.

Computation time: based on the mean times reported in Table 6.1. The distribution-moment model is by far the slowest of the four models. The fastest models are the Haeufle and multiscale models followed by the work-dependent deactivation model.

Activation: based on what kind of activation dynamics are used by the model. The activation of the Haeufle model is a function between 0 and 1. The activation of the three other models is based on the calcium reactions with the muscle. The distribution-moment and multiscale model also present a recruitment level of the muscle fibers as activation element.

Inputs: based on what are the inputs needed by the model. All of them take as input an activation element. For the Haeufle model it is the activation function. For the distribution-moment model it is the impulse train function $\chi(t)$ as well as the fraction of cross-bridges available for interaction with the actin filament. The work-dependent deactivation model takes as input a stimulation time. The multiscale model takes as input a pulse function with a specific intensity and width.

Outputs: based on what does the model generate on basis of the inputs. All models have as output the force-response of the muscle to the inputs. It is the only output of the Haeufle and work-dependent deactivation models. The two other models give additional outputs. The multiscale model also gives the muscle stiffness as a function of time. The distribution-moment model also gives the muscle stiffness and additionally the stored elastic energy inside the contractile element.

Muscle-dependent parameters: whether the model needs many parameters describing the muscle. In the Haeufle and work-deactivation models only a few are needed: the muscle and contractile element optimal lengths. Most parameters of these models are fitting parameters without a physiological meaning. The distribution-moment model needs many muscle dependent parameters: all the activation parameters such as $c*$, ρ, τ_0^{-1} or the rate functions f and g. They all have a physiological meaning and have to be measured experimentally. The multiscale model is in between these two extremes: based on the distribution-moment model, it still needs more parameters than the Haeufle or work-dependent deactivation model but because of the simplified activation dynamics it needs less then the distribution-moment model itself.

Pennation: whether the pennation of a muscle is taken into account in the model or if it could be added to the model. All four models do not take muscle pennation into account but for three the models, it could be added as discussed in Section 6.4.

Physical meaning: whether the model is more phenomenological or biophysical. The most phenomenological model is the Haeufle model which is a Hill-type model. The model with the most biophysical meaning is the distribution-moment model where almost any constant or rate has a physiological meaning. The two other models are somewhere in between these two extremes.

Criteria	**Hill-type**	**DM**	**WDD**	**Multiscale**
Computation time	Fast	Slow	Rather fast	Fast
Activation	Function between 0 and 1	Based on sarcoplasmic Ca^{++} release + fraction α	Based on sarcoplasmic Ca^{++} release	Based on sarcoplasmic Ca^{++} release + recruitment level α
Inputs	- Activation function	- Impulse function $\chi(t)$ + fraction α	- Stimulation time	- Pulse intensity I and width PW
	- Initial muscle and contractile element lengths and velocities	- Initial muscle length and velocity	- Initial muscle and contractile element lengths and velocities	- Initial sarcomere or muscle length and velocity
Outputs	- Muscle force	- Muscle stiffness, force and stored elastic energy	- Muscle force	- Muscle stiffness and force
	- New values for lengths and velocities	- New values for lengths and velocities	- New values for lengths and velocities	- New values for lengths and velocities
Muscle-dependent parameters	Few	Many	Few	Intermediate
Pennation	Can be incorporated	No	Can be incorporated	Can be incorporated
Physical meaning	Phenomenological	Biophysical	Both	Both

Table 6.2: Comparison table of the different models according to the computation time, the activation mechanics, the inputs/outputs, the needed parameters, whether the muscle pennation is taken into account as well as the biophysical meaning of the model.

6.6 Comparison of the force responses for similar activations

Each model gives an output muscle force to an input activation, muscle length and velocity but each model computes it differently. For the same inputs, the models compute the force differently on the basis of what the model focuses upon and the mathematical formulations it uses. How similar or dissimilar are these force responses to the same inputs? To compare them, the normalized force response for similar activations of the different muscle models have been computed in Figure 6.4 and Figure 6.5.

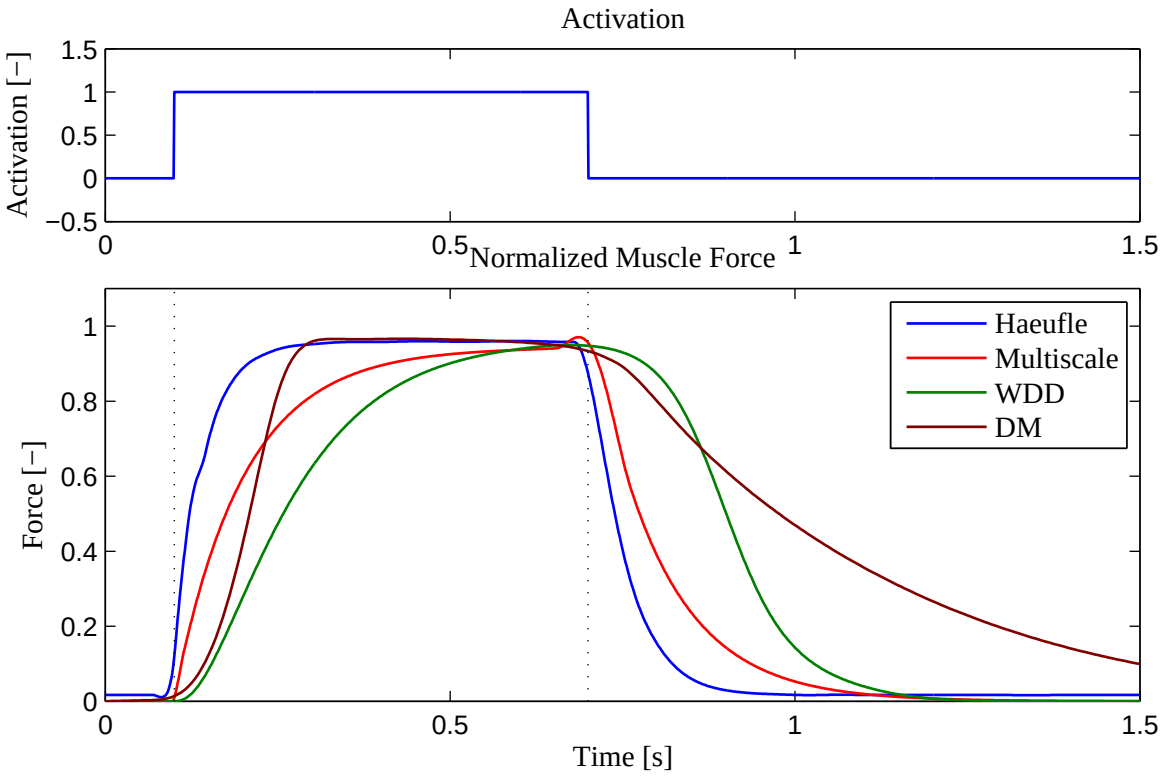

Figure 6.4: Comparison of the isometric force response for a similar activation. For the work-dependent deactivation model (WDD), the activation input is the stimulation time and the stimulation is on when the activation function on the upper graph is equal to one. DM corresponds to the distribution-moment model. The activation time starts after 0.1 seconds and lasts for 0.6 seconds

Figure 6.4 shows the force response for a single activation that lasts 0.6 seconds for the different models. The force responses are quite similar and start decreasing when the stimulation stops. Only the work-dependent deactivation model (WDD) starts decreasing later because the controllable activation is the stimulation time. It was already shown in Chapter 4 that the force starts decreasing a bit later than the deactivation stops.
The time needed by each model to reach the peak force and to go back to a force value close to zero are quite dissimilar.
The Haeufle model reaches its peak value the fastest and has thus a longer plateau. It is also the model where the force response decreases the fastest after the end of the stimulation.
The work-dependent deactivation model reaches its peak value the latest and does not present a plateau. It is due to the fact that the activation is controlled by the stimulation time mechanism which is too short. A longer activation time would have induced a plateau for this model as well.
The distribution-moment model (DM) reaches its peak value second and presents a plateau like the Haeufle model. It is the model that starts decreasing first and needs the longest to go back

to its initial state.
The multiscale and Haeufle model present a rather abrupt change in force when the activation stops unlike the work-dependent deactivation and distribution-moment models which decrease smoothly. It is even more blatant in Figure 6.5 with an oscillating activation.

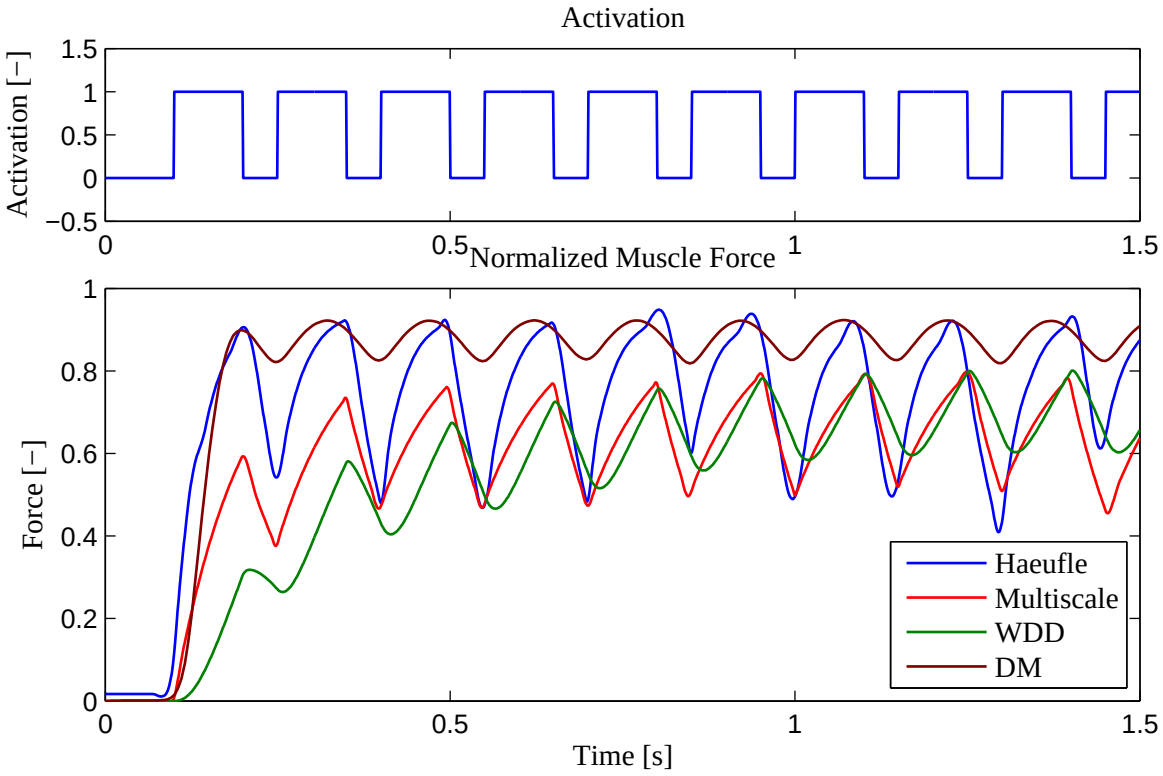

Figure 6.5: Comparison of the force response for a similar oscillating activation with a period of 0.15 seconds. For the work-dependent deactivation model (WDD), the activation input is the stimulation time and the stimulation is on when the activation function on the upper graph is equal to one. DM corresponds to the distribution-moment model.

Figure 6.5 presents an oscillating activation of 0.1seconds with a period of 0.15 seconds varying between 0 and 1. It can be observed that the force-response simulated with the work-dependent deactivation model presents an increasing unfused tetanus that comes closest to what is represented in Figure 1.8 of Chapter 1. The three other models reach the peak force at the first activation step. This is probably due to the fact that the work-dependent deactivation model takes the longest to reach its peak force in isometric condition as can be observed in Figure 6.4.

Unlike the other three models, the distribution-moment model does not present an abrupt change in force when the activation stops. The force response of this model corresponds the most to the unfused tetanus presented in Figure 1.8. This is due to the activation dynamics based on the calcium concentration. The activation of the distribution moment is controlled by the impulse function $\chi(t)$ (here impulses with a period of 0.15 seconds). The impulse function controls the calcium concentration and thus the activation factor r. The complex activation dynamics of this model give a smooth oscillating response for an oscillating activation.
The work-dependent deactivation model activation dynamics are also based upon the calcium concentration but are simplified and controlled somewhat like a switch: the rate k_1 in Equation 4.1 is negligible when the stimulus is off and the rate k_2 is negligible when the stimulus is on. The concentration of free calcium concentration C_a decreases abruptly when the stimulus stops. The concentration of bound calcium does not change as abruptly but depends on the free calcium

concentration that does. This can be observed on Figure 4.2. For a single activation an in Figure 6.4, the decrease after the activation stops is smooth. For an oscillating activation however, the force response is not as smooth anymore.
The multiscale model simplified even more the activation dynamics making the force change at the end of the activation more abrupt than for the work-dependent deactivation and distribution-moment models.
The Haeufle model drops also quite abruptly when the activation stops. This is because of the too simple activation dynamics of this model.

6.7 Discussion

All models have specific features and focus on different elements. The distribution-moment model has the most physiological meaning from the four in the mechanical model as well as the activation dynamics. The outputs of this model are the muscle stiffness, generated force and stored elastic energy unlike most models where the only output is the generated muscle force. However, it is also the slowest to compute due to its higher complexity. The high biophysical meaning of the model requires to experimentally measure the constants and rates needed by the model which may be difficult or impossible to measure directly.

The multiscale model is partially based on the Huxley and distribution-moment model and is faster than the distribution-moment model. The simplifications made the model faster but some physiological veracity was lost in the process. The outputs of the model are the generated force as well as the stiffness of the muscle. Its main strength compared to the other models is that it models the muscle force-response and stiffness on microscopic and macroscopic level.

The work-dependent deactivation model is a fast and simple in comparison to the distribution-moment and multiscale models. The activation dynamics are simpler compared to the activation dynamics of the distribution-moment model but the attachment and detachment rates have lost their physiological meaning. This model also considers the stiffness to be variable depending on the calcium concentration instead of a constant making the model more realistic than models that consider it as a constant.

The Hill-type model has the least physiological meaning from the four analysed models but is the simplest. Despite that, the force response of the muscle is similar to the other models. The focus of this Hill-type model, which added a damper in parallel to the series elastic element, is set upon the eccentric movements unlike other Hill-type models which focus on something else.

None of the presented models take into consideration the pennation or the fatigue of the muscles. Even a complex model such as the Huxley or distribution moment model do not take all the characteristics of muscles into account.

Finally, the comparison of the force responses for a single activation or an oscillating activation shows that the distribution moment model has the most physiological response as it does not change too abruptly when the activation stops and restarts before the muscle relaxed. This comes however with a price: a high computation time. The work-dependent deactivation model has also a smooth force decrease after the end of the stimulation but only in the case where there is only one activation and no second activation starts before the end of the muscle relaxation. In the case of oscillating activation, the force response is still smoother than for the multiscale and Haeufle model, especially when a new stimulation starts. The Haeufle and multiscale models present force responses with more abrupt changes when the activation stops or restart in both activation cases.

Chapter 7

Mechanical impedance of the isolated muscle

The previous chapter partially analysed the force response to an oscillating activation. How does the muscle react to a variable, sinusoidal velocity with specific frequency? How differently, or similarly, do the muscle models respond to such a perturbation? The purpose of this chapter is to answer these questions. First, the mechanical impedance will be defined. Then the simulation protocol used to calculate the impedance will be explained. Before looking at the impedance as a function of frequency, the force response in the time domain for a few perturbation frequencies will be shown and commented. Finally, the impedance, in the frequency domain, will be given for the four models and discussed.

7.1 Definition

The mechanical impedance is defined as the relationship between the deformation kinematics, the velocity, and the resulting dynamics, the force. It corresponds to the ratio between the force change to the displacement change that are acting on a mechanical system. It defines the linear or rotational stiffness and damping characteristics of the system under consideration which are important for the functioning of the limbs. [47]

A linked concept to the mechanical impedance is the admittance. The admittance relates the input dynamics to the resulting output kinematics. [47]

7.2 Simulation protocol

The impedance of the muscle models presented in part II were computed. In order to do this, the velocity of the whole muscle was controlled and set to a sine wave

$$v(t) = A\sin(\omega t)$$

with $\omega = 2\pi f$, the angular frequency in rad/sec and A the amplitude of the perturbation signal.

The resulting force output, after a certain stabilization time, is a signal that can be approximated by a sine wave of the form

$$F(t) = B\sin(\omega t - \varphi)$$

with B the amplitude of the output signal and φ the phase shift in radians. If the models were Linear Time Invariant (LTI), the output signal would be a perfect sine wave but since it is not the case with the presented muscular models, the output can only be approximated by a sine function. The graphs of the force responses to a sinusoidal velocity input shown later in this chapter show

that the force responses have a sinusoidal-like behaviour and that this approximation can be made.

The time frame was set so that the activations, and thus the force-responses, had the time to stabilize. The activation was set to its maximum for all models. The impedance amplitude corresponds to the amplitude of the output force signal, B, divided by the amplitude of the input velocity amplitude, A, at different frequencies.

The next section discusses the force-responses of the models in the time domain to velocities of a few selected frequencies. This first step allows to see how the muscle responds to an input velocity. In the section after that, the same has been done except that not only a few frequencies were selected but a frequency range up to 100 Hz has been chosen. For each frequency, the force amplitude has been measured and divided by the velocity amplitude to obtain the impedance. The impedance is then represented in a graph in frequency domain and not in the time domain as in the preceding section.

7.3 Force-responses of the models to velocities with different frequencies

Before discussing the impedance of the different models, the force responses of the models to a same velocity amplitude with different frequencies are analysed. Figure 7.1 shows some input velocities and the force responses of the different models. For all the models, the activation was set to its maximum and stabilized around a constant value. The force responses presented in Figure 7.1 are represented between two and four seconds, after the models reached their constant maximum activation value.

It can be observed in Figure 7.1 that the force responses to a same velocity input differ for each model. The multiscale and work-dependent deactivation models have very similar force responses. The Haeufle model gives similar force responses but with a higher amplitude than with the two other models. The distribution-moment model presents a higher amplitude at a frequency of 10Hz than below unlike the other models.

For the work-dependent deactivation model and distribution-moment models, the force response to the velocities are centred around the isometric force-response whereas for the multiscale model is is slightly shifted below the isometric force. In the Haeufle model, it is shifted upwards. This can be explained by the fact that this model focuses on eccentric muscle movements and the force response is bigger for lengthening velocities ($V > 0$) than for shortening velocities ($V < 0$). In his article presenting the model [10], it was stated that in eccentric contractions, and thus during positive contraction velocities, the muscle produces forces exceeding the forces produces in isometric conditions. This can be observed in the four presented models but is more expressed in the Haeufle model.

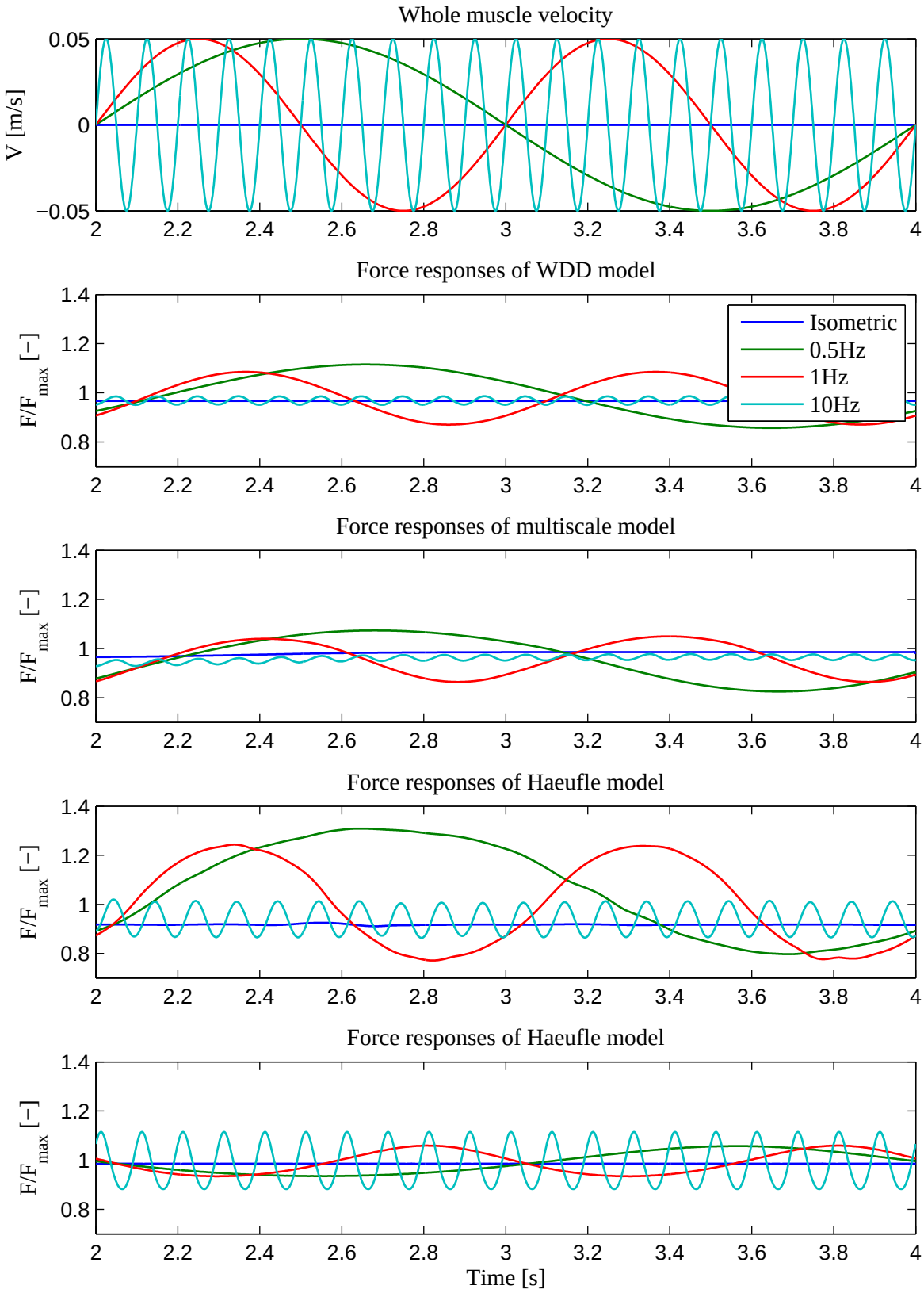

Figure 7.1: Force responses of the different models to input velocities for different frequencies. The first graph shows the different velocities, of same amplitude but different frequencies. The other graphs show the corresponding force responses for the different models.

7.4 Impedance of the isolated muscle models

For the impedance, the same was done as in the previous section except that a wider range of frequency values were used. For each frequency, going up to 100Hz, the force amplitude was calculated.
The amplitudes of the force responses divided by the velocity amplitude were determined for each frequency between 1 and 100 Hz and can be observed in Figure 7.2.

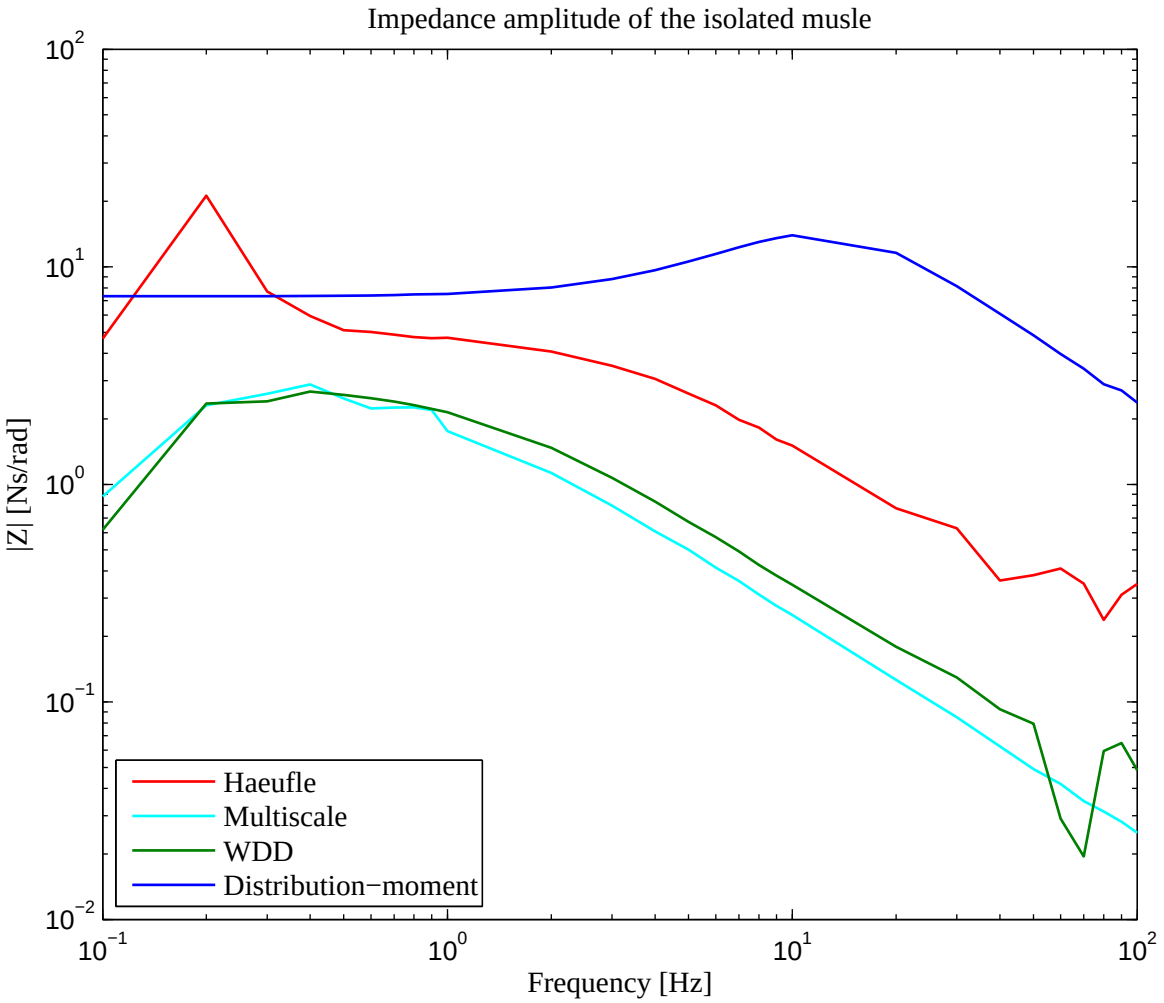

Figure 7.2: Amplitude of the impedance of the different models with normalized force response

At lower frequencies, the impedance is higher than at higher frequencies (above 10Hz). This means that the force amplitude is smaller at higher frequencies than at lower ones. This can be observed on Figure 7.1 (except for the distribution-moment model where the amplitude starts decreasing at a frequency level not represented on this figure): the higher the frequency, the smaller the force amplitude and the closer it gets to the isometric force response.

The impedance curves for the multiscale and work-dependent deactivation (WDD) models are very similar. The impedance increases for frequencies below approximately 0.2Hz and decreases for frequencies above this value. At the impedance peak, the force amplitude is the biggest. At high frequencies, the force amplitude becomes smaller and smaller.
Even though their impedance curves are quite similar, the force equations of these two models are quite different: the mechanical portion of the work dependent model is based on a Hill type model whereas the mechanical portion of the multiscale model is based on a Hill-type model as

well as the Huxley model.
For both models, the force depends on the muscle velocity and a variable muscle stiffness. Equation 7.1 hereunder gives the force response of the contractile element for the work-dependent deactivation model and Equation 7.2 for the multiscale model (only F_{cu} and not F_{ru} since there is no muscle relaxation in this case).

$$Pc = \lambda(l_c)\left(1 + \alpha_1 V - \frac{\alpha_1}{\mu}\frac{dP}{dt}\right) \tag{7.1}$$

$$\begin{aligned} k_{cu}(t) &= -(U_c + a.|\dot{\varepsilon}_c|)k_{cu} + \alpha.N.U_c.\frac{S_0}{L_{c0}}k_0.fl(\varepsilon_c) \\ F_{cu}(t) &= -(U_c + a.|\dot{\varepsilon}_c|)F_{cu} + k_{cu}.L_{c0}.\dot{\varepsilon}_c + \frac{1}{2}.\alpha.N.U_c.k_0.h.(1 + 2.y_0).fl(\varepsilon_c) \end{aligned} \tag{7.2}$$

Here, the activation reached a constant level ($C_{af} = 1$ and thus $dC_{af}/dt = 0$) and since the muscle stiffness varies with the activation in the work-dependent deactivation model, it tends to be constant in this case. In the multiscale model, the stiffness varies with the activation, constant here, but also with the velocity of the contractile element.
Despite these differences, the resulting impedances are quite similar.

The impedance curve of the Haeufle model is similar to the multiscale and work-dependent deactivation models but has a higher impedance for the same range of frequencies. The mechanical portion of this model is based on the Hill model just as for the work-dependent deactivation model. The force produced by the contractile element in this model is given by Equation 7.3 to see how it differs from the other ones.

$$F_{CE}(\dot{l}_{CE}) = F_{max}\left(\frac{A.F_{isom} + A_{rel}}{1 - \frac{\dot{l}_{CE}}{B_{rel}.l_{CE,opt}}} - A_{rel}\right) \tag{7.3}$$

As a reminder, F_{isom} is the force-length relationship. It depends on the contractile element velocity (which itself depends on the whole muscle velocity) as well as the muscle length. This relationship, as show in Section 2.3 of Chapter 2 varies more with eccentric lengths than the others. Unlike for the other two models, no differential equation of the muscle force is involved.

The distribution-moment model is the one that differs the most from the other ones in terms of impedance. It stays relatively constant up to 1 Hz, increases up to 10Hz and then decreases reaching an impedance value at 100Hz bigger than the other three models. The force amplitude of this model does not change much over the range of frequencies compared to the other three models and is greater than for the other models.
Its force response is based on the microscopic Huxley model and the normalized force Q_1 is given by Equation 7.4. The force response depends on the muscle stiffness Q_0 as well as the elastic energy stored in the muscle Q_2 and the scaled myofilament sliding velocity. The activation factor r has also reached a constant value $r = 1$ as for the other models.

$$\frac{dQ_\lambda}{dt} = r.\alpha.\beta_\lambda - r.\phi_{1\lambda}(Q_0, Q_1, Q_2) - \phi_{2\lambda}(Q_0, Q_1, Q_2) - \lambda u(t) Q_{\lambda-1} \tag{7.4}$$

The difference between the distribution-moment model and the other three probably arises from the fact that distribution-moment model computes the muscle force not only from the stiffness of the muscle but also from the elastic energy stored inside the muscle.

7.5 Discussion

In this chapter, the impedance of the muscles, how the muscle reacts to a velocity input, has been analysed. The impedance curves of the different models allowed to see that the force responses to a same velocity input of the muscles differ for the models. The multiscale and work-dependent deactivation models present the most similarities in terms of muscle impedance. They have similar shapes and amplitudes even though their force equations as function of the muscle-tendon unit and contractile element velocities are quite different. The Haeufle model has a similar shape than the two previous models but has a higher impedance amplitude. The distribution-moment model presents the biggest differences with respect to the other models which is probably due to the fact that it considers the elastic energy stored in the muscle as well in the computation of the muscle force.

Part IV

Comparison of the models for agonist/antagonist muscles

Introduction of Part IV

In the previous part, isolated muscle implemented with the different models were compared. This allowed to identify the key features of each model such as their computation time or phyiscal meaning for example.

However, comparing isolated muscle has its limitations since skeletal muscles are usually connected to bones inside the body. Hence, this part will focus on a human articulation.

The primary role of skeletal muscles is to move the body segments. It was stated in Section 1.6 from Chapter 1 that there are three types of muscle contraction: isometric, concentric and eccentric. These types of contraction give the living beings with muscles the possibility to move their body segments toward them or away from them. The contraction of an agonist muscle allows to move a body segment in one direction and the eccentric muscle contraction can be achieved by an external force or an antagonist muscle.

Since an agonist-antagonist muscle system is what allows us to move our body parts and is the primary role of skeletal muscles, such a system was implemented in this chapter with the different muscular models. Only three of the four models will be used to simulate the multi-muscle single-joint system: the Haeufle, the work-dependent deactivation and the multiscale models. The distribution-moment model will not be implemented for this articulation due to its high complexity and heavy computational burden. For this chapter, the ankle articulation which allows the movement of the foot with respect to the tibia was chosen.

The first chapter analyses the ankle dynamics. First, the geometry of the ankle with two muscles is detailed. Then a simulation protocol telling how the results were obtained is given. Finally, the force responses, change in angle and torque for each model with the same activation are given and compared.

The second chapter analyses the impedance of the ankle where the muscles are implemented with the different models. It is based on the dynamics obtained in the previous chapter. The activations will be set to constants and a sine perturbation will be added to the system.

Chapter 8

Multi-muscle single joint system: ankle articulation

8.1 Geometry

The articulation studied with the previously introduced muscular models is the ankle. The geometry of the problem is shown schematically in Figure 8.1. To simplify the problem, only two monoarticular muscles are taken into account: the tibialis anterior and the soleus. These two muscles are represented in red in the scheme. In this geometry, the rest of the body is ignored, only the tibia and the foot linked by the ankle are taken into account. This is not physiologically correct since the gastrocnemius mulitiarticular muscle links the ankle to the femur for instance which is ignored here.

The tibia is fixed and only the foot is allowed to move. The values of the different segments of Figure 8.1 can be found in Table 8.1. The muscle tendon unit parameters of the two muscles can be found in Table 8.2 [21].

Parameter	**Value**	**Parameter**	**Value**
T1	26 [cm]	T3	29 [cm]
T2	2 [cm]	T4	1 [cm]
T5	3 [cm]	m	1.25 [kg]
θ_0	100^o		

Table 8.1: Chosen geometrical parameters. Ti represent the segment lengths in centimeters represented on Figure 8.1. m is the mass of the foot and θ_0 is the initial angle of the foot with respect to the tibia. $L_1(\theta)$ is the whole muscle length with respect to ankle angle of the tibialis anterior and $L_2(\theta)$ is the muscle length of the soleus muscle.

	SOL	**TA**
F_{max} [N]	4000	800
v_{max} $[l_{opt}s^{-1}]$	6	12
l_{opt} [cm]	4	6
l_{slack} [cm]	26	24

Table 8.2: Muscle specific parameters for the soleus (SOL) and tibialis anterior (TA) muscles. F_{max} is the muscle maximum force in Newton in isometric condition. v_{max} is the maximum contraction velocity represented as a function of the muscle optimal length. l_{opt} is the optimal length of the contractile element of the muscle in centimeters and l_{slack} is the length in centimeters of the tendon. From [21]

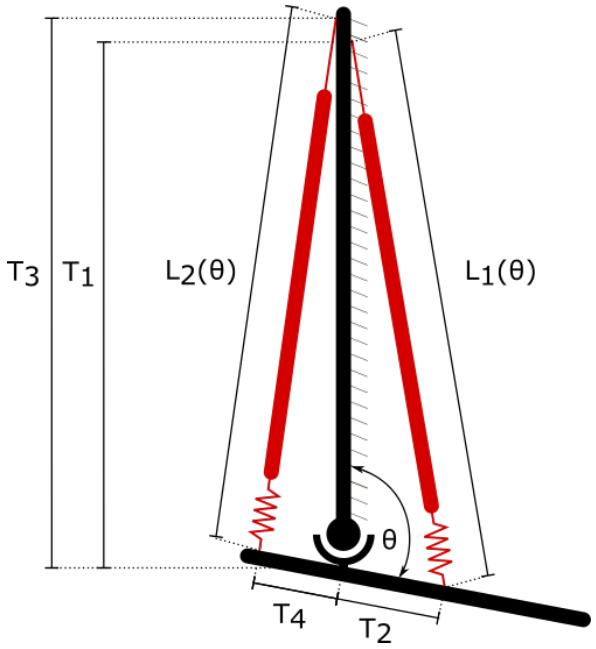

Figure 8.1: Schematic representation of the ankle geometry. In red, the muscles with a spring representing the tendon. In black, the tibia and foot connected by a joint representing the ankle. The tibia is fixed and only the foot can move.

Only the dorsi- and plantar flexion are analysed here. The term "plantarflexion" refers to the extension of the foot at the ankle to move the foot downward whereas the term "dorsiflexion" refers to the flexion of the foot to move it upwards [49]. Both types of flexions are represented in Figure 8.2. The range of physiological angle values in plantar- and dorsiflexion were measured on human subjects [50] [51]. The foot can move in dorsiflexion up to 20^o from its neutral position (which corresponds to $\theta = 90^o$ in Figure 8.1). It can move in plantar flexion up to 50^o from it neutral position. Hence, the range of θ values can be set between 70^o and 140^o.

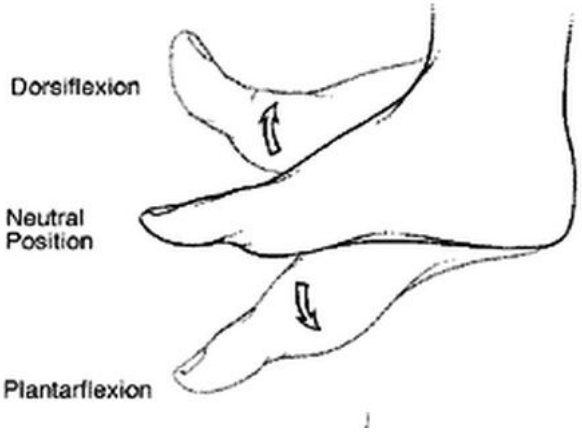

Figure 8.2: Schematic representation of the foot moving upwards (Dorsiflexion) or downwards(Plantarflexion) from its neutral position. From [48]

8.2 Simulation protocol

The simulation of the ankle movement due to the contraction of one of the two muscles or both has been implemented. In order to do this, a time frame of 3 seconds has been set. The simulation scheme has been represented schematically in Figure 8.3.

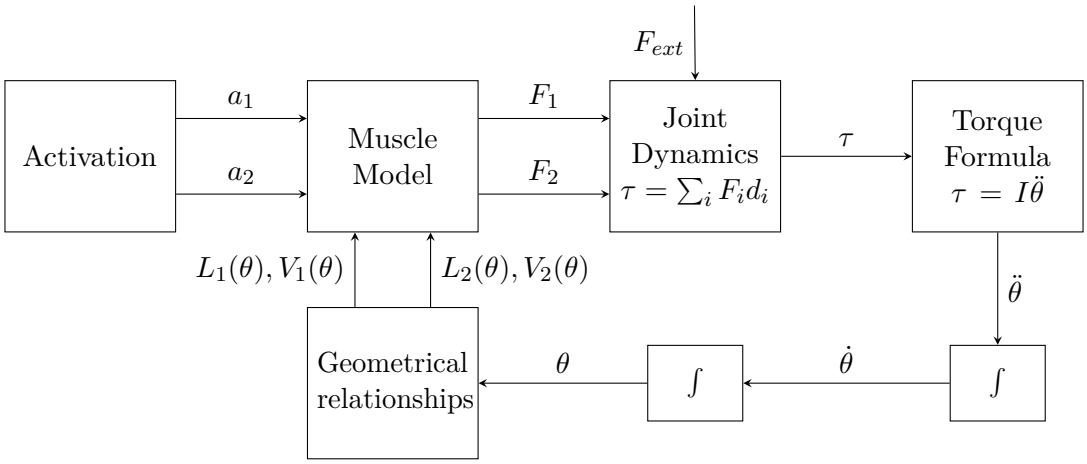

Figure 8.3: Scheme of the simulation protocol. The inputs of the muscle model at each time step are the activations of the two muscles (a_i) as well as the respective lengths and velocities of the muscles ($L_i(\theta)$, $V_i(\theta)$). The output are the forces generated by each muscle (F_i). These forces and external forces such as the gravity are used to compute the torque (τ) which is the sum of each force with its lever arm (d). The torque is then used to find the angular acceleration $\ddot{\theta}$ by using the ankle inertia (I). This acceleration is integrated twice to obtain the angular velocity ($\dot{\theta}$) and displacement (θ) respectively. These are used to compute the new muscle lengths and velocities that will be used in the next time step.

The muscle model takes as input the activation, the length and velocity of the muscle.
For the Haeufle model, the activation is a number between 0 and 1. For the work-dependent deactivation model, the activation corresponds to a stimulation time in seconds. The activation function, or stimulation time, is a pulse function with an amplitude between 0 and 1 during a certain period of time.

Due to the geometry presented in Figure 8.1, the lengths of the two muscles, $L_1(\theta)$ and $L_2(\theta)$, can be calculated by the laws of sine and cosine with respect to the ankle angle θ. The angle theta varies with time, $\theta(t)$, and a new θ is computed at each time step.

$$L_1(\theta(t)) = \sqrt{T_1^2 + T_2^2 - 2T_1T_2\cos(\theta(t))} \tag{8.1}$$

$$L_2(\theta(t)) = \sqrt{T_3^2 + T_4^2 + 2T_3T_4\cos(\theta(t))} \tag{8.2}$$

The velocity of contraction of the muscles can be easily found from Equation 8.1 and Equation 8.2 by deriving the muscle length, $V_i = \frac{dL(\theta(t))}{dt}$.

$$V_1(\theta(t)) = \frac{(T_1T_2\omega(t)\sin(\theta(t)))}{\sqrt{T_1^2 + T_2^2 - 2T_1T_2\cos(\theta(t)))}} \tag{8.3}$$

$$V_2(\theta(t)) = \frac{(T_3T_4\omega(t)\sin(\theta(t)))}{\sqrt{T_3^2 + T_4^2 + 2T_3T_4\cos(\theta(t))}} \tag{8.4}$$

where ω is the angular velocity ($\omega = d\theta/dt$.)
Thus, the length and velocity of the muscles depend on the geometry of the problem. The only controllable input for the muscle models is hence the muscle activation.

At each time step, the muscle forces are computed from the muscle models which uses as

inputs the previously computed muscle lengths and velocities as well as the current activation level.

From there, the torque can be computed. As a reminder, the torque is a force exerted a certain distance from the joint, that tends to change the rotational motion [52]. It corresponds to the product between a force F and its lever arm d which is the distance between the joint and the force application point. The total torque is the sum of the torques induced by the two muscles, the torque induced by gravity and a potential external torque.

Once the total torque is found, the corresponding angular acceleration $\ddot{\theta}$ can be calculated from the torque formula $\tau = I\ddot{\theta}$ where I corresponds to the ankle inertia.

The angular acceleration is integrated twice to obtain the new angle θ. By virtually adding springs with a high stiffness, the angles between which the foot can move were restricted between 70 and 140^o to remain biologically correct. The new lengths and velocities are calculated and the cycle begins again until the end of simulation time.

This was done with the different muscular models with the same muscle parameters, segment lengths as well as initial conditions and activations. The next sections shows the dynamical responses for the different models.

8.3 Comparison of the dynamic responses generated by the different models

As said previously, the only controllable input is the muscle activation which is represented for both muscles. In this ankle movement simulation, the tibialis anterior muscle is stimulated first, at 0.1 seconds, and stops after one second. The soleus muscle is then activated 0.2 seconds after the activation of the tibialis anterior stops. These activation curves can be seen in the first graph of Figure 8.4. The dotted curve corresponds to the activation of the tibialis anterior and the solid curve corresponds to the activation of the soleus muscle.

Since the activation is now set and the muscle lengths and velocities fixed by the geometry of the articulation, the muscle models can calculate the force-response of each muscle. The force-responses for the three models is represented in the second graph of Figure 8.4. The blue, green and red curves correspond to the forces generated with the multiscale, Haeufle and work-dependent deactivation models respectively. The dotted curve represents the tibialis anterior and the solid line to the soleus as for the activation. This color code is maintained for the next graphs.

The individual torques created by the two muscles and the gravity can be calculated as mentioned in Section 8.2. The total torque is the sum of the individual torques and is represented for the three models in the third graph of Figure 8.4.

This torque allows to find the angular acceleration as mentioned in Section 8.2. After integrating the acceleration twice, the angle is obtained. The angle change resulting from the torque is represented for the three models in the last graph of Figure 8.4.

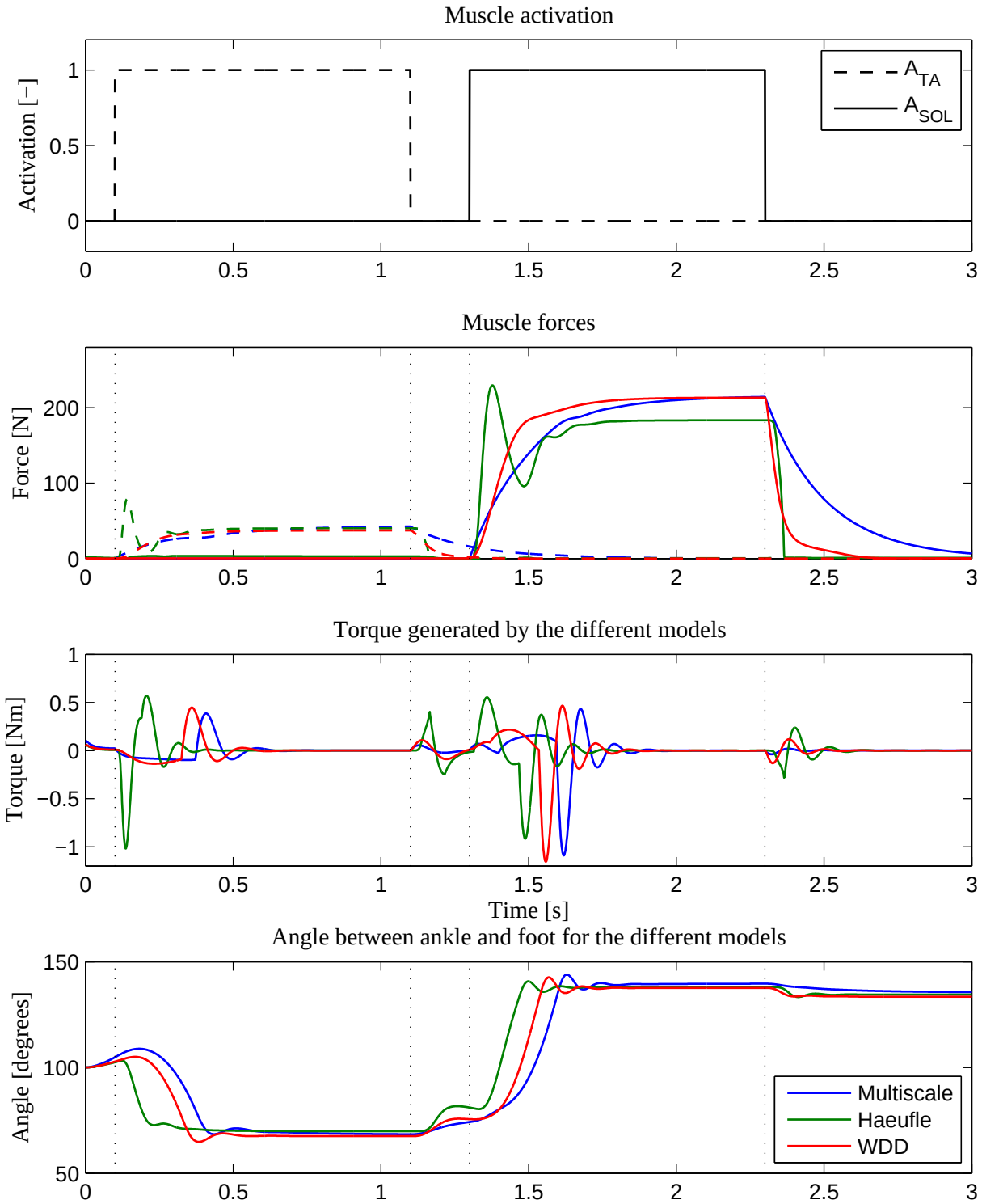

Figure 8.4: Activation of the tibialis anterior and soleus muscles, generated forces, torque and angle found with the three models.
The first graph represents the muscle activations (dotted: tibialis anterior; solid: soleus). The second graph represents the generated muscle forces by each muscle with the multiscale (blue), Haeufle (green) and work-dependent deactivation (red) models. The third graph represents the change in torque and the last graph represents the change in angle of the foot with respect to the tibia.

Now that the ankle articulation has been simulated in the same conditions for all three models, they can be described and compared.

When the tibialis anterior is activated, the angle between tibia and foot decreases as is to be expected. Once it reaches the physiological angle limit in dorsiflexion of 70 degrees, it stays constant at this limit value until the activation stops or the antagonist muscle is activated.
When the activation of the tibialis anterior stops, the angle starts increasing again due to the gravity.
Once the soleus muscle is activated, the angle increases to its plantarflexion angle limit of 140 degrees. Even though the activation of the soleus muscle stops, the angle barely changes due to the gravity.

The responses are similar for the three models as can be expected but there are some dissimilarities nonetheless. The work-dependent deactivation and Haeufle forces decrease faster after the activation stops than the multiscale model. The force responses to the activations are smoother for the work-dependent and multiscale models than for the Haeufle model which reaches rapidly a peak value before decreasing and attaining a plateau value.

During the first 0.1 seconds, no muscle is activated. The angles in all three cases increase slightly due to gravity. After 0.1 seconds, the tibialis anterior is activated (first dotted line). The angle induced by the Haeufle model starts decreasing first and reaches the physiological minimum angle limit first. The angle decrease at the beginning of the activation is much faster than 0.1 seconds after the beginning of the activation. This is probably due to the force peak of the tibialis anterior at the beginning of the contraction. The torque created by this model right after the activation starts is the biggest of the three models and starts the fastest just as for the angle change.
The angle induced by the work-dependent deactivation model starts decreasing later than for the Haeufle model because the generated force increases slower at the beginning of the activation than the Haeufle model. Additionally to that, the angle shows no peak decrease. The torque after the beginning of the stimulation is the weakest but a change in torque can be observed later on when the foot reaches is limit maximum angle.
The multiscale model reaches the highest angle value before decreasing because the generated force right after the beginning of the activation is smaller than for the two other models. It is the model that takes the most time to reach its force peak value and thus the limit angle value.

All three models have reached the minimum limit angle before the activation stops. After the end of the tibialis anterior activation, the angles start increasing again due to the gravity. The angles induced by the work-dependent deactivation and Haeufle models increase a bit faster than the multiscale model. The torques created by the three models are quite similar except for a small time shift and a slightly larger torque for the Haeufle model. The time shift is due to the fact that the models reach their plateau force values at different times.

When the activation of the soleus muscle starts, all three angles induces by the different muscular models reach the maximum limit angle value similarly, only a small time shift is observed. The same can be observed for the torque.

Finally, when the stimulation of the soleus stops, only a small angle change is observed and the foot keeps an angle close to its maximum limit value due to the gravity. It can however be observed that the work-dependent deactivation and Haeufle model stabilize much faster than the multiscale model.

8.4 Discussion

The aim of this chapter was to analyse the dynamics of a bi-muscular single joint articulation namely the ankle implemented with three different muscular models. The main agonist-antagonist muscles responsible for the plantar an dorsiflexion of the ankle that were implemented here are the tibialis anterior and the soleus muscles. The muscles lengths and velocities could be calculated thanks to the geometry of the articulation. The only controllable input for the muscle models was the muscle activation. The output force of the models allowed to calculate new values for the torque and angle between foot and tibia. The same activation signals were used for all three models in order to compare them.

The change in angle and torque were similar for the three models. It is the time to attain the limit minimum angle value when the tibialis anterior was activated that presented the greatest difference between the models. The Haeufle model reached it the fastest followed by the work-dependent and the multiscale model.

The Haeufle model may be chosen in cases where the movement is faster for example. The article of this model [10] used it to model the eccentric force in rapid arm movements where a faster change in angle is more realistic. The multiscale model may be chosen in cases where a slower response is wanted. The work-dependent deactivation and multiscale models present the most similarities just as in the case of an isolated muscle discussed in the previous part.

Chapter 9

Impedance of the multi-muscle single-joint articulation

In this part, the ankle articulation is moved by two antagonist muscles, the tibialis anterior and the soleus. A motor task such as the ankle movement is normally performed by the co-contraction of more muscles than seem to be required and the same task can be carried out in several ways [47]. This means that different activation intensity combinations of the antagonist muscles can produce the same torque. From a physiological point of view, the co-contraction of muscles facilitates the stability and controllability and motion [47]. How does the ankle articulation resists and tries to stabilize to an oscillatory perturbation when one or both muscles are activated? In this chapter, the mechanical impedance of the system using the different muscular models with different levels of co-activation will be implemented and compared.

9.1 Definition of mechanical impedance for an articulation

The definition of mechanical impedance has been given in Chapter 7 where the mechanical impedance of a single muscle has been computed. In this chapter, the mechanical impedance of the ankle articulation with two muscles is computed.

The mechanical impedance can be defined as the relationship between deformation kinematics such as the angular displacement and the dynamics such as the torque. The mechanical impedance defines here the rotational stiffness and damping characteristics of the system, the ankle for instance [47].

The mechanical impedance of the ankle is interesting in order to understand how the ankle supports the lower extremity function during physical interaction with the environment. Those interactions can be for example stabilization or propulsion during walking [53].

9.2 Simulation protocol

The impedance simulation has been performed on the mechanical model presented in the previous chapter with the different muscular models.

The simulation protocol is based on experimental protocols that have been described in the literature to measure the ankle impedance [53] [54]. In these experiments, the subject is seated and his tibia and foot are fixed in a robot called "Anklebot" [55]. This robot was initially developed as a rehabilitation tool and used later as an experimental tool [53] [54]. The Anklebot prototype is represented in Figure 9.1a and in action in Figure 9.1b.

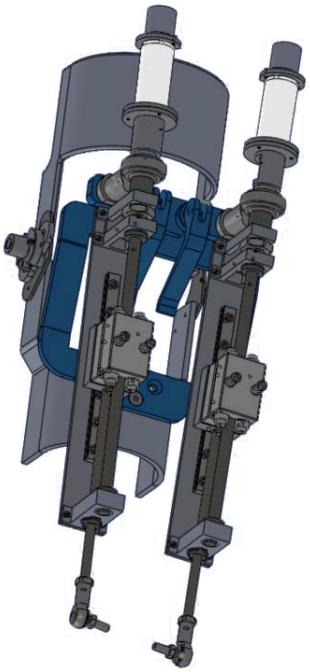

(a) Anklebot prototype. From [55]

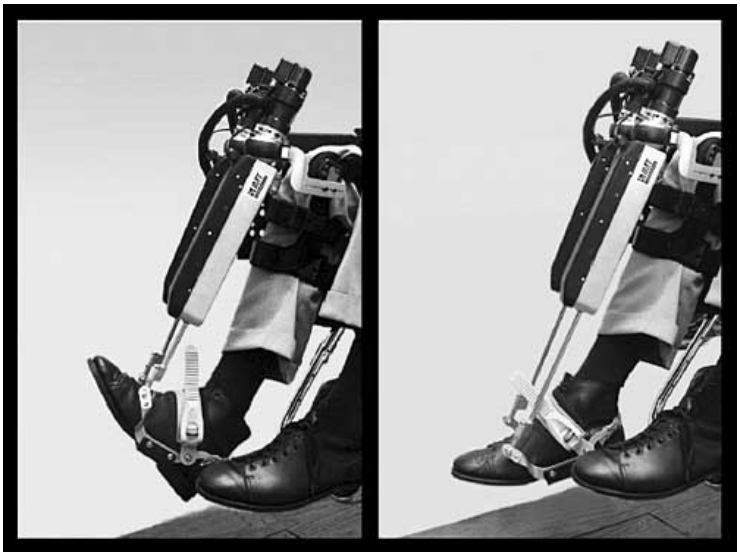

(b) Picture of the Anklebot in action. Left: Anklebot applies torque to move the ankle joint in dorsiflexion. Right: same but in plantarflexion. From [56]

Figure 9.1: Robot to measure the human ankle impedance. The prototype in depicted on the left and the robot in action to move a human foot is depicted on the right.

This robot is attached to a knee brace on the subject and connected to a shoe in which the foot of the subject is. The robot, by applying torques, can move the foot along a given trajectory in dorsi-plantar flexion and/or inversion-eversion. Since only the dorsi-plantar flexion has been analysed in the previous chapter, only a dorsi-plantar flexion perturbation will be introduced here.
The trajectories are limited in the normal range of ankle motion. In order to measure the angular displacement and torque at the joint, sensors were added to the robot [54].

First, the subject is asked to completely relax the soleus and tibialis anterior, the two muscles considered for the ankle joint movement. An external sinusoidal torque is applied to the foot through the Anklebot. The according angular displacement between the tibia and the foot is then measured. In real human experiments, torque perturbations are used instead of position perturbations. The reason for this is that position perturbations can cause excessive displacement of the ankle and hurt the subject. This is not a problem for the numerical simulations performed in this thesis and the angular displacement perturbation could be used.
The same was done for activated muscles: the subject was asked to activate one of the two muscles or both at the same time at a low activation level, about 10% of the maximum voluntary contraction (MVC) [57].
A sinusoidal torque perturbation was introduced at different frequencies, going from 0 Hz to 100 Hz, and the corresponding angle displacement was measured in order to find the impedance.

The same was done numerically by using the previously implemented muscle models and ankle articulation in MATLAB®. A sinusoidal angular displacement of the ankle with a certain frequency was set. The corresponding torque could be obtained trough the muscle model. Since the muscular system is non-linear, the output torque has been approximated by a sinusoidal function as has been done in Chapter 7.

This was done for the same cases as the experimental protocol: first, the muscles were completely relaxed by setting their activation level to zero. Then, the tibialis anterior was activated while the soleus muscle remained relaxed. The opposite was done as well: the soleus muscle was activated while the tibialis anterior was relaxed. Finally, both muscles were activated.

The output torque were taken over a certain time frame where the ankle had the time to adjust to the muscle activations. With this, the amplitude of the torque signal could be obtained. This has been repeated for frequencies up to 100 Hz. The impedance could then be calculated according to Equation 9.1.

$$Z(\omega) = \frac{\tau(\omega)}{\theta(\omega)} \tag{9.1}$$

Where $Z(w)$, $\tau(\omega)$ and $\theta(\omega)$ represent the impedance, torque and angular displacement in the frequency domain respectively.

The impedance of the ankle articulation has been calculated for the three muscular models. The results can be observed in Figure 9.2. The first graph shows the impedance, in frequency domain, in the case where both muscles are completely relaxed. In the second graph, the tibialis anterior muscle is activated while the soleus muscle remains relaxed. The blue, green and red curves correspond to the impedances of the multiscale, Haeufle and work-dependent deactivation models respectively. This color code is kept for all the graphs in Figure 9.2. The third graph represents the impedance when the soleus muscle is activated and the tibialis anterior relaxed. The last graph represents the case where both muscles are activated and thus in co-contraction.

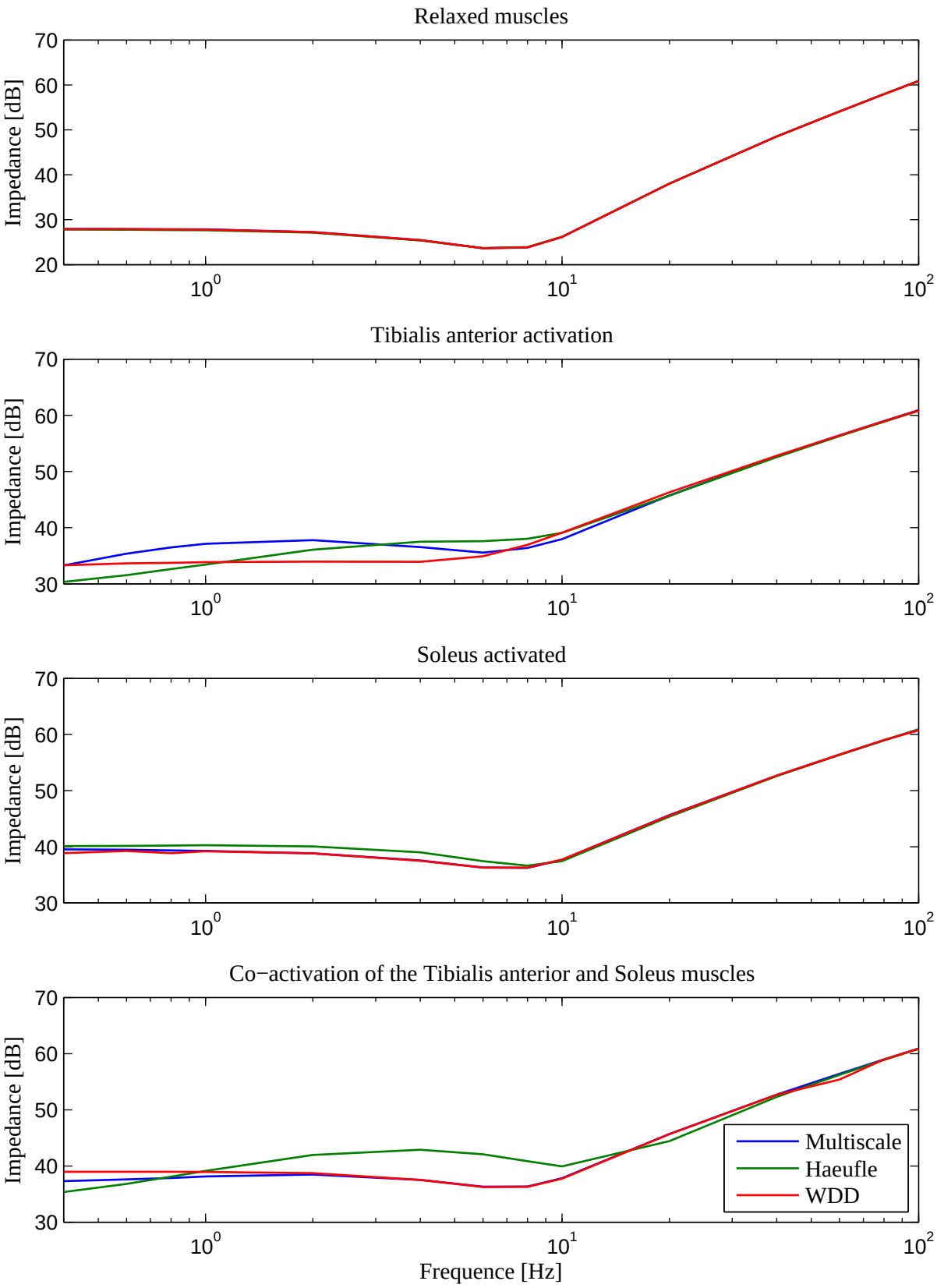

Figure 9.2: Amplitude of the ankle impedance for different levels of activations of the different muscles for the models. The first graph represents the impedances of the muscle models in the relaxed muscles case. In the second graph, the tibialis anterior was activated. In the third graph, the soleus was activated. In the last graph, both muscles were co-activated.

Several things can be observed on Figure 9.2. First of all, the impedance has been represented in decibel in order to compare with the ankle impedance measured by Hyunglae Lee et al. by using the Anklebot [57]. Their impedance graph for the dorsi-plantar flexion of the ankle is given in Figure 9.3. It can be observed that the values obtained with the muscle models and the ones from Hyunglae Lee et al. at low and high frequencies are quite similar.

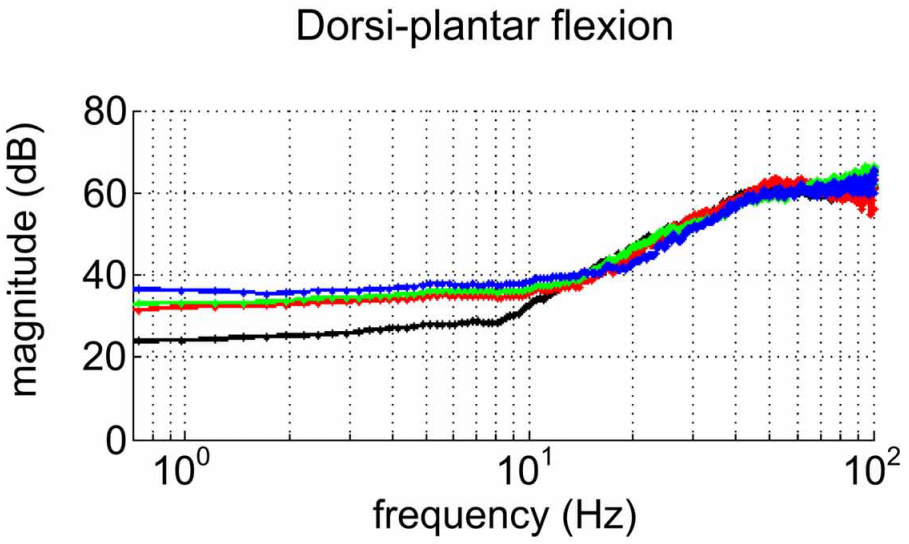

Figure 9.3: Impedance of the ankle articulation with different activation levels of the soleus and tibialis anterior muscles. Black: relaxed muscles. Red: tibialis anterior activated. Green: soleus muscle activated. Blue: both muscles activated. From [57].

Secondly, the impedance is almost identical for the three models in the case where no muscle is activated. The impedance values at lower frequencies are smaller than in the cases where one or both muscles are activated. Some differences at frequencies below 10 Hz can be observed between the models when one or both muscles are activated.

Thirdly, the impedance values for all activations and muscles tend to the same value for frequencies above 10Hz. This can be explained by looking at the equation of motion Equation 9.2 [58].

$$\tau = I\ddot{q} + B(\dot{q}, q) + K(q) \tag{9.2}$$

Where I corresponds to the inertial term, B the viscous term and K the stiffness term. q represents the generalized coordinates and corresponds to θ here since the ankle joint can be represented by a revolute joint. This equation can be rewritten to show the relation between the angular displacement of the ankle θ and the resulting ankle torque τ [58].

$$\tau = I\ddot{\theta} + B(\alpha)\dot{\theta} + K(\alpha)\theta \tag{9.3}$$

With α the activation level of the muscles. In Equation 9.3, the viscous and stiffness terms are function of the muscles activation level while the inertial term remains constant. Indeed, the moment of inertia depends on the mass of an object, the foot here, and the square distance of its center of gravity to the joint [52].

The angular position perturbation has the form of a sine wave with a specific amplitude (the amplitude of the perturbation) and an angular frequency $\omega = 2\pi f$ in radians per second with f the ordinary frequency in Hz. The higher the angular frequency of the position sine wave, the bigger will be the acceleration. This means that the higher the frequency, the more the inertial

term $I\ddot{\theta}$ will dominate while the effects of the the stiffness and viscosity are negligible. This explains why all the impedance values tend to the same value at higher frequencies.

At low frequencies, under one Hz, it is the stiffness term that dominates while the inertia and viscosity are negligible. The Haeufle model presents the lowest impedance when the tibialis anterior is activated or in co-contraction with the soleus muscle.

At intermediate frequencies, the damping term dominates. In all cases with muscle activation, the Haeufle model presents the highest impedance. Indeed, one of the particularities of this Hill-type model to others is that it added a damping element in the muscle-tendon structure.

9.3 Discussion

In this chapter, the impedance of the ankle articulation has been implemented and analysed. In Chapter 7, the impedance of the isolated muscle was measured and analysed for the different models. In this chapter, the same was done but for a bi-muscular single-joint articulation, the ankle.

The ankle articulation impedance tends to the same value for all the models and activation levels at frequencies above 10Hz. This has been explained to be due to the moment of inertia of the ankle, term which dominated at higher frequencies.

The impedance of the articulation is the smallest at lower frequencies when no muscle is activated. This seems natural: the articulation resists more to an external perturbation when one or two muscles are activated. In that case, the impedance is almost identical for all the muscular models.

The impedance varies between the models when the muscles are activated for frequencies below 10 Hz. As for the isolated muscle impedance, the Haeufle model has a higher impedance than the other models. As in the isolated muscle case, the multiscale and work-dependent deactivation models are quite similar to each other.

Conclusion

This master thesis has been divided in four parts. The first part reviewed the muscle physiology upon which the different muscular models have been build. It showed how complex a muscle is and works. The second part described four different muscle models: the Hill and Hill-type models, the Huxley and distribution-moment models, the work-deactivation model and the multiscale model. Each model was described individually and insight about their particularities was given. The third and fourth part focused on the comparison of the different muscular models. The third part compared the models in the case of an isolated muscle whereas the fourth part compared the models in the case of a human articulation, the ankle.

After the comparison of these models, it is easy to understand why the Hill-type model belongs to the most used ones: even with less physiological meaning than the other ones, it gives a similarly good force-response with the advantage of being fast and easy to implement in multibody systems. The distribution moment model is interesting for the purpose of understanding how the muscle works on the microscopic scale. Of the four models, it is the one with the most physiological meaning. Additional outputs of this model are the muscle stiffness and stored elastic energy unlike the three other discussed models. It showed, among other things, the best response for an oscillating activation compared to the other models. However, the price for this accuracy is the computational time which is much higher than for the other models. Because of this complexity and high computation time, it is not suited for multi-body articulations simulations.
The work-dependent deactivation and multiscale models are in between the Hill and Huxley models in terms of accuracy and efficiency. These two models present the most similarities in terms of force output and impedance. The multiscale model is an interesting model if the microscopic as well macroscopic levels need to be analysed. However, the activation dynamics are too simplified. The work-dependent deactivation model has also simplified activation dynamics compared to the distribution-moment. However, the force response for an oscillating activation is better than for the multiscale and Haeufle models.

The ankle articulation implemented with two muscles modelled with the three models gave similar results in terms of torque and change in angle. The muscles modelled with the Haeufle model were the fastest to react in terms of torque and angle, followed by the work-dependent deactivation and multiscale models. The ankle impedance measured with the models was similar too.

It can be concluded that the best model from the four presented depends on the situation and purpose of use. No model, not even the Huxley model, takes the whole complexity of the muscle into account. Each model has strengths, weaknesses and focuses on some specific characteristics of the muscle.

This master thesis gave some insight over the muscle models existing in the literature and the difficulty to model a muscle. There are other muscle models present in the literature, apart from Hill-type models, with their own particularities. These other models could be implemented and added to this comparison.

Bibliography

[1] K. A. Zimmermann, "Muscular system: Facts, functions & diseases." http://www.livescience.com/26854-muscular-system-facts-functions-diseases.html, 2016. Accessed: 2017-05-28.

[2] E. P. Widmaier, H. Raff, and K. T. Strang, *Vander's Human Physiology: The Mechanisms of Body Function*, ch. 9, pp. 267 – 301. McGraw-Hill Science, 9 ed., 2003.

[3] J. P. Johnson, "Animal electricity, circa 1781," September 2011. [Online; posted 28/11/2011].

[4] "Types of muscular contractions." http://www.hawaiianshirtray.com/wp-content/uploads/2011/02/contractions21.jpg. Accessed: 2016-12-11.

[5] L. H. Hyman, *Hyman's Comparative Vertebrate Anatomy*, ch. 9, pp. 327 – 332. University of Chicago Press, third ed., 1992.

[6] M. G. Dongwoon Lee, A. Khan, E. Fiume, and K. Jackson, "Modeling and simulation of skeletal muscle for computer graphics: A survey," *Computer Graphics and Vision*, vol. 7, no. 4, p. 229 – 276, 2011.

[7] U. S. University, "Cartilage and bone connective tissue." https://s3.amazonaws.com/classconnection/818/flashcards/7206818/jpg/periosteum_growth-14FD75D53584A4E3F6C.jpg. Accessed: 2017-05-24.

[8] D. Kirkendall and W. Garrett, "Function and biomechanics of tendons," *Scand J Med Sci Sports*, vol. 7, pp. 62 – 66, 1997:.

[9] A. Hill, "The heat of shortening and the dynamic constants of muscle," *Proceedings of the Royal Society of London B: Biological Sciences*, vol. 126, no. 843, pp. 136 – 195, 1938.

[10] D. Haeufle, M. Günther, A. Bayer, and S. Schmitt, "Hill-type muscle model with serial damping and eccentric force–velocity relation," *Journal of Biomechanics*, vol. 47, no. 6, pp. 1531 – 1536, 2014.

[11] A. Huxley, *Progress in piophysics and biophysical chemistry*, vol. 7, ch. 6, pp. 257 – 310. The MacMillan company, first ed., 1957.

[12] G. I. Zahalak, "A distribution-moment approximation for kinetic theories of muscular contraction," *Journal of biomechanical engineering*, vol. 55, pp. 89 – 114, 1981.

[13] T. L. Williams, "A new model for force generation by skeletal muscle, incorporating work-dependent deactivation," *J Exp Biol.*, vol. 213, no. 4, pp. 643 – 650, 2010.

[14] H. E. Makssoud, D. Guiraud, P. Poignet, M. Hayashibe, P.-B. Wieber, K. Yoshida, and C. Azevedo-Coste, "Multiscale modeling of skeletal muscle properties and experimental validations in isometric conditions," *Computer Graphics and Vision*, vol. 105, no. 2, p. 121 – 138, 2011.

[15] T. McMahon, *Muscles, reflexes, and locomotion*, ch. 1, pp. 3 – 25. Princeton University Press, first ed., 1984.

[16] J. M. Winters and S. L.-Y. Woo, *Multiple Muscle Systems: Biomechanics and Movement Organization*, ch. 1, pp. 1 – 23. Springer-Verlag, 1990.

[17] A. Hill, "The maximum work and mechanical efficiency of human muscles, and their most economical speed," *Journal of Physiology*, vol. 56, pp. 19 – 45, 1922.

[18] H. Gasser and A. Hill, "The dynamics of muscle contraction," *Proceedings of the Royal Society of London B: Biological Sciences*, vol. 96, pp. 398 – 437, 1924.

[19] A. Hill, "The effect of load on the heat of shortening of muscle," *Proceedings of the Royal Society of London B: Biological Sciences*, vol. 159, pp. 297 – 318, 1964.

[20] H. Geyer, A. Seyfarth, and R. Blickhan, "Positive force feedback in bouncing gaits?," *Proc Biol Sci.*, vol. 270, no. 1529, pp. 2173 – 83, 2003.

[21] H. Geyer and H. Herr, "A muscle-reflex model that encodes principles of legged mechanics produces human walking dynamics and muscle activities," *IEEE Trans Neural Syst Rehabil Eng.*, vol. 18, no. 3, pp. 263 – 73, 2010.

[22] "Youngmok yun: Roboticist in the univ. of texas at austin." http://youngmok.com/hill-type-muscle-model-with-matlab-code/. Accessed: 19-12-2016.

[23] Y. Gao and C. Zhang, "Structure–function relationship of skeletal muscle provides inspiration for design of new artificial muscle," *Smart Materials and Structures*, vol. 24, pp. 1 – 16, 2015.

[24] A. Huxley and R. Simmons, "Proposed mechanism of force generation in striated muscle," *Nature*, vol. 233, no. 5321, p. 833 – 838, 1971.

[25] S. Gestrelius and P. Borgström, "A dynamic model of smooth muscle contraction," *Biophys J*, vol. 50, no. 1, pp. 157 – 169, 1986.

[26] G. I. Zahalak and I. Motabarzadeh, "A re-examination of calcium activation in the huxley cross-bridge model," *Mathematical biosciences*, vol. 119, pp. 20 – 29, 1997.

[27] G. I. Zahalak and S.-P. Ma, "Muscle activation and contraction: Constitutive relations based directly on cross-bridge kinetics," *Journal of Biomechanical Engineering*, vol. 112, pp. 52 – 62, 1990.

[28] E. J. Rouse, R. D. Gregg, L. J. Hargrove, and J. W. Sensinger, "The difference between stiffness and quasi-stiffness in the context of biomechanical modeling," *IEEE Transactions on Biomedical Engineering*, vol. 60, no. 2, pp. 562 – 568, 2013.

[29] G. I. Zahalak and S.-P. Ma, "A distribution-moment model of energetics in skeletal muscle," *Journal of Biomechanics*, vol. 24, no. 1, pp. 21 – 31, 1991.

[30] T. McMillen, T. Williams, and P. Holmes, "Nonlinear muscles, passive viscoelasticity and body taper conspire to create neuromechanical phase lags in anguilliform swimmers," *PLoS Comput Biol*, vol. 4, no. 8, pp. 1 – 16, 2008.

[31] D. T. Corr and W. Herzog, "Force recovery after activated shortening in whole skeletal muscle: transient and steady-state aspects of force depression," *Journal of Applied Physiology*, vol. 99, p. 252 – 260, 2005.

[32] K. Edman and R. Josephson, "Determinants of rise time during isometric contraction of frog muscle fibers," *J Physiol*, vol. 580, p. 1007 – 1019, 2007.

[33] M. Hayashibe, D. Guiraud, and P. Poignet, "In-vivo identication of skeletal muscle dynamics with nonlinear kalman filter - comparison between ekf and spkf," *ISRN Rehabilitation*, p. 1 – 10, 2013.

[34] M. Hayashibe and D. Guiraudt, "Voluntary emg-to-force estimation with a multi-scale physiological muscle model," *BioMedical Engineering OnLine*, vol. 12, no. 86, p. 1 – 18, 2013.

[35] T. Siebert, C. Rode, W. Herzog, O. Till, and R. Blickhan, "Nonlinearities make a difference: comparison of two common Hill-type models with real muscle," *Biol Cybern*, vol. 98, pp. 133 – 143, 2008.

[36] F. R. ans F.J. Alonso, "A comparison among different hill-type contraction dynamics formulations for muscle estimation," *Mechanical Sciences*, vol. 7, pp. 19 – 29, 2016.

[37] P. Weiss, I. Hunter, and R. Kearney, "Phenomenological models of the dynamics of muscle during isotonic shortening," *Journal of Biomechanics*, vol. 46, p. 2419–2425, 2013.

[38] K. Jovanović, J. Vranić, and N. Miljković, "Hill's and Huxley's muscle models – Tools for simulations in biomechanics," *Serbian journal of electrical engineering*, vol. 12, no. 1, pp. 53 – 67, 2015.

[39] W. Herzog, *Skeletal Muscle Mechanics: From Mechanisms to Function*, ch. 7, pp. 95 – 125. John Wiley and Sons, 2000.

[40] J. M. Winters and S. L.-Y. Woo, *Multiple Muscle Systems: Biomechanics and Movement Organization*, ch. 5, pp. 1 – 23. Springer-Verlag, 1990.

[41] T. S. Buchanan, D. G. Lloyd, K. Manal, and T. F. Besier, "Neuromusculoskeletal modeling: Estimation of muscle forces and joint moments and movements from measurements of neural command," *J Appl Biomech*, vol. 20, no. 4, p. 367 – 395, 2004.

[42] F. Fuchs, "Cooperative interactions between calcium-binding sites on glycerinated muscle fibers - the influence of cross-bridge attachment," *Biochim. Biophys. Acta*, vol. 462, pp. 314 – 322, 1977.

[43] A. Bahler, "The series elastic element of mamalian skeletal muscle," *Am. J. Physiol.*, vol. 213, pp. 1560 – 1564, 1967.

[44] P. Rack and D. Westbury, "The effects of length and stimulus rate on tension in isometric cat soleus muscle," *J. Physiol.*, vol. 204, pp. 443 – 460, 1969.

[45] D. Thelen, "Adjustment of muscle mechanics model parameters to simulate dynamic contractions in older adults," *ASME Journal of Biomechanical Engineering*, pp. 70 – 77, 2003.

[46] F. Zajac, "Muscle and tendon: properties, models, scaling, and application to biomechanics and motor control," *Crit Rev Biomed Eng.*, vol. 17, no. 4, pp. 443 – 460, 1989.

[47] J. Mizrahi, "Mechanical impedance and its relations to motor control, limb dynamics, and motion biomechanics," *Journal of Medical and Biological Engineering*, vol. 35, pp. 1 – 20, 2015.

[48] "Dorsi-plantar flexions." https://s-media-cache-ak0.pinimg.com/736x/8f/b9/d8/8fb9d8185c6c79fd776d1e1adb177db3.jpg. Last accessed on 28-05-2017.

[49] Saunders, "Dorland's medical dictionary for health consumers," 2007.

[50] D. K. A. trial management group, "Range of movement guide – aim trial v1.0," 2010.

[51] Physiopedia, "Ankle impingement." http://www.physio-pedia.com/Ankle_Impingement. Last accessed on 28-05-2017.

[52] B. Physics, "Torque and rotational inertia." http://physics.bu.edu/~duffy/py105/Torque.html. Last accessed on 28-05-2017.

[53] H. Lee, P. Ho, M. Rastgaar, H. I. Krebs, and N. Hogan, "Multivariable static ankle mechanical impedance with active muscles," *IEEE Transactions on Neural Systems and Rehabilitation Engineering*, vol. 22, no. 1, pp. 44 – 52, 2014.

[54] H. Lee, H. I. Krebs, and N. Hogan, "Multivariable dynamic ankle mechanical impedance with active muscles," *IEEE Transactions on Neural Systems and Rehabilitation Engineering*, vol. 22, no. 5, pp. 971 – 981, 2014.

[55] H. Krebs, S. Rossi, S. Kim, P. Artemiadis, D. Williams, E. Castelli, and P. Cappa, "Pediatric anklebot," *IEEE International Conference on Rehabilitation Robotics*, 2011.

[56] A. Roy, H. Krebs, C. Bever, L. Forrester, R. Macko, and N. Hogan, "Measurement of passive ankle stiffness in subjects with chronic hemiparesis using a novel ankle robot," *Journal of Neurophysiology*, 2011.

[57] N. Hogan and D. Sternad, "Dynamic primitives in the control of locomotion," *Frontiers in Computational Neuroscience*, vol. 7, pp. 1–16, 2013.

[58] S. H. Yeo, J. A. Monroy, A. K. Lappin, K. C. Nishikawa, and D. K.Pai, "Human ankle joint stiffness over the full range of muscle activation levels," *Journal of Biomechanics*, vol. 21, pp. 539–544, 1988.

[59] A. Rohatgi, "Webplotdigitizer." http://arohatgi.info/WebPlotDigitizer, 2017. Version 3.11. Last accessed on 17-05-2017.

Appendix A

Moment-Distribution: ϕ_λ functions

In this appendix, the explicit constructions for ϕ_λ are given for the cases of tight and loose coupling. For the case of loose coupling, it is just a reminder of the equations that can be found in [12]. It was expanded on the same basis for the case of tight coupling. A comparison of the force response for constant or oscillating velocity for the two couplings is given at the end of this appendix in Figure A.1.

A.1 Loose coupling

The ϕ_λ function is defined as follow:

$$\phi_\lambda = \int_{-\infty}^{+\infty} \xi^\lambda . \left[f(\xi) + g(\xi) \right] . n\left(\xi, t\right) d\xi \tag{A.1}$$

With:

$$n(\xi, t) = \frac{Q_0}{\sqrt{2\pi} q} \exp\left(\frac{-(\xi - p)^2}{2q^2} \right) \tag{A.2}$$

$$p(Q_0, Q_1) = \frac{Q_1}{Q_0} \tag{A.3}$$

$$q(Q_0, Q_1, Q_2) = \sqrt{\frac{Q_2}{Q_0} - \left(\frac{Q_1}{Q_0} \right)^2} \tag{A.4}$$

And $f(\xi)$, $g(\xi)$ are defined as follow

$$f(\xi) = \begin{cases} 0 & \text{if} \quad \xi < 0 \\ f_1 \xi & \text{if} \quad 0 < \xi < 1 \\ 0 & \text{if} \quad \xi > 1 \end{cases} \qquad g(\xi) = \begin{cases} g_2 & \text{if} \quad \xi < 0 \\ g_1 \xi & \text{if} \quad 0 < \xi < 1 \\ g_1 \xi + g_3(\xi - 1) & \text{if} \quad \xi > 1 \end{cases} \tag{A.5}$$

By incorporating Equation A.5 into Equation A.1, Equation A.6 was obtained.

$$\begin{aligned} \phi_\lambda = g_2 \int_{-\infty}^{0} \xi^\lambda . n(\xi, t) d\xi + (f_1 + g_1) \int_{0}^{1} \xi^{\lambda+1} . n(\xi, t) d\xi \\ + (g_1 + g_3) \int_{1}^{+\infty} \xi^{\lambda+1} . n(\xi, t) d\xi - g_3 \int_{1}^{+\infty} \xi^\lambda . n(\xi, t) d\xi \end{aligned} \tag{A.6}$$

G. I. Zahalak defined the following integral

$$\begin{aligned} J_\lambda(\eta) &= \frac{1}{\sqrt{2\pi} q} \int_{-\infty}^{\eta} \xi^\lambda \exp\left(\frac{-(\xi - p)^2}{2q^2} \right) d\xi \\ &= \frac{1}{Q_0} \int_{-\infty}^{\eta} \xi^\lambda . n(\xi, t) d\xi \end{aligned} \tag{A.7}$$

And by the change of variables $\zeta = (\xi - p)/q$ and $\tau = (\eta - p)/q$, Equation A.7 becomes

$$J_\lambda(\tau) = \frac{1}{\sqrt{2\pi}} \int_{-infty}^{\tau} (p + q\zeta)^\lambda \exp\left(\frac{-\zeta^2}{2}\right) d\zeta \tag{A.8}$$

By expanding the integrand of Equation A.8, the following series of integrals are obtained:

$$I_\lambda(\tau) = \frac{1}{\sqrt{2\pi}} \int_{-\infty}^{\tau} \zeta^\lambda \exp\left(\frac{-\zeta^2}{2}\right) d\zeta \tag{A.9}$$

And by integrating Equation A.9 by parts, the following recurrence formula is found:

$$\lambda . I_{\lambda-1} = \frac{\tau^\lambda \exp(-\tau^2/2)}{\sqrt{2\pi}} + I_{\lambda+1} \tag{A.10}$$

Equation A.6 becomes finally

$$\begin{aligned} \frac{\phi_0}{Q_0} &= g_2 J_0\left(-\frac{p}{q}\right) + (f_1 + g_1)\left[J_1\left(\frac{1-p}{q}\right) - J_1\left(-\frac{p}{q}\right)\right] \\ &\quad + g_1\left[p - J_1\left(\frac{1-p}{q}\right)\right] + g_3\left[p - J_1\left(\frac{1-p}{q}\right) - 1 + J_0\left(\frac{1-p}{q}\right)\right] \end{aligned} \tag{A.11}$$

$$\begin{aligned} \frac{\phi_1}{Q_0} &= g_2 J_1\left(-\frac{p}{q}\right) + (f_1 + g_1)\left[J_2\left(\frac{1-p}{q}\right) - J_2\left(-\frac{p}{q}\right)\right] \\ &\quad + g_1\left[p^2 + q^2 - J_2\left(\frac{1-p}{q}\right)\right] + g_3\left[p^2 + q^2 - J_2\left(\frac{1-p}{q}\right) - p + J_1\left(\frac{1-p}{q}\right)\right] \end{aligned} \tag{A.12}$$

$$\begin{aligned} \frac{\phi_2}{Q_0} &= g_2 J_2\left(-\frac{p}{q}\right) + (f_1 + g_1)\left[J_3\left(\frac{1-p}{q}\right) - J_3\left(-\frac{p}{q}\right)\right] \\ &\quad + g_1\left[p^3 + 3pq^2 - J_3\left(\frac{1-p}{q}\right)\right] \\ &\quad + g_3\left[p^3 + 3pq^2 - J_1\left(\frac{1-p}{q}\right) - (p^2 + q^2) + J_0\left(\frac{1-p}{q}\right)\right] \end{aligned} \tag{A.13}$$

A.2 Tight coupling

The same was done for the tight coupling knowing from [12] that

$$\phi_{1\lambda} = \int_{-\infty}^{+\infty} \xi^\lambda . \left[f(\xi) + g'(\xi)\right] . n\left(\xi, t\right) d\xi \tag{A.14}$$

$$\phi_{2\lambda} = \int_{-\infty}^{+\infty} \xi^\lambda . \left[g(\xi) + f'(\xi)\right] . n\left(\xi, t\right) d\xi \tag{A.15}$$

G. I. Zahalak defined in [16] the function $f(\xi)$, $g(\xi)$, $f'(\xi)$ and $g'(\xi)$ as follow

$$f(\xi) = \begin{cases} 0 \\ f_1\xi \\ 0 \end{cases} \quad g(\xi) = \begin{cases} g_2 \\ g_1\xi \\ 0 \end{cases} \quad f'(\xi) = \begin{cases} 0 & \text{if} \quad \xi < 0 \\ 0 & \text{if} \quad 0 < \xi < 1 \\ f'_0 + f'_1(\xi - 1) & \text{if} \quad \xi > 1 \end{cases} \tag{A.16}$$

and $g'(\xi) \approx 0$.

However, by looking at the $f(\xi)$ and $g(\xi)$ defined in [12] (Equation A.5), $g(\xi)$ and $f'(\xi)$ from

Equation A.16 can be summarized by the $g(\xi)$ from Equation A.5 with $f_0' = g_1$ and $f_1' = g_3$.

Thus, Equation A.14 and Equation A.15 become

$$\phi_{1\lambda} = \int_{-\infty}^{+\infty} \xi^{\lambda}.f(\xi).n\left(\xi,t\right)d\xi \tag{A.17}$$

$$\phi_{2\lambda} = \int_{-\infty}^{+\infty} \xi^{\lambda}.g(\xi).n\left(\xi,t\right)d\xi \tag{A.18}$$

where $g(\xi)$ is the one defined in Equation A.5.

Thus, $\phi_{\lambda} = \phi_{1\lambda} + \phi_{2\lambda}$

$$\frac{\phi_{1,0}}{Q_0} = f_1\left[J_1\left(\frac{1-p}{q}\right) - J_1\left(-\frac{p}{q}\right)\right] \tag{A.19}$$

$$\frac{\phi_{1,1}}{Q_0} = f_1\left[J_2\left(\frac{1-p}{q}\right) - J_2\left(-\frac{p}{q}\right)\right] \tag{A.20}$$

$$\frac{\phi_{1,2}}{Q_0} = f_1\left[J_3\left(\frac{1-p}{q}\right) - J_3\left(-\frac{p}{q}\right)\right] \tag{A.21}$$

$$\begin{aligned}\frac{\phi_{2,0}}{Q_0} &= g_2 J_0\left(-\frac{p}{q}\right) + g_1\left[J_1\left(\frac{1-p}{q}\right) - J_1\left(-\frac{p}{q}\right)\right] \\ &+ g_1\left[p - J_1\left(\frac{1-p}{q}\right)\right] + g_3\left[p - J_1\left(\frac{1-p}{q}\right) - 1 + J_0\left(\frac{1-p}{q}\right)\right]\end{aligned} \tag{A.22}$$

$$\begin{aligned}\frac{\phi_{2,1}}{Q_0} &= g_2 J_1\left(-\frac{p}{q}\right) + g_1\left[J_2\left(\frac{1-p}{q}\right) - J_2\left(-\frac{p}{q}\right)\right] \\ &+ g_1\left[p^2 + q^2 - J_2\left(\frac{1-p}{q}\right)\right] + g_3\left[p^2 + q^2 - J_2\left(\frac{1-p}{q}\right) - p + J_1\left(\frac{1-p}{q}\right)\right]\end{aligned} \tag{A.23}$$

$$\begin{aligned}\frac{\phi_{2,2}}{Q_0} &= g_2 J_2\left(-\frac{p}{q}\right) + g_1\left[J_3\left(\frac{1-p}{q}\right) - J_3\left(-\frac{p}{q}\right)\right] \\ &+ g_1\left[p^3 + 3pq^2 - J_3\left(\frac{1-p}{q}\right)\right] \\ &+ g_3\left[p^3 + 3pq^2 - J_1\left(\frac{1-p}{q}\right) - (p^2+q^2) + J_0\left(\frac{1-p}{q}\right)\right]\end{aligned} \tag{A.24}$$

A.3 Graphical comparison between the loose and tight coupling

Figure A.1 shows the force-response in the case of constant and oscillating contraction velocity (10Hz) of the sarcomeres. No significant difference between the two models can be observed.

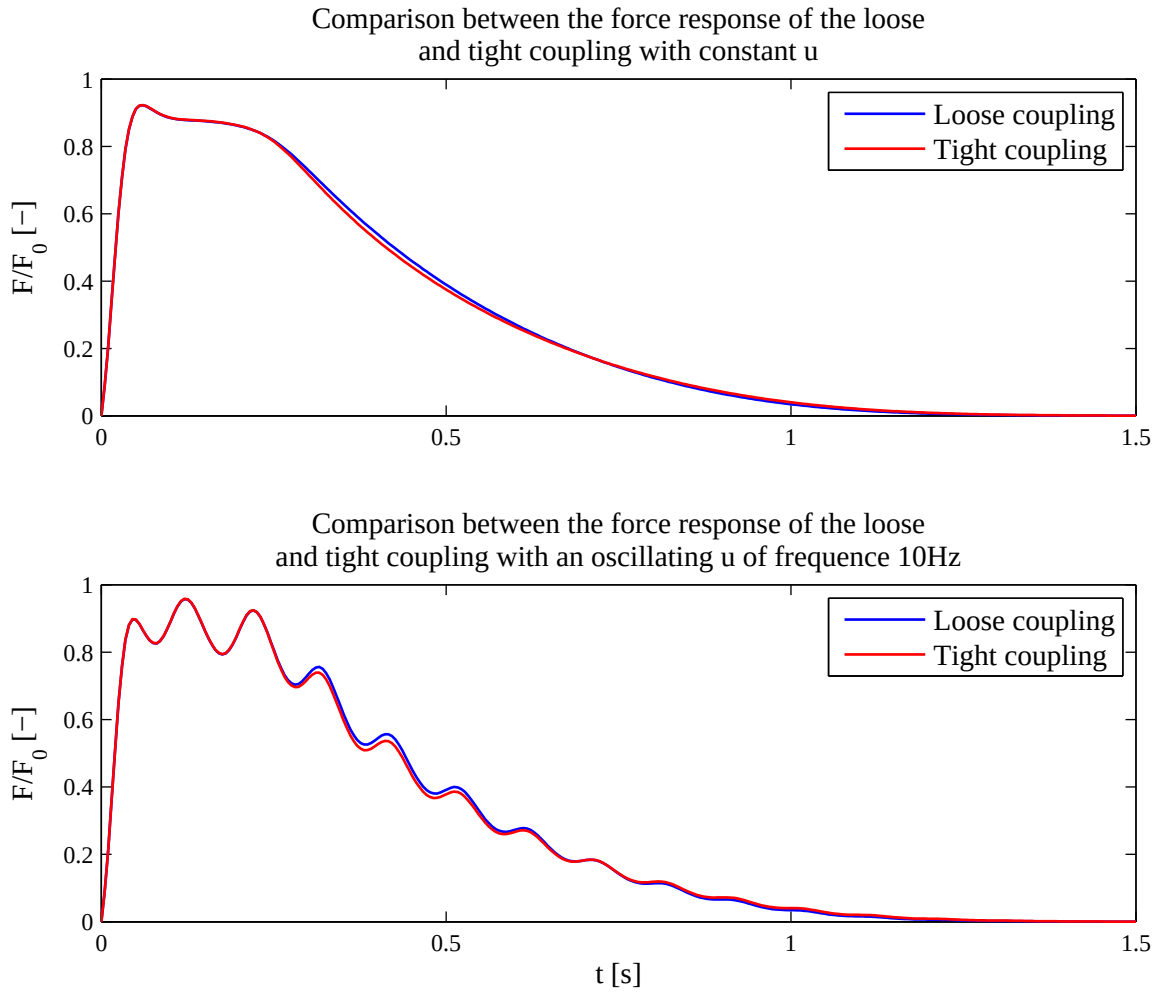

Figure A.1: u is the contraction velocity of the sarcomeres. The first graph shows the force response with a constant $u(t) = -100s^{-1}$ for the loose coupling (blue) and the tight coupling (red). The second graph shows the force response with an oscillating $u(t) = -20\sin(2\pi ft) - 100$ with a frequence $f = 10Hz$

Appendix B

Model validations

The models presented in the second part of this master thesis were all implemented in MATLAB®, following the equations provided in the corresponding references. The goal of this chapter is to report the validation of these models, i.e. graphs of the force response, produced as output of these different models, and compared to the data provided in the corresponding references.

Since the reference data were available as graphical figures, a digitized version of the data had to be produced first. To do this, the free software "WebPlotDigitizer" was used [59]. The graph is loaded in the software as a picture. The axis are calibrated by the user who puts two points on each axis where the coordinates are known. This allows the software to calibrate the plot. Then, the user manually adds sampling points to reproduce the desired graph. As many points as wanted can be added and the more there are, the more the data will fit the graph on the image. However, since it is the user who manually adds the sample points, some precision is inevitably lost.

A.1 Work-dependent deactivation model

For this model, Figure 2(A) in [13] was chosen. This figure represents the normalized force response of the muscle in isometric conditions for a stimulation time of about 0.34 seconds.
With the same parameter values given in the article, the given model was implemented for the same conditions. The obtained force response with the model and the one given in the article are both represented in Figure B.1. The red curve represents the curve numerically extracted from the article figure and the blue curve corresponds to what was obtained with our implementation of the model.

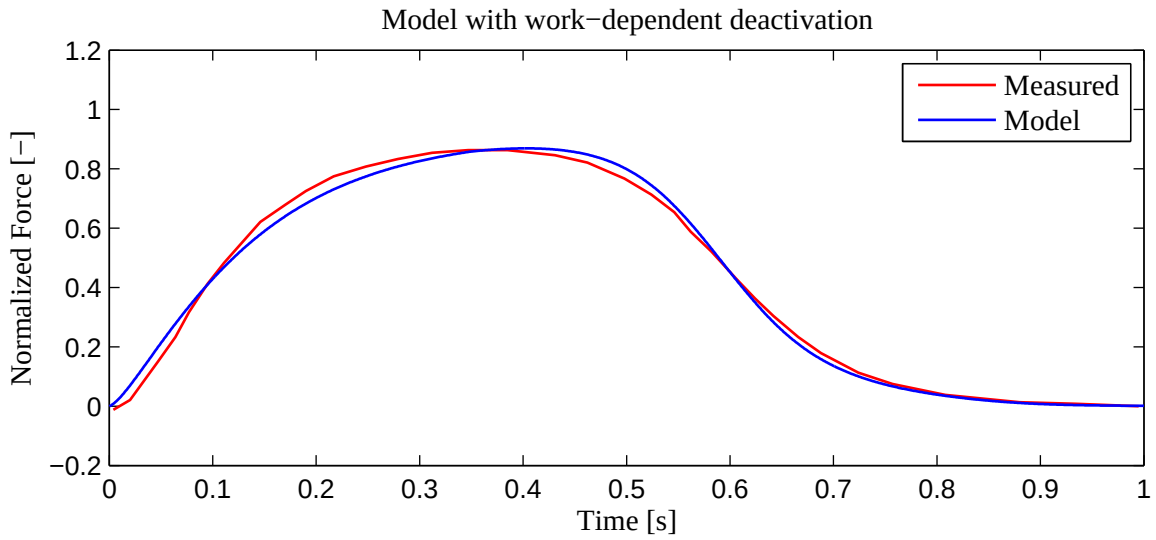

Figure B.1: Implemented WDD model (blue curve) compared reference data (red curve) [13] in isometric condition

It can be observed that the two curves are very similar. The small dissimilarities are probably due to the loss of precision in the numerical data extraction since the figure in the article is quite small.

A.2 Multiscale model

To validate this model, Figure 18 from [14] was chosen. This figure represents force responses at two different frequencies, 15 and 20 Hz. In this figure, measured data on subject was compared to the the force-response obtained by the model.
The curve obtained with the reference model was numerically extracted and compared to the implemented model. This can be seen in Figure B.2. Again, the red curve represents the curved that was numerically extracted from the article and the blue curve corresponds to what was obtained with the implementation of the model in the same conditions.

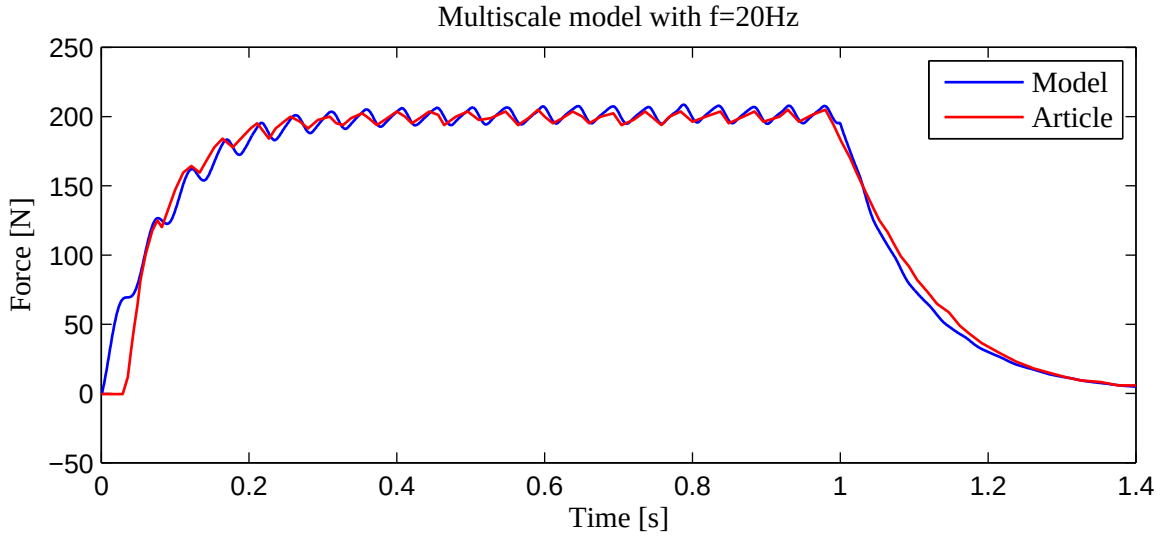

Figure B.2: Implemented multiscale model (blue curve) compared to what was obtained in the article (red curve) [14] Fig. 18 with a frequency of 20 Hz

It can again be observed that the two curves are very similar. The small dissimilarities are probably due to the lack of precision during the numerical data extraction. It can also be due to the fact that some parameter had to be estimated since their value was not given in the literature.

A.3 Distribution-moment model

For this model, Figure 3 in [12] was chosen. This figure gives the force response for specific bonding and unbonding rates. The computed force response with the model and the one given in the article are both represented in Figure B.3. The red curve represents the curve numerically extracted from the article figure while the blue curve corresponds to what was obtained with the computed model.

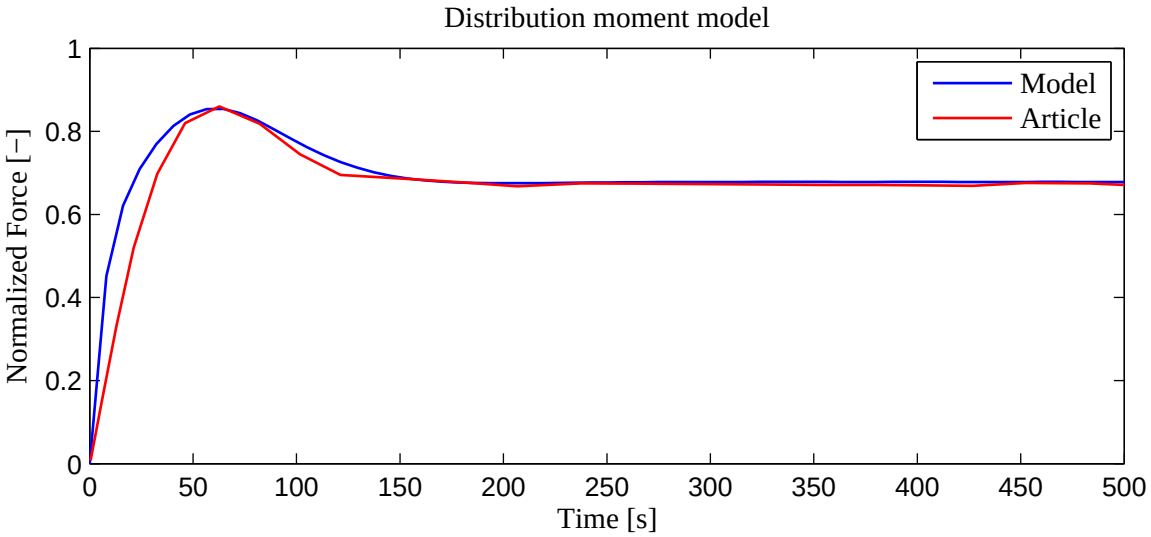

Figure B.3: Implemented distribution-moment model (blue curve) compared to what was obtained in the article (red curve) [12]

Even though both curves are similar, there are some dissimilarities. This can be due partially to the lack of precision during the numerical extraction but also due to the fact that some of the many parameters needed by the model were not specified for this case.

Rue Archimède, 1 bte L6.11.01, 1348 Louvain-la-Neuve **www.uclouvain.be/epl**